I. STUDIES TOWARD THE TOTAL CHEMICAL

SYNTHESIS OF CYCLIC ADENOSINE 5'-

DIPHOSPHATE RIBOSE (CADPR)

II. SELECTIVE PHOSPHITYLATION OF

UNPROTECTED CARBOHYDRATES

III. THE SOLUTION STRUCTURE OF CADPR

By

SARAH CHRISTINE POPE

Bachelor of Arts

Earlham College

1994

Submitted to the Faculty of the
Graduate College of the
Oklahoma State University
in partial fulfillment of
the requirements for
the degree of
DOCTOR OF PHILOSOPHY
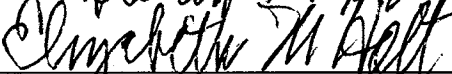December, 1999

I. STUDIES TOWARD THE TOTAL CHEMICAL

SYNTHESIS OF CYCLIC ADENOSINE 5'-

DIPHOSPHATE RIBOSE (CADPR)

II. SELECTIVE PHOSPHITYLATION OF

UNPROTECTED CARBOHYDRATES

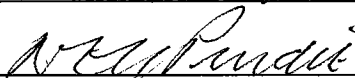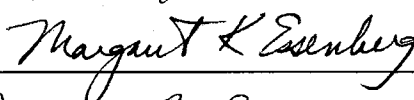III. THE SOLUTION STRUCTURE OF CADPR

Thesis Approved:

_____

Thesis Advisor

_____

_____

_____

_____

_____
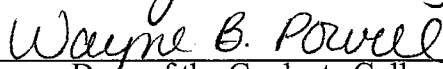
Dean of the Graduate College

This thesis was completed in loving memory of
my grandfather, Hughlan William Pope

Although I knew you for just a short time, you
continue to be an inspiration for me.
I miss you.

July 12, 1914 - August 15, 1980

ACKNOWLEDGEMENTS

Additionally, I want to acknowledge and thank those people who make up my soul. Many have been around for quite some time, and I consider myself blessed to have them in my life. Sangbo, Laura, Karen, Tess, Jeremy, Medea, Tammy, Jill, Tina, Diane, and Devon. If a person is truly a reflection of their friends, I am a very fortunate person.

Finally, I would like to express my deepest love and appreciation for my family. My parents (Charles and Mary) have shown by example the importance of ethics, happiness, and true success, while teaching me how to live and work responsibly. My beloved younger siblings (Jim and Leah) have continually provided comic relief for the unwavering pressure of graduate school!

Thank you all so very much.

TABLE OF CONTENTS

CHAPTER IV. THE SOLUTION STRUCTURE OF CADPR

LIST OF TABLES

LIST OF FIGURES

xi

CHAPTER I

GENERAL BACKGROUND

Calcium Release and Second Messengers

Introduction

Intracellular calcium release from calcium vesicles into the cellular cytosol plays

an integral role in numerous cellular events including muscle contraction, fertilization,

and regulation of metabolic cascades.[1-3] Within the past twenty years, several novel

Ca^{2+}-releasing molecules have been discovered (Figure 1), and a new understanding of

the involved biochemical mechanisms is emerging. This increased understanding

provides new insights concerning intracellular Ca^{2+} regulation, as it prompts further

Inositol 1,4,5-triphosphate
(IP_3, **1**)

Cyclic adenosine
5'-diphosphate ribose
(cADPR, **2**)

Nicotinic acid adenine
dinucleotide phosphate
(NAADP, **3**)
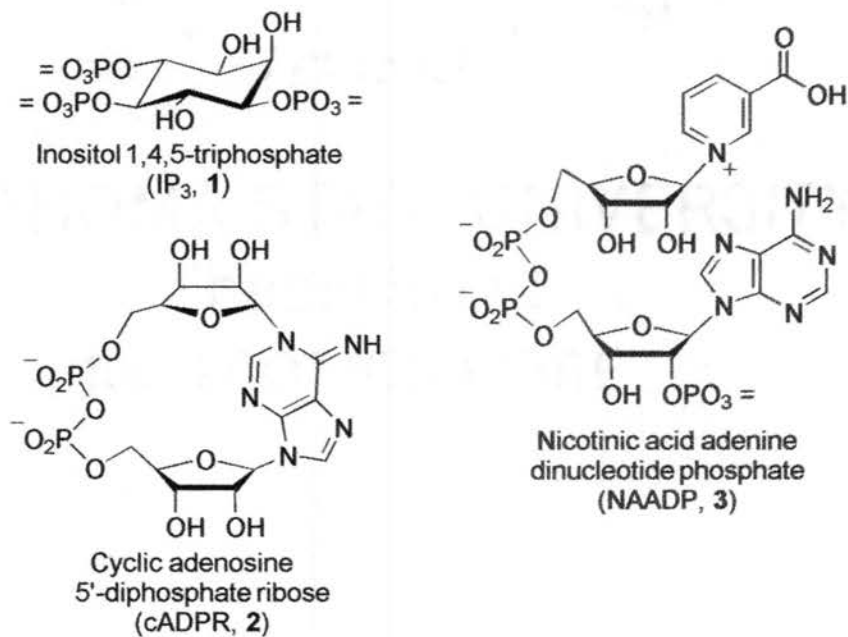
Figure 1. Three Ca^{2+}-releasing molecules.

investigations into the resulting biological implications.

Much recent interest has focussed on the investigation of calcium-releasing agents hypothesized to play a particular intermediate role in cellular transmembrane signal transduction. To date, three such molecules (Figure 1, **1-3**) have been identified and postulated[4-6] to play key roles in transmitting an extracellular signal into the interior of the cell. Accordingly, these three molecules, as well as their respective transduction cascades, are attractive targets for further investigation.

Generally, second messenger molecules facilitate signal transduction across plasma membranes, thereby transmitting an extracellular stimulus to affect an intracellular response (Figure 2).[7] Initially, the external signal binds to an appropriate receptor in the plasma membrane. This binding, in turn, initiates a cascade of events, which ultimately results in the formation of the biologically active second messenger from its precursor. Once the active form of the second messenger is present in the cell, it is then capable of causing Ca^{2+} release by interacting directly or indirectly with receptors on the Ca^{2+} vesicle surface. The released Ca^{2+} is then free to activate cellular proteins,
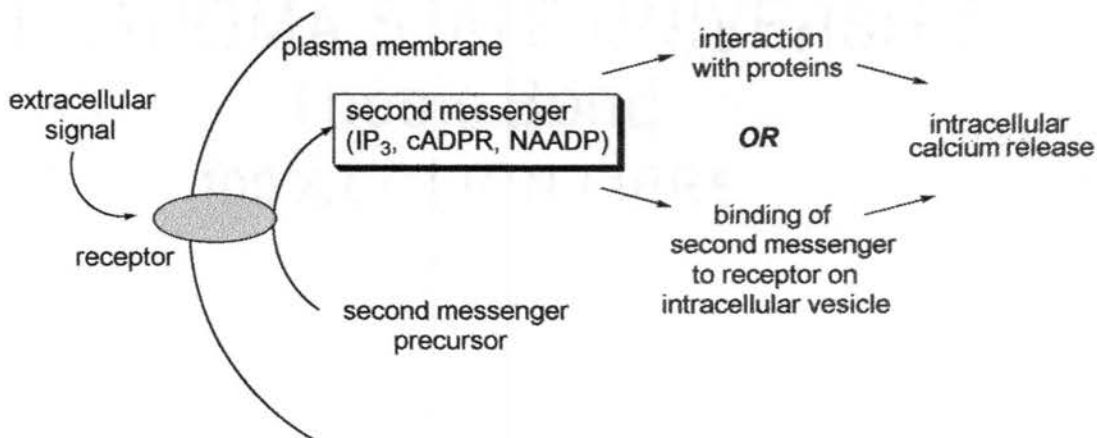
Figure 2. A general model for second messenger-induced calcium release.

consequently generating the final cellular response.

The intracellular Ca^{2+} release caused by second messengers is categorized into two groups.[8] One division includes Ca^{2+} release within electrically-excitable cells (such as nerve and muscle), while the other involves Ca^{2+} release within electrically-inexcitable cells (such as epithelial and blood). Both cell types incorporate Ca^{2+} release as a key event in cellular signaling; however, the mechanisms of that release differ, and the putative second messengers vary.

Inositol 1,4,5-triphosphate as a second messenger

In 1983, inositol 1,4,5-triphosphate (IP_3, 1) was identified as the first Ca^{2+}-releasing second messenger.[9] At the time of its discovery, IP_3 was postulated to release calcium ions from intracellular Ca^{2+} stores, with a half-maximal calcium release (ED_{50}) at an intracellular IP_3 concentration of 50-60 nM.[10] Additionally, IP_3 plays an integral role in the calcium-dependent induction of the cellular cortical reaction, which follows egg fertilization and is often observed visually (in certain species) with the formation of the fertilization envelope.[11]

Shortly after its initial discovery, IP_3 was chemically synthesized via two similar routes.[12,13] Both strategies, starting from a commercially-available inositol derivative, incorporate the use of hydroxyl protections and subsequent polyphosphorylation via the phosphoramidite approach to yield racemic IP_3. Enantiomerically pure IP_3 was obtained by performing a similar synthesis,[13] starting from an enantiomerically pure starting material.
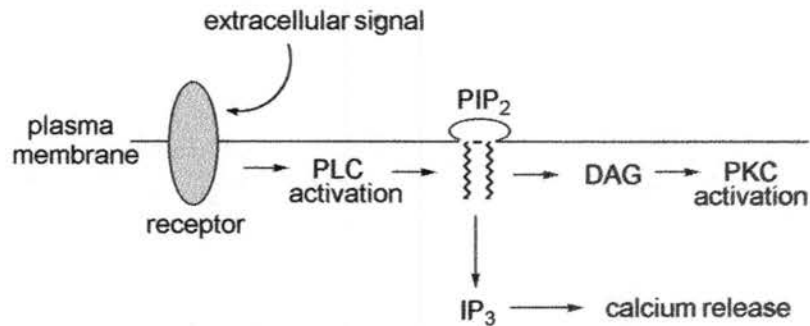
Figure 3. The IP_3 signal transduction cascade.

Much more detail has been revealed about the IP_3 pathway in the two decades following its discovery, and the IP_3 signal transduction cascade has emerged as proportionately more intricate.[4] IP_3 is currently known to perform as a second messenger in two major signaling pathways, initiated by ligand binding to one of two types of cell surface receptors. The first includes a family of G-protein linked receptors (receptors dependent on the binding of guanosine triphosphate, GTP); the second involves receptors coupled, either directly or indirectly, to tyrosine kinases (enzymes that phosphorylate the amino acid tyrosine). In both cases (Figure 3), receptor binding of the extracellular ligand initiates the activation of phospholipase C (PLC), which consequently hydrolyzes the membrane-bound phosphatidylinositol 4,5-bisphosphate (PIP_2), generating the products IP_3 and diacylglycerol (DAG). Interestingly, an entire family of related membrane-bound phosphoinositides has also been uncovered.[2] Although PIP_2 is the only substrate hydrolyzed in the IP_3 cascade, the other phosphorylated inositol molecules play key roles in other cellular events, such as endocytosis and cellular trafficking.

Once the signal has been transmitted through the plasma membrane, the produced second messengers (IP_3 and DAG) proceed to affect the corresponding intracellular

vicinal 4- and 5-
phosphate groups
required for
calcium release

1-phosphate and 6-hydroxyl necessary
for receptor affinity
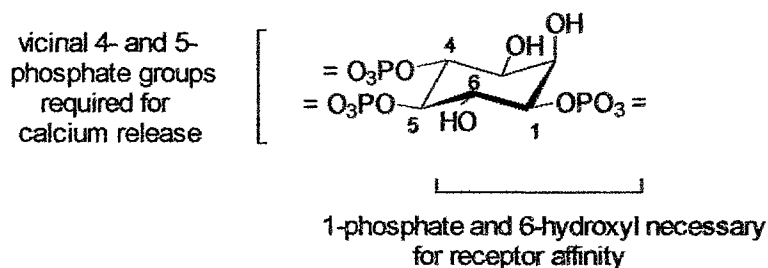
Figure 4. Key structural elements of IP $_3$.

responses. Diacylglycerol, which is not a Ca^{2+}-releasing molecule, activates protein

kinase C (PKC), which then phosphorylates other key proteins essential in cellular

function. As a Ca^{2+}-releasing agent, IP$_3$ advances further to bind to its receptor on the

calcium vesicles , causing the resultant efflux of Ca^{2+} ions.

Structure-activity studies of IP$_3$ have determined that two main structural

components are integral for the observed biological activity (Figure 4). First, the vicinal

4-5 bisphosphate arrangement is essential for Ca^{2+}-releasing activity.[14] Second, the 1-

phosphate and the 6-hydroxyl groups are required for enhanced affinity for the IP$_3$

receptor.[15,16] Recent evidence has indicated that the cyclohexane ring is not required for

the calcium-releasing action of IP$_3$, as several cyclopentane-based analogues

demonstrated activity comparable to that of IP$_3$.[16]

The ryanodine receptors

Following the elucidation of the IP$_3$ pathway, a second receptor on the

intracellular Ca^{2+} vesicle, insensitive to IP$_3$, was discovered. Both receptors are located

on the sarcoplasmic reticulum of muscle cells, and both regulate their respective calcium

channels; however, the two vary in their specific agonists and antagonists.

The IP_3 receptor (IP_3R), found in a number of cell types, is both positively and negatively regulated by IP_3, dependent on cytosolic calcium levels.[4,17] When [Ca^{2+}] is low (<300 nM), IP_3R is activated to release Ca^{2+} from the intracellular vesicles. When [Ca^{2+}] is high (>300 nM), IP_3R is inactivated towards further Ca^{2+} release. Although the mechanism of this calcium-induced calcium release (CICR) is not completely known, it is currently thought to include changes in affinity states of IP_3R.[17] When [Ca^{2+}] is low, IP_3R may exist in an activated/high affinity state for IP_3 (IP_3R_h), while high [Ca^{2+}] may trigger the conversion of IP_3R_h to its inactivated/low affinity state for IP_3 (IP_3R_l). Other intermediate proteins, such as the Ca^{2+}-binding calmodulin, may play key roles in this regulation. IP_3R agonists include various sulfhydryl reagents, such as thimerosal, while antagonists include heparin.[17]

Similarly, the IP_3-insensitive ryanodine receptor (RyR), sensitive to the plant alkaloid ryanodine, appears to be up- and down-regulated by cytosolic calcium concentrations in CICR.[18] However, while RyR is IP_3-insensitive, it is sensitive to another organic phosphate, cyclic adenosine 5'-diphosphate ribose (cADPR).[19,20] In fact, recent evidence has demonstrated that the ED_{50} for cADPR-induced Ca^{2+} release is 18 nM,[11] making it much more potent than the aforementioned IP_3R/IP_3 interaction.

To date, three different types of ryanodine receptors (RyR1, RyR2, and RyR3) have been discovered in various types of organisms including rabbit, mink, and rat.[21] While RyRs are most prominently expressed in skeletal muscle, they are also present in stomach, spleen, brain, and cardiac cells.[22] The observed variety of RyR isoforms in

various tissues indicates possible variations in calcium release channels and/or cascades, relative to the different cell types.[21,22]

The general RyR, as characterized by electron microscopy, possesses a fourfold symmetry with a tetrameric structure (~2240 kDa total).[21] It has been postulated that the transmembrane domains of each subunit collaborate to form the actual RyR Ca^{2+} channel. Several potential Ca^{2+} and calmodulin-binding sites have been identified in the primary sequence of RyR.[21]

Changes in the primary sequence of RyR have caused certain disease states.[21] In fact, a single point mutation (from arginine-615 to cysteine-615 in the DNA sequence) in RyR1 has been identified as a probable cause for malignant hyperthermia,[21] a potentially fatal metabolic condition. In humans, the condition has been attributed to a defect in the calcium channels of skeletal muscle sarcoplasmic reticulum. The region thought to be involved is homologous to the IP_3-binding region of IP_3R.

Although the three ryanodine receptors appear to possess considerable (~70%) homology,[21] the exact mechanism of RyR activation remains unknown. Interestingly, the actual pathways may differ for the various RyR gene products. For example, the cardiac RyR Ca^{2+} channel is activated by phosphorylation by a Ca^{2+}/calmodulin-dependent (CAM) kinase, while the skeletal RyR Ca^{2+} channel is neither phosphorylated nor activated by CAM kinase. In fact, phosphorylation of the skeletal RyR actually appears to inhibit Ca^{2+} release.[21]

Rationale for investigation

Even with the currently available information on RyR, much remains to be elucidated regarding the exact pathways of Ca^{2+} release from the involved intracellular stores. For example, exactly which Ca^{2+} stores are implicated in RyR Ca^{2+} release? Which proteins and/or small molecules are involved, and what are the roles of such agents in the pathway? What is the endogenous regulator of RyR? What are the roles, if any, of IP_3 and IP_3R in the cascade? What are the energy requirements for the process, and how are these attained? What are the biological implications of the resultant Ca^{2+} release? What are the biological implications of inhibiting these pathways?

The current projects have preliminarily addressed such questions by examining the putative RyR regulator cADPR. Although relatively little is known regarding Ca^{2+} release by cADPR, it is believed to be a key player in cellular signal transduction leading to intracellular events. Accordingly, elucidation of its mechanism of action will potentially lead to a significantly increased understanding of not only the implicated Ca^{2+} release, but also, of cellular signal transduction as a whole.

Cyclic adenosine 5'-diphosphate ribose

cADPR emerged in 1987 as another potent intracellular Ca^{2+} release agent.[5] It has been postulated that the cyclic nucleotide collaborates with IP_3 to regulate intracellular Ca^{2+} levels in inexcitable and excitable cells (Figure 5).[11,23] Although the exact mechanism of Ca^{2+} regulation by cADPR remains unknown, cADPR has been

identified as a RyR regulator in skeletal, cardiac, and pancreatic cells.[24-26] Calmodulin

has also been proposed as a mediator of cADPR-induced calcium release.[27]

Recent evidence has demonstrated that while cADPR is much more potent than

IP_3 in releasing intracellular calcium, the resultant Ca^{2+} release is due to a combination of

both pathways.[23] In fact, blockage of either pathway during Ca^{2+}-dependent fertilization

of sea urchin eggs does not completely block fertilization from taking place; rather, the

process is slowed, as demonstrated by the delay in fertilization envelope formation.[11]

Similarly to IP_3, cADPR appears to release Ca^{2+} as a second messenger, thereby

causing an increase in intracellular $[Ca^{2+}]$ following ligand binding to a membrane-bound

receptor.[28,29] cADPR is also postulated to act via a CICR mechanism, in which the

binding affinity of RyR is altered, dependent on cytosolic $[Ca^{2+}]$. This CICR has been

observed to be synergistic with another RyR regulator, caffeine.[30] The structural isomer

isocaffeine was four to five times less effective than caffeine in the activation of RyR

towards calcium release.

Additional evidence indicates that IP_3 and cADPR regulate different intracellular

calcium stores. Sea urchin egg homogenates, upon treatment with cADPR, became
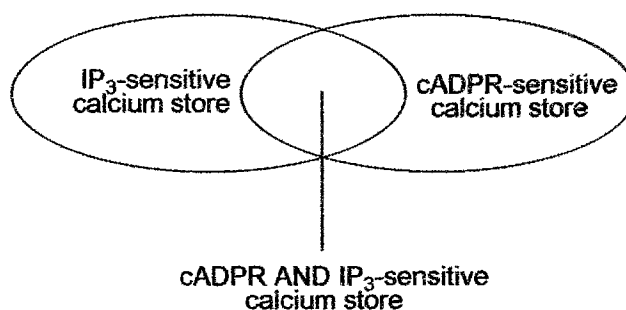
Figure 5. Postulated distribution of intracellular calcium.

insensitive to further Ca^{2+} release from cADPR-sensitive stores. However, these same

homogenates were still IP_3-sensitive, thereby suggesting that the two agents do not

significantly alter the affinity of the other ligand for its own receptor.[11] Likewise,

treatment of RyR homogenates with the IP_3 antagonist heparin resulted in no change for

cADPR-induced calcium release. However, although cADPR and IP_3 do act on different

receptors, a relatively small amount of intracellular calcium does appear to be susceptible

to both agents.

Biologically, cADPR is synthesized from nicotinamide adenine dinucleotide

(NAD^+) by the ubiquitous ADP-ribosyl cyclase (Figure 6).[31] This monofunctional

enzyme is found in many tissues including brain, heart, spleen, kidney, and liver,[32-34]

demonstrating its potential as a widespread producer of cADPR. The cyclase activity is

activated by the putative extracellular ligand cyclic 3',5'-guanosine monophosphate

(cGMP).[35] In contrast to other NAD^+-utilizing enzymes which bind NAD^+ in an
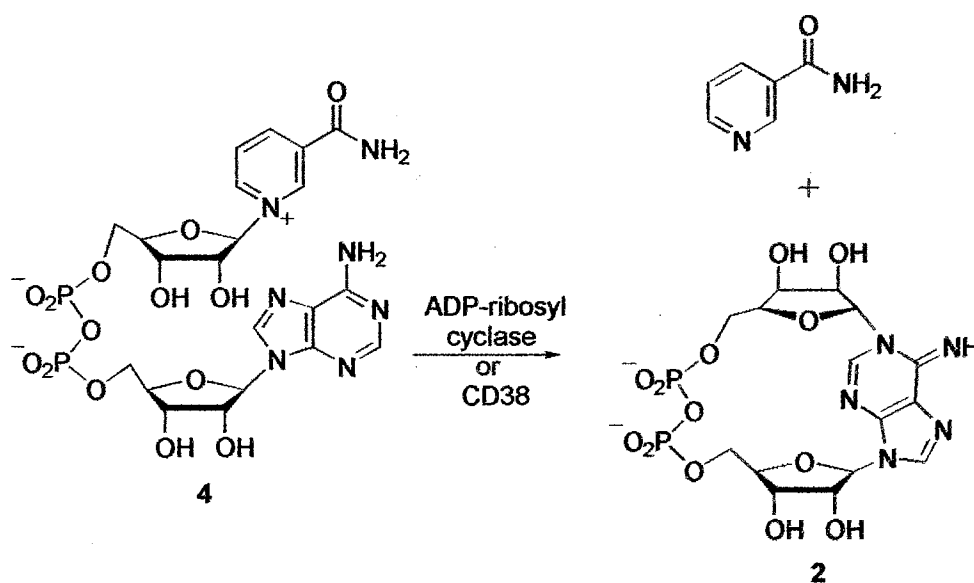
Figure 6. Biological synthesis of cADPR.

2'- and 3'- hydroxyls
necessary for biological
activity
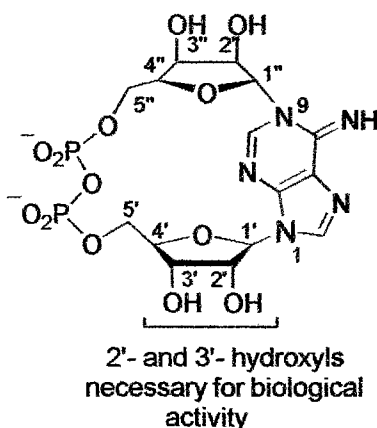
Figure 7. cADPR structural details.

extended conformation, ADP ribosyl cyclase is postulated to bind NAD^+ in a folded

conformation, in order to facilitate the necessary cyclization.

Another route for cADPR synthesis involves the human lymphocyte antigen

CD38 in both the synthesis and hydrolysis of cADPR.[36] The bifunctional CD38 has been

isolated from various types of cells[37,38] and appears to share a high degree of amino acid

sequence identity with ADP-ribosyl cyclase.[39] Additionally, several CD38 site mutations

analyses have been performed, and the hydrolase and cyclase activities were altered

accordingly.[39]

Structurally, cADPR consists of a cyclic ADP-ribose unit containing an *N*-

glycosyl linkage, joining C1'' of one ribose fragment with N1 of the adenine ring.[40,41]

The cyclic nature is completed by a bond between the adenine N9 and C1' of the

remaining furanose ring.[42] According to the determined torsional angles, the adenine is

syn with respect to the C1'-N1 bond, while it is *anti* with respect to the C1''-N9

linkage.[43]

Current evidence supports the necessity of the furanosyl hydroxyl groups for

cADPR's observed biological activity (Figure 7).[44] Analogues containing 2'- or 3'-

deoxyribose have substantially decreased Ca^{2+}-releasing abilities (100 times lower),

relative to that observed with cADPR. Additional studies have determined that the

3'hydroxyl group is especially instrumental in cADPR-induced calcium release.

Throughout the past few years, many cADPR analogues have been synthesized

and evaluated with respect to their Ca^{2+}-releasing activity (Figure 8). A 1997 study

introduced the triphosphate analog, cyclic adenosine triphosphate ribose (cATPR, 5), as

a more potent RyR agonist.[45] In contrast, calcium mobilization was significantly
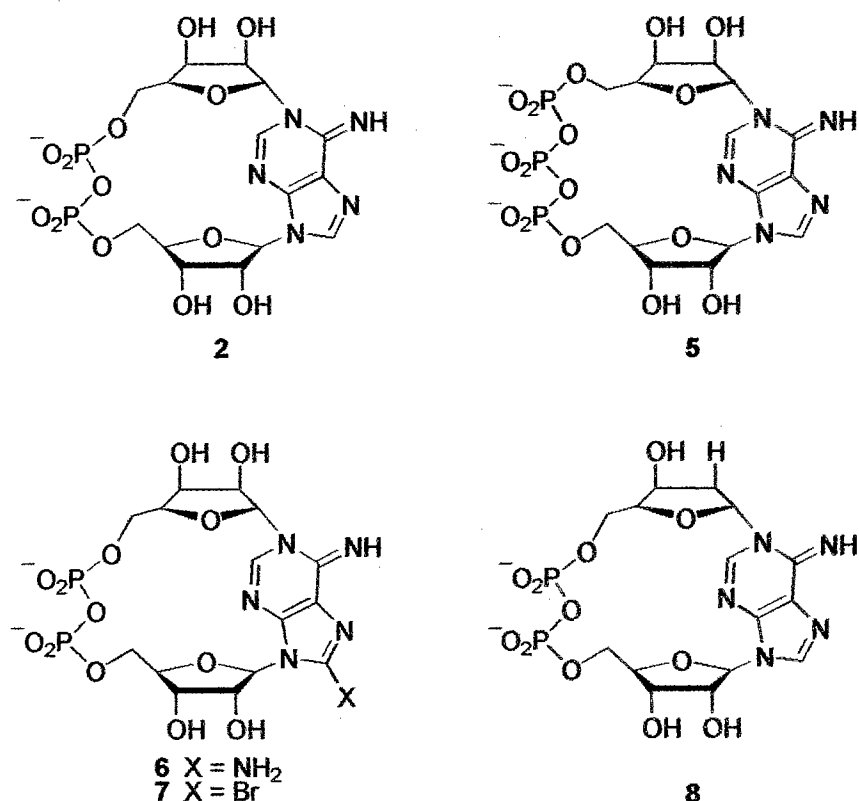
Figure 8. cADPR and some synthesized analogues.

decreased when the 8-position of the adenine ring was substituted with an amino (6) or bromo (7) group.[46] In the latter cases, the analogues were able to bind to RyR, but were ineffective as calcium release agents. Additional modification of the 7-position produced further inhibition of calcium release.

Although many of the details for cADPR's role in intracellular signal transduction remain elusive, a general model has been proposed for its mechanism (Figure 9).[1] In the cascade, the extracellular ligand binds and activates a membrane-bound receptor which, in turn, initiates a series of signals. Potentially, one or more of the resulting signals triggers cADPR synthesis by ADP-ribosyl cyclase. Once synthesized, cADPR acts in some way on RyR, perhaps in concert with a calmodulin/Ca^{2+} complex, resulting in the final intracellular calcium release. A second potential role for cADPR in the cascade is as a RyR activator, thereby directly sensitizing RyR to cytosolic calcium levels. Once sensitized, RyR is then free to respond to the intracellular $[Ca^{2+}]$, resulting in CICR and cellular protein activation.

The current studies offer preliminary avenues into the further study of cADPR-
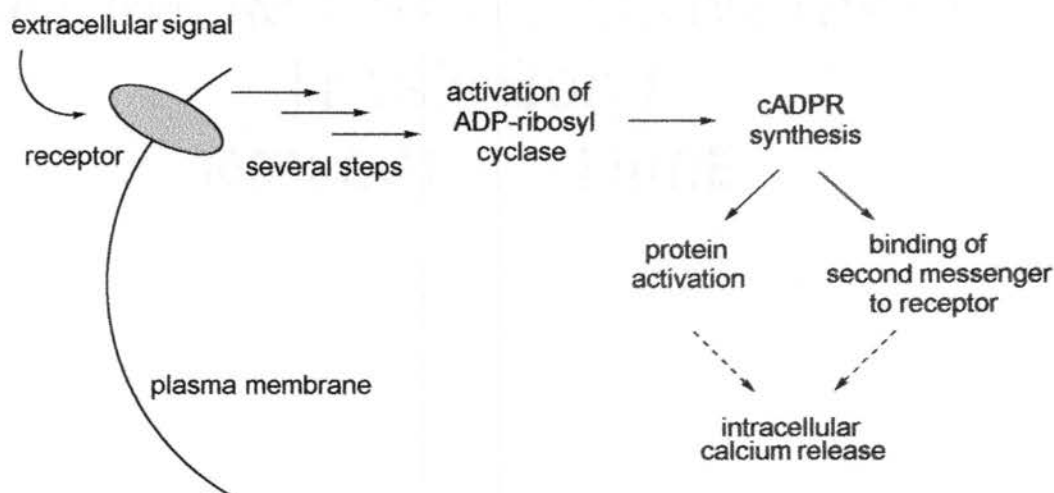
Figure 9. Proposed calcium release by cADPR.

induced calcium release. The development of a total chemical synthesis, along with solution structure elucidation, provides more detail to the current knowledge surrounding the cADPR cascade. The potential applications are far-reaching, and might include cADPR photoaffinity labels, cADPR analog studies, and determination of the binding site and/or conformation of cADPR.

Future research foci

With the recent discovery of another calcium-releasing agent, nicotinic acid adenine dinucleotide phosphate (3, NAADP, Figure 1),[6] regulation of intracellular $[Ca^{2+}]$ occupies a promising place in the identification and treatment of certain cellular disease states. Due to the structural similarities among IP_3, cADPR, and NAADP, it is possible that an entire family of calcium-releasing, low molecular weight phosphates exists. As research progresses, further elucidation of the mechanisms and implicated pathways of calcium regulation will continue to enhance the understanding of this significant biological process.

References

1. Dousa, T. P.; Chini, E. N.; Beers, K. W. *Am. J. Phys.*, **1996**, *271*, C1007-C1024.

2. De Camilli, P.; Emr, S. D.; McPherson, P. S.; Novick, P. *Science*, **1996**, *271*, 1533-1539.

3. Takasawa, S.; Nata, K.; Yonekura, H.; Okamoto, H. *Science*, **1993**, *259*, 370-372.

4. Berridge, M. J. *Nature*, **1993**, *361*, 315-325.

5. Aarhus, R.; Graeff, R.; Dickey, D. M.; Walseth, T.; Lee, H. C. *J. Biol. Chem*, **1995**, *270*, 3037-3033.

6. Lee, H. C.; Aarhus, R. *J. Biol. Chem*, **1995**, *270*, 2152-2157.

7. Berridge, M. J. *Nature*, **1993**, *361*, 142-152.

8. Putney, J. W. *Science*, **1993**, *262*, 676-678.

9. Streb, H.; Irvine, R. F.; Berridge, M. J. *Nature*, **1983**, *306*, 67-69.

10. Clapper, D. L.; Lee, H. C. *J. Biol. Chem*, **1995**, *260*, 13947-13954.

11. Dargie, P. J.; Agre, M. C.; Lee, H. C. *Cell Regul.*, **1990**, *1*, 279-290.

12. Cooke, A. M.; Potter, B. V. L. *Tetrahedron Lett.*, **1987**, *28*, 2305-2308.

13. Reese, C. B.; Ward, J. G. *Tetrahedron Lett.*, **1987**, *28*, 2309-2312.

14. Poirot, E.; Bourdon, H.; Chretien, F.; Chapleur, Y.; Berthon, B.; Hilly, M.; Mauger, J.-P.; Guillon, G. *Bioorg. Med. Chem. Lett.*, **1995**, *5*, 569-572.

15. Liu, C.; Potter, B. V. L. *J. Org. Chem.*, **1997**, *62*, 8335-8340.

16. Jenkins, D. J.; Riley, A. M.; Potter, B. V. L. *J. Org. Chem.*, **1996**, *61*, 7719-7726.

17. Lee, H. C.; Aarhus, R.; Walseth, T. F. *Science*, **1993**, *261*, 352-355.

18. Galione, A.; McDougall, A.; Busa, W. B.; Willmont, N.; Gillot, I.; Whitaker, M. *Science*, **1993**, *261*, 348-351.

19. Thorn, P.; Gerasimenko, O.; Petersen, O. H. *EMBO J.*, **1994**, *13*, 2038-2043.

20. Meszaros, L. G.; Bak, J.; Chu, A. *Nature*, **1993**, *364*, 76-79.

21. Sorrentino, V.; Volpe, P. *TiPS*, **1993**, *14*, 98-102.

22. Giannini, G.; Conti, A.; Mammarella, S.; Scrobogna, M.; Sorrentino, V. *J. Cell Biol.*, **1995**, *128*, 893-904.

23. Clapper, D. L.; Walseth, T. F.; Dargie, P. J.; Lee, H. C. *J. Biol. Chem*, **1987**, *262*, 9561-9568.

24. Galione, A. *TiPS*, **1992**, *13*, 304-306.

25. White, A. M.; Watson, S. P.; Galione, A. *FEBS Lett.*, **1993**, *318*, 259-263.

26. Jacobson, M. K.; Ame, J.-C.; Lin, W.; Coyle, D. L.; Jacobson, E. L. *Receptor*, **1995**, *5*, 43-49.

27. Lee, H. C.; Aarhus, R.; Graeff, R.; Gurnack, M. E.; Walseth, T. F. *Nature*, **1994**, *370*, 307-309.

28. Sih, C. J.; Gu, Q. M.; Yamada, S.; Zhang, F.-J. *Youji Huaxue*, **1997**, *17*, 43-46.

29. Lee, H. C.; Aarhus, R.; Graeff, R. M. *J. Biol. Chem*, **1995**, *270*, 9060-9066.

30. Lee, H. C. *J. Biol. Chem*, **1993**, *268*, 293-299.

31. Lee, H. C.; Aarhus, R. *Cell Regul.*, **1991**, *2*, 203-209.

32. Chini, E. N.; Klener, P.; Beers, K. W.; Chini, C. C. S.; Grande, J. P.; Dousa, T. P. *Kidney Int.*, **1997**, *51*, 1500-1506.

33. Rusinko, N.; Lee, H. C. *J. Biol. Chem*, **1989**, *264*, 11725-11731.

34. Prasad, G. S.; Levitt, D. G.; Lee, H. C.; Stout, C. D. *Prot. Struc. Func. Gen.*, **1996**, *24*, 138-140.

35. Galione, A.; White, A.; Willmont, N.; Turner, M.; Potter, B. V. L.; Watson, S. P. *Nature*, **1993**, *365*, 456-459.

36. Funaro, A.; Horenstein, A. L.; Calosso, L.; Morra, M.; Tarocco, R. P.; Franco, L.; De Flora, A.; Malavasi, F. *Int. Immun.*, **1996**, *8*, 1643-1650.

37. Fryxell, K. B.; O'Donoghue, K.; Graeff, R. M.; Lee, H. C.; Branton, W. D. *Prot. Exp. Purif.*, **1995**, *6*, 329-336.

38. Mizuguchi, M.; Otsuka, N.; Sato, M.; Ishii, Y.; Kon, S.; Yamada, M.; Nishina, H.; Katada, T.; Ikeda, K. *Brain Res.*, **1995**, *697*, 235-240.

39. Tohgo, A.; Takasawa, S.; Noguchi, N.; Koguma, T.; Nata, K.; Sugimoto, T.; Furuya, Y.; Yonekura, H.; Okamoto, H. *J. Biol. Chem*, **1994**, *269*, 28555-28557.

40. Lee, H. C.; Walseth, T. F.; Bratt, G. T.; Hayes, R. N.; Clapper, D. L. *J. Biol. Chem*, **1989**, *264*, 1608-1615.

41. Gu, Q. M.; Sih, C. J. *J. Am. Chem. Soc.*, **1994**, *116*, 7481-7486.

42. Kim, H.; Jacobson, E. L.; Jacobson, M. K. *Biochem. Biophys. Res. Comm.*, **1993**, *194*, 1143-1147.

43. Lee, H. C.; Aarhus, R.; Levitt, D. *Struc. Biol.*, **1994**, *1*, 143-144.

44. Ashamu, G. A.; Sethi, J. K.; Galione, A.; Potter, B. V. L. *Biochemistry*, **1997**, *36*, 9509-9517.

45. Zhang, F. J.; Yamada, S.; Gu, Q. M.; Sih, C. J. *Bioorg. Med. Chem. Lett.*, **1996**, *6*, 1203-1208.

46. Bailey, V. C.; Sethi, J. K.; Potter, B. V. L. *Chem. Comm.*, **1997**, 695-696.

CHAPTER II

STUDIES TOWARD THE TOTAL CHEMICAL

SYNTHESIS OF CADPR

Synthesis of a Postulated cADPR Precursor

Introduction

The 1987 discovery of cADPR[1] fueled various research efforts into the relatively new field of second messengers and their resulting biological effects. While many of the initial investigations[1-3] concerned the actual discovery and isolation of cADPR itself, additional studies[2,4] were directed toward further characterization of the molecule. Logical extensions included cADPR structural elucidation and characterization, as well as synthetic studies. The resulting knowledge continues to offer insight into the mechanism of the cADPR cascade.

A key requirement for the study of the cADPR pathway (or for that of any biological molecule) is a method for the production of the actual agent. Ideally, this protocol would be relatively easy and would provide substantial quantities of the desired molecule for further study. A successful procedure should also be economical.

Many potential areas for future cADPR research depend on the development of a successful synthetic route (Figure 10). Techniques such as affinity chromatography resins, photoaffinity labels,[5] and the synthesis of cADPR analogues[6-8] rely heavily on the ability to initially produce authentic cADPR. Once available, the route can then be adjusted and modified for experiments leading to further pathway elucidation.
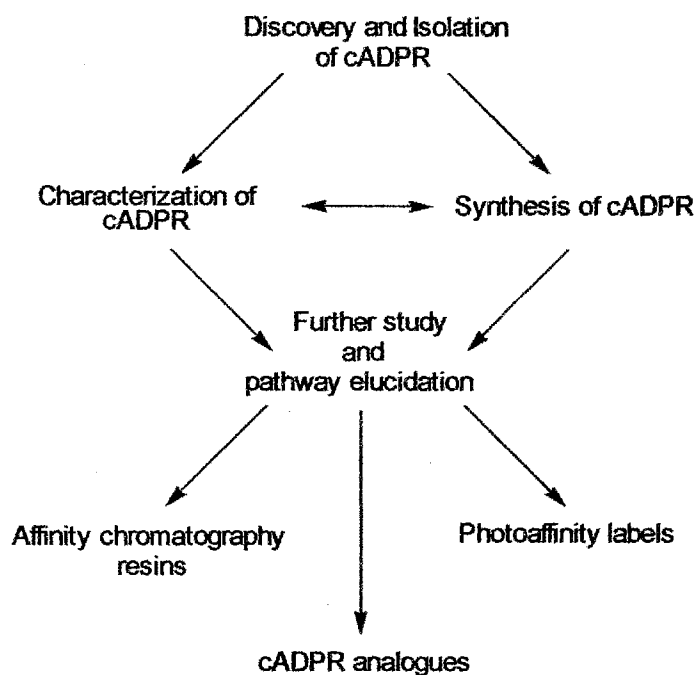
Figure 10. Flow chart for cADPR pathway elucidation.

Current cADPR syntheses

Currently, two methods exist for the synthesis of cADPR.[1,9] The first[1] incorporates an enzymatic cyclization of the commercially available NAD$^+$ (4, cADPR's biological precursor) to form the new N-glycosidic bond (Figure 11). One main advantage of the route results from the relative lack of specificity of the active enzyme, ADP-ribosyl cyclase. Due to its ubiquity,[1,10,11] the cyclase has been used in syntheses of authentic cADPR, as well as for some cADPR analogues.

However, some disadvantages do exist for the enzymatic synthesis of cADPR. One major synthetic challenge results from the use of the cyclase, as enzymatic protocols must be utilized. Additional drawbacks may be present in the inherent specificity of the cyclase; while relatively non-discriminatory among enzymes,[1] ADP-ribosyl cyclase does possess a certain specificity, which may or may not prove to be a factor in future syntheses of cADPR analogues.
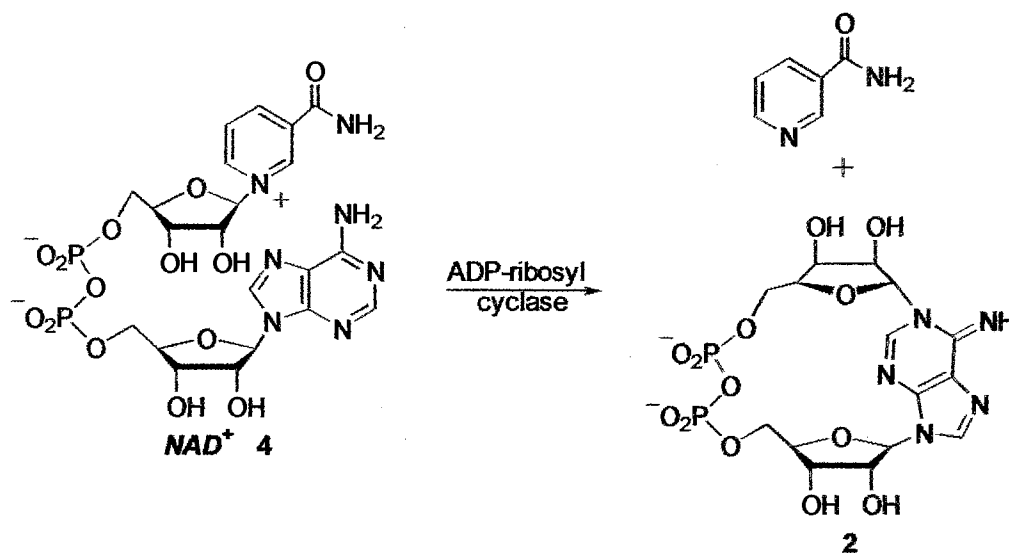
Figure 11. Enzymatic synthesis of cADPR.

Perhaps most prominently, the overall reaction yield for the enzymatic cyclization is also very low (~5-10%).[9] While the yield is quite respectable for an enzymatic protocol, it remains very limiting for cADPR study. This is apparent in the exorbitant current selling price of cADPR from various chemical manufacturers ($166 per mg).[12]

The enzymatic cyclization of NAD^+ (4) has been closely replicated in a biomimetic chemical synthesis of cADPR (Figure 12).[9] The route includes the same
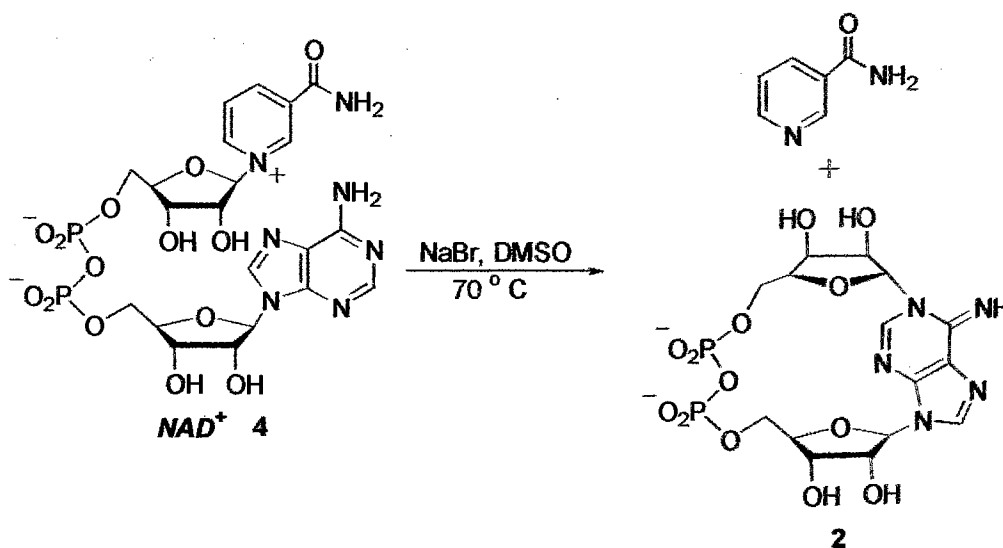
Figure 12. Chemical synthesis of cADPR.
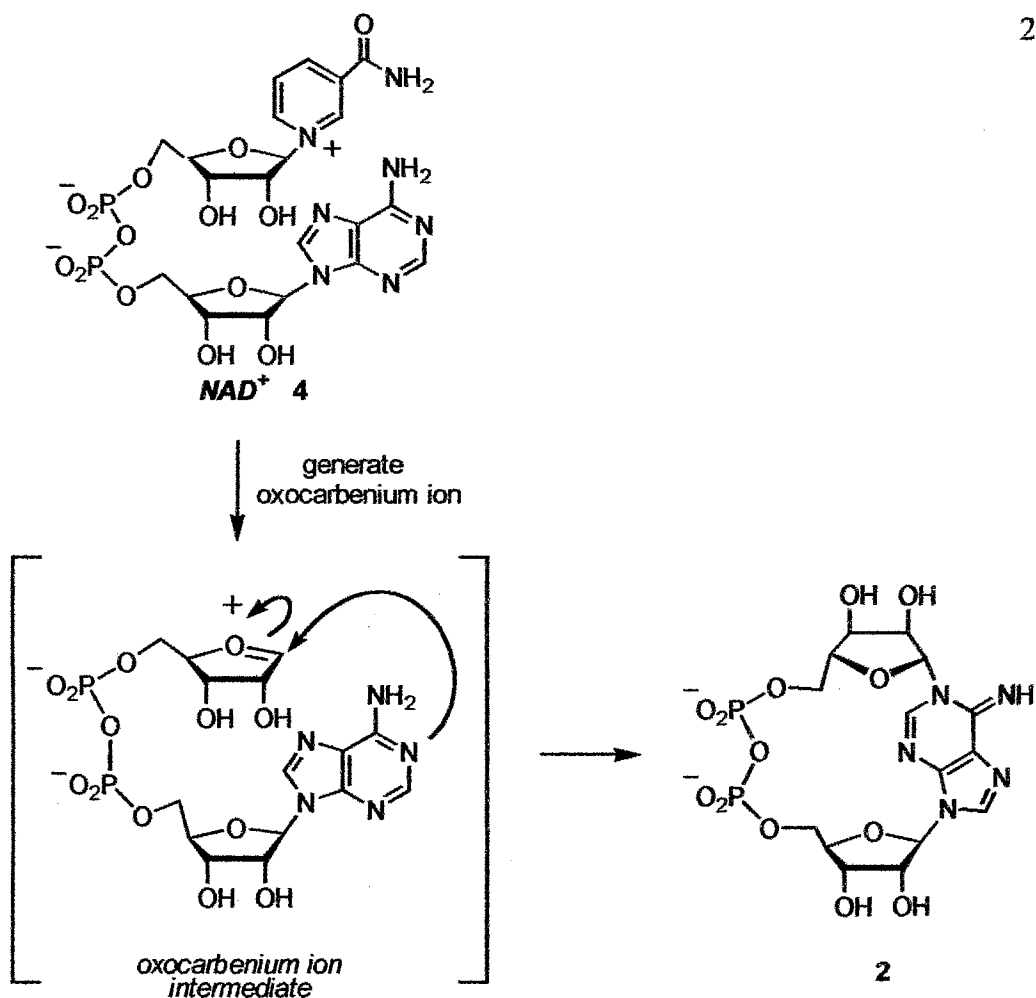
Figure 13. Proposed oxocarbenium ion intermediate.

starting material (NAD⁺) as the enzymatic approach and utilizes sodium bromide at an elevated temperature to affect the intramolecular cyclization.

Both synthetic routes are postulated to proceed through identical oxocarbenium ion intermediates (Figure 13).[13,14] Once the intermediate has been formed (either chemically or enzymatically), the lone electron pair on the adenine nitrogen-1 attacks the sp^2-hybridized oxocarbenium carbon. Interestingly, the resulting cyclization produces some loss of aromaticity in the adenine ring. This is further apparent in the high temperature necessary for the non-enzymatic cADPR synthesis.
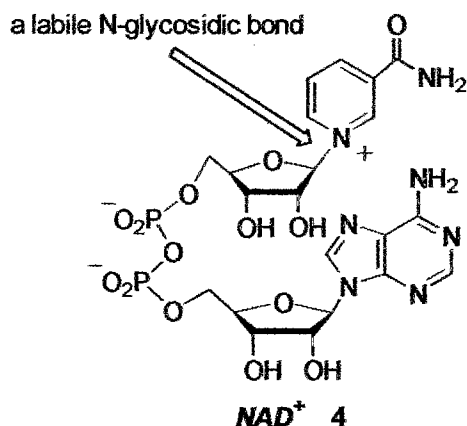
Figure 14. The relatively labile N-glycosidic bond in nicotinamide dinucleotide.

While both cADPR syntheses are successful in modest yields, they also possess

some common disadvantages. A major shortcoming is present in the starting material

NAD$^+$, used in both routes. Due to the presence of the nicotinamide moiety at the

anomeric position of the corresponding sugar ring, the resulting linkage is relatively

susceptible to nucleophilic attack (Figure 14). As a result, NAD$^+$ would pose some

potential problems as a starting material for various cADPR analogues. Additionally,

while the degree of similarity between NAD$^+$ and the cyclized cADPR is helpful in the

enzymatic and chemical routes, it may provide a large challenge when trying to

manipulate some of the finer details of cADPR.

Rationale for total chemical synthesis of cADPR (2)

The rationale behind the current study is outlined in Figure 15. Due to the

shortcomings of the reported cADPR syntheses, the current study proposes a *total*

chemical synthesis of cADPR. The developed protocol avoids many of the challenges of

the enzymatic and chemical routes from NAD$^+$, while providing an efficient and cost-
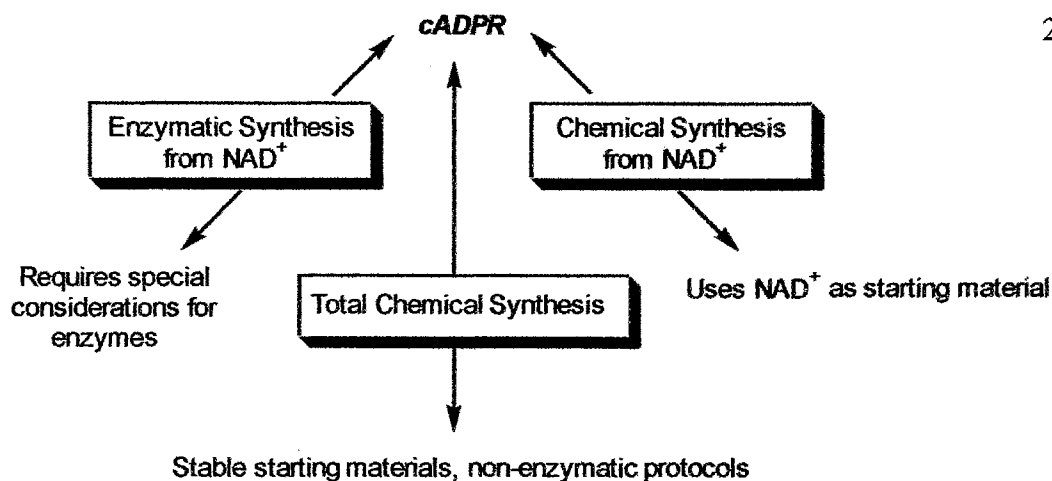
Figure 15. Rationale behind the total chemical synthesis of cADPR.

effective procedure for cADPR, based on established synthetic methodology and readily available starting materials.

Synthetic strategy

The proposed synthetic sequence is based primarily on the synthesis of a key cADPR precursor 9 (Figure 16). This molecule incorporates an alkenyl (n-pentenyl) side chain in place of the nicotinamide moiety of NAD^+. Due to the relative stability of the
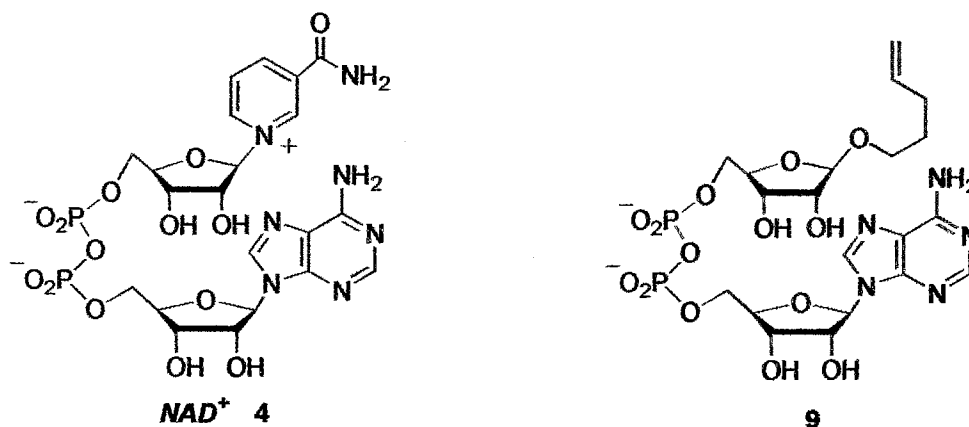
Figure 16. Starting material for the total chemical synthesis of cADPR, relative to nicotinamide dinucleotide (4).
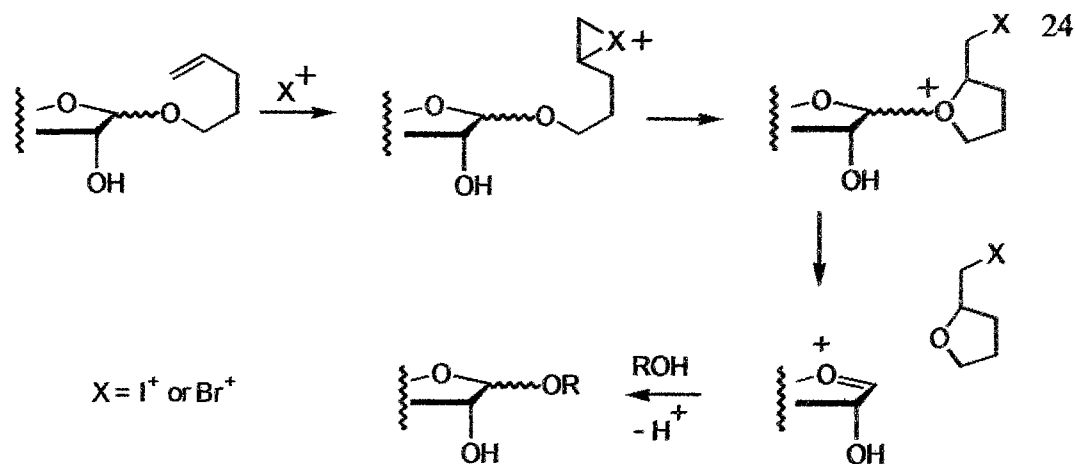
Figure 17. The *n*-pentenyl group used in the construction of *O*-glycosidic bonds.

O-glycosidic linkage, the substitution produces a more stable cADPR precursor, relative

to NAD^+. Additionally, the replacement creates a precursor that is capable of generating

the desired oxocarbenium ion intermediate (above, Figure 17).

The *n*-pentenyl group was recently reported[15] to produce an effective leaving

group in oligosaccharide synthesis. Upon treatment with a halonium ion (usually I^+ or

Br^+), the pentenyl double bond reacts, and the resulting cyclic halonium rearranges into a

substituted tetrahydrofuran (Figure 17). Donation of an oxygen lone pair then stabilizes

the produced positive charge (producing the oxocarbenium ion intermediate), and the sp^2-

hybridized anomeric carbon is then susceptible to further nucleophilic attack. Treatment

of the intermediate with the desired coupling component affords the final *O*-linkage.

A similar observation was made in the construction of *N*-glycosidic bonds (Figure

18) using the same *n*-pentenyl group.[16] In this case, mechanistic details remain

analogous to those of Fraser-Reid.[15] The slight variation is present in the identity of the

attacking nucleophile **10** (nitrogen instead of oxygen). Accordingly, the successful

inclusion of the *n*-pentenyl side chain in the construction of such *N*-glycosidic bonds (as

in **12**) became a fundamental aspect of the proposed synthesis.
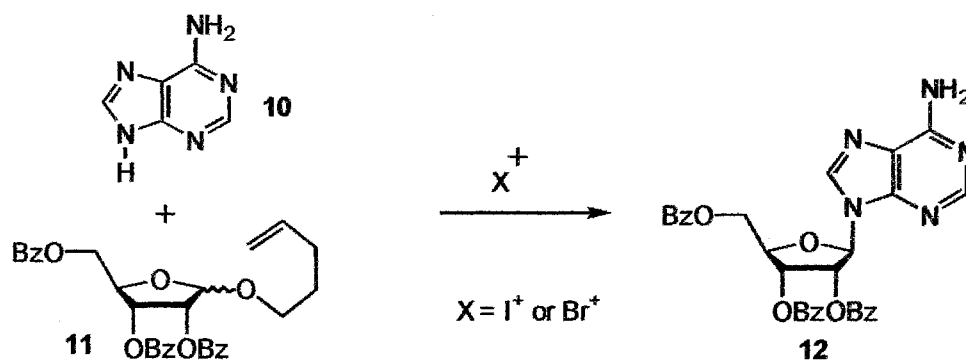
Figure 18. The n-pentenyl group used in the construction of N-glycosidic bonds.

A retrosynthetic approach to the current study includes a two-step process (Figure 19). The first step involves the synthesis of a 5'-monophosphate (13) suitable for a subsequent coupling with adenosine monophosphate (AMP, 14). The second phase incorporates this coupling in the formation of the pyrophosphate bond in the acyclic precursor (9), which is followed by a final cyclization to yield the product cADPR (2).

A major advantage of the n-pentenyl side chain is its requisite stability towards a variety of synthetic manipulations. While some consideration must be given to the reactivity and reticent basicity of the double bond, the moiety remains generally hearty, and thus, may be incorporated into the early stages of the synthesis. Accordingly, the pentenyl group can also confer some of its own organic properties to some of the more polar molecules (in particular, phosphates) produced later on in the synthesis.

Another advantage to the proposed route involves the use of AMP as the other coupling fragment in the construction of the pyrophosphate bond. The commercial availability and low cost of AMP, as well as its ultraviolet absorption properties, make it a useful component of the acyclic precursor 9.
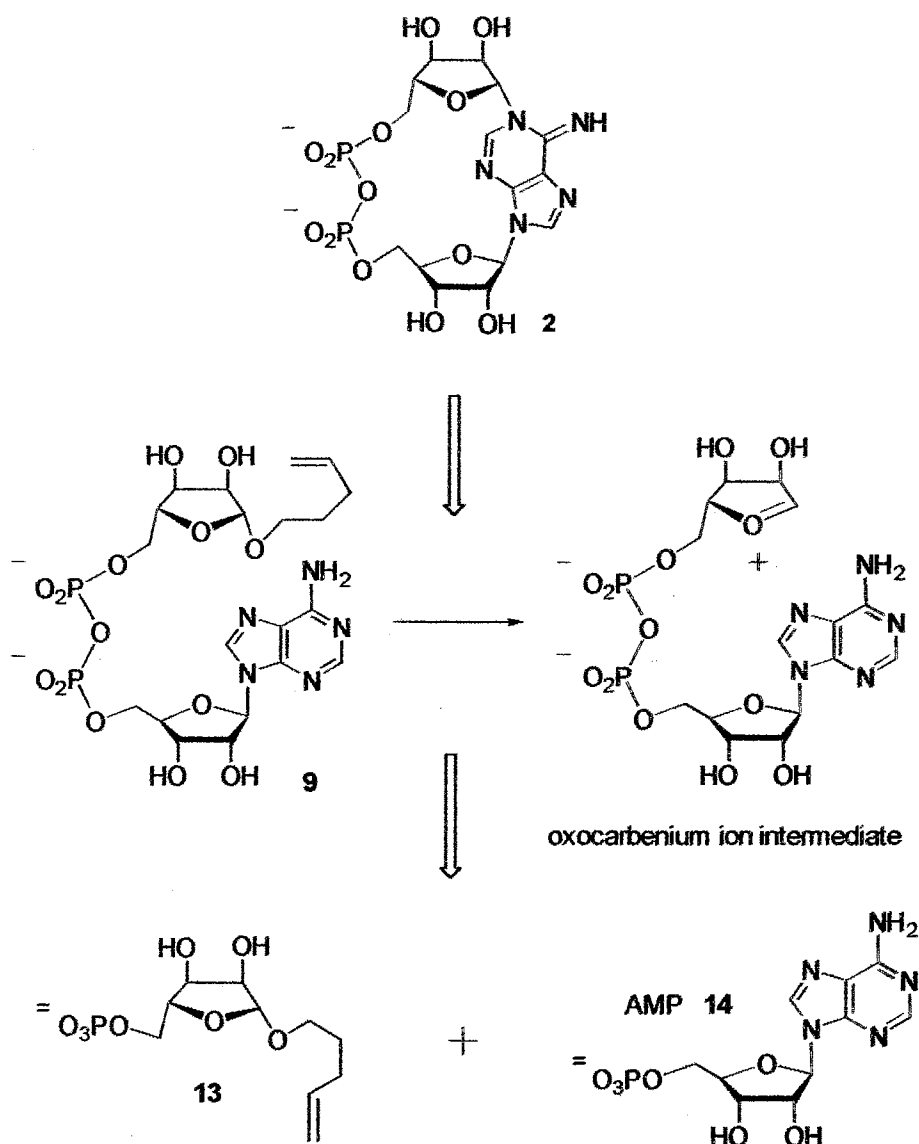
Figure 19. A retrosynthesis of cADPR.

Synthetic Phases

The pentenyl 5'-monophosphate (13) is not commercially available and has to be independently synthesized. Due to the presence of the phosphate moiety exclusively at the 5'-position, the resulting synthetic strategy encompassed several selectivity issues.
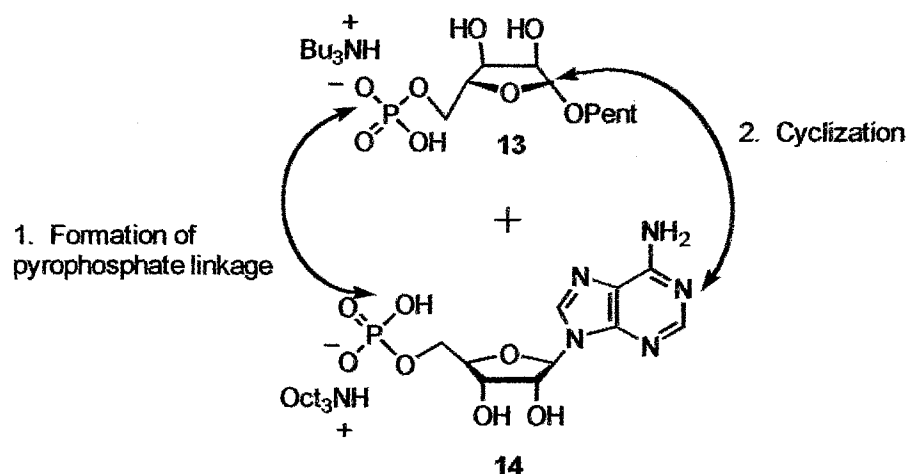
Figure 20. The final steps in the synthesis of cADPR.

Additionally, the charged nature of **13** presented considerable challenges in synthesis, characterization, and final purification.

The second phase of the synthesis involves the formation of the pyrophosphate bond and the final cyclization to yield cADPR (Figure 20). While the incorporation of AMP introduces a chromophore into these final cADPR precursors (simplifying detection), additional challenges are present in the isolation and purification procedures (see below). The final cADPR product can then be characterized relative to its known properties.

Results and Discussion

The initial step in the synthesis of the pentenyl phosphate **13** involved the substitution of the *n*-pentenyl side chain at the anomeric position of D-ribose (**15**, Figure 21). In accordance with the published procedure,[16] the reaction was very successful and alpha (α, **16**) and beta (β, **17**) products were observed in a high yield (>80%).
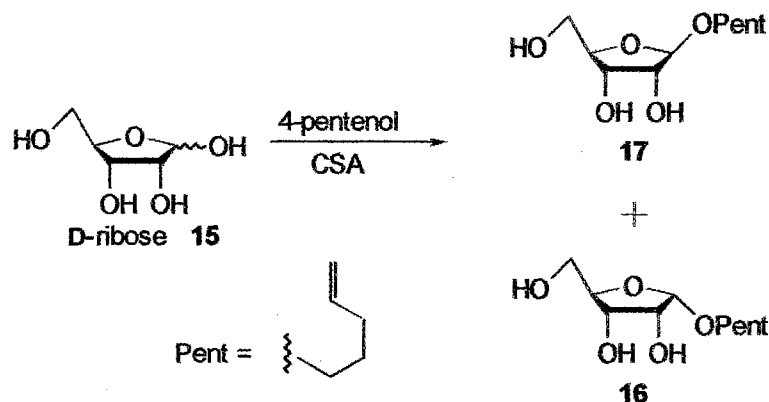
Figure 21. Formation of the pentenyl riboside.

Although either anomer would potentially be a successful candidate for the final cyclization of the acyclic precursor (the oxocarbenium ion intermediate has an sp^2-hybridized anomeric carbon), the β-pentenyl riboside (17) was chosen for further synthetic study. This was largely due to its increased production in the glycosylation reaction, as well as its observed thermodynamic properties. It was noted that the *beta* anomer (17) possessed a higher melting point than the *alpha* anomer (16). In most experimental scenarios, the *alpha* pentenyl riboside remained a clear oil; in identical situations, the *beta* anomer became a solid. Interestingly, this was only true for pure (chromatographed) *beta* product.

Key spectroscopic elements also became apparent in this first synthetic step. For example, it was noted that the two anomers included one basic difference in the corresponding proton spectra (Figure 22). Specifically, the two anomers could be spectroscopically differentiated by the position of the intense H1' signal relative to the nearby H5 signals (each is a doublet of quartets). If the sample consisted of the *alpha* anomer, the H1' resonance was located downfield (δ 4.992) from H5; if the sample contained the *beta* anomer, H1' is located upfield (δ 4.914) from H5.
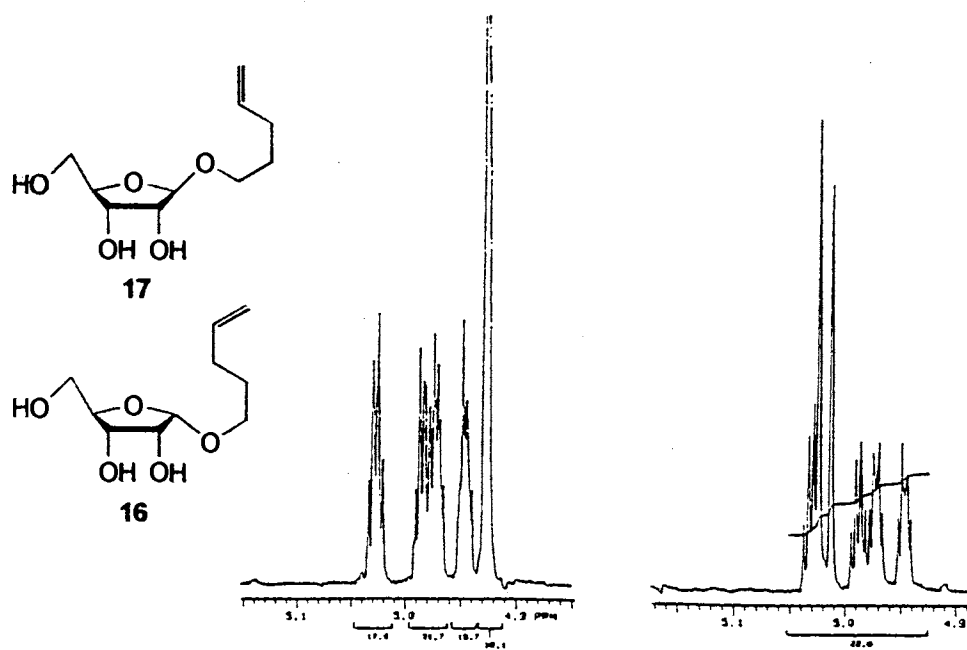
Figure 22. Spectral variations between **16** and **17**.
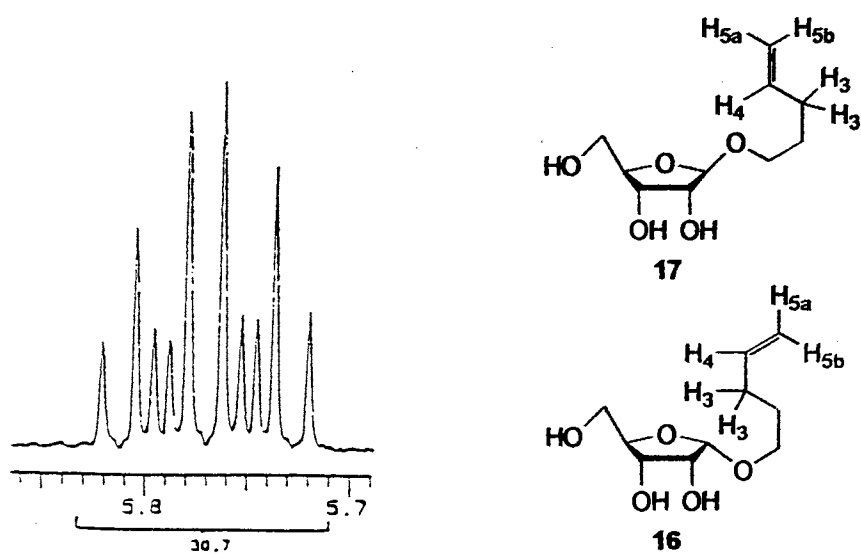
Figure 23. Characteristic signal for the pentenyl H4 in **16** and **17**.

Another significant feature of the pentenyl riboside (either anomer) is the

characteristic pattern of the pentenyl H4 signal (Figure 23). Due to the *cis* and *trans*

alkene splitting and the additional coupling of H3, H4 is observed to be a noticeable ten-

peak pattern (ddt). Considering that the pentenyl group is present throughout most of the

overall synthesis, this pattern quickly evolved into a prime indication of the continuing

presence (and stability) of the *n*-pentenyl side chain.

Once the pentenyl riboside **17** had been synthesized and purified, the next steps

were designed to include some type of protection strategy for the three reactive

hydroxyls. Given that the final pentenyl phosphate fragment **13** is a 5'-monophosphate, a

method for the selective incorporation of the phosphate at only the 5'-position had to be

developed.

Characteristically, carbohydrate-based protection strategies[17] include an initial

substitution of a sterically-hindered (and relatively labile) group at the 1'-position (Figure

24). This is followed by protection of the secondary hydroxyls with a less labile moiety,
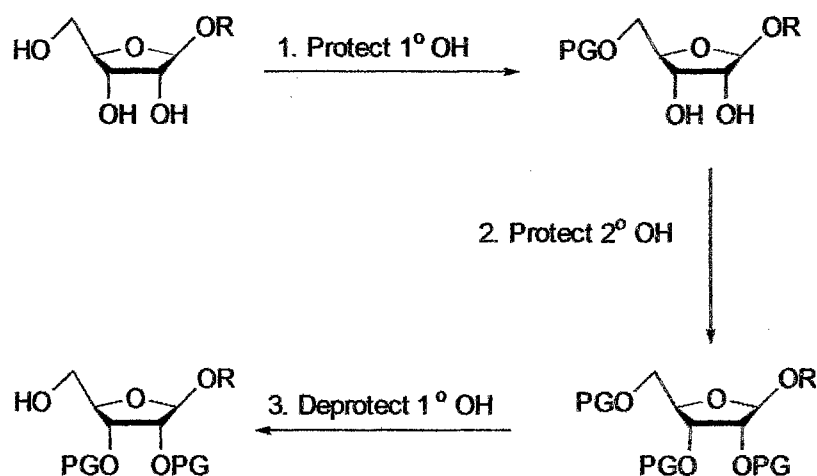
Figure 24. A general protection/deprotection strategy
for carbohydrates.

to yield a fully protected molecule. Selective removal of the protecting group on the primary hydroxyl then produces a compound ready for nucleophilic attack at the center of a phosphorylating (or phosphitylating) reagent. Obviously, in this protocol, care must be taken to ensure that removal and addition of protecting groups does not interfere with any functionalities already present on the reacting molecule.

This approach was utilized in initial attempts (Figures 25-27) for the synthesis of
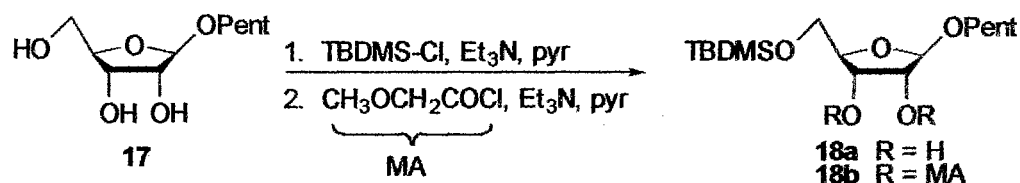
Figure 25. Synthesis of **18** via a protection strategy.
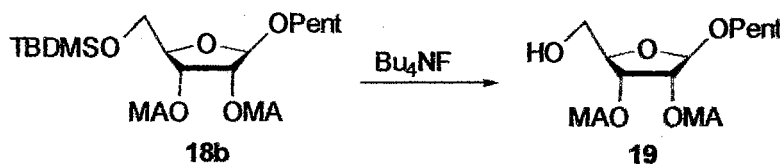
Figure 26. Attempted deprotection of **18b** .

			96:4 CHCl$_3$:MeOH
O	o		R$_f$ = 0.49
	o		R$_f$ = 0.34
	o		R$_f$ = 0.26
	o		R$_f$ = 0.14
		o	R$_f$ = 0.03
18b	Rxn	TBAF	
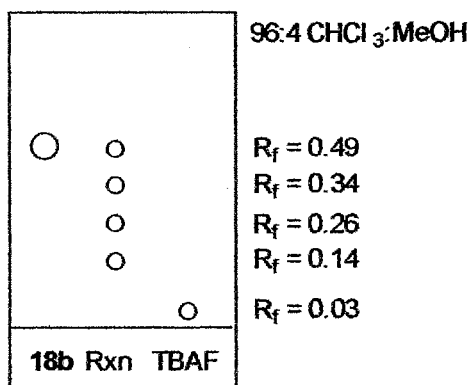
Figure 27. TLC analysis of the attempted desilylation of **18b.**

the monophosphate **13**. Early trials included protection of the primary hydroxyl of **17**

with the sterically demanding *tert*-butyldimethylsilyl (TBDMS) group.[18-20] Secondary

hydroxyls were then protected successfully[21] as their corresponding methoxyacetyl (MA)

esters to yield **18b** (Figure 25). However, problems were encountered with the attempted

deprotection.[18] of **18b** with tetrabutylammonium fluoride (TBAF) in the synthesis of **19**

(Figure 26). TLC analysis (Figure 27) indicated that many side products were present,

and the strategy was abandoned, due to this complexity.

The second strategy (Figure 28) incorporated the labile 4,4'-dimethoxytrityl

(DMT) group at the primary position.[22] Similar to the previous protocol, secondary
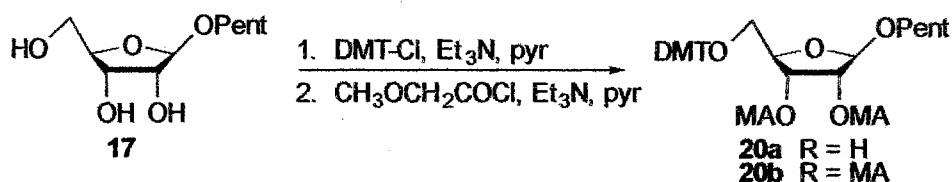
Figure 28. Synthesis of **20** via a protection strategy.

hydroxyls were then protected as their methoxyacetyl esters[21] to yield **20b**. Acid-

catalyzed cleavage (Figure 29) of the dimethoxytrityl ether linkage[23,24] in **20b** (by
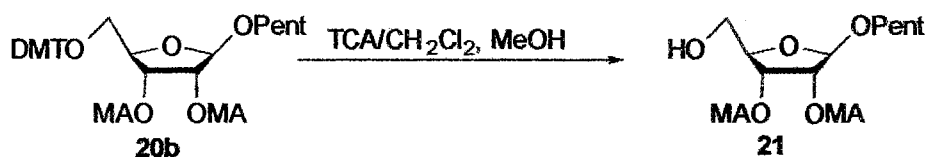
Figure 29. Deprotection of the protected pentenyl riboside **20b**.

trichloroacetic acid, TCA) subsequently produced the 5'-deprotected product **21**.

Once the 5'-hydroxyl was available for nucleophilic attack, attention shifted to

possible routes for the necessary incorporation of a phosphate group. Fortunately,
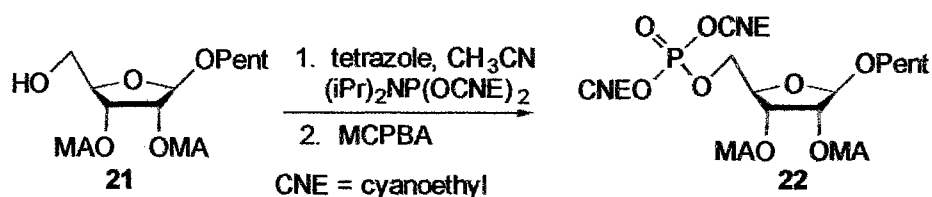
Figure 30. Synthesis of the fully protected phosphate 22.

favorable results were obtained (Figure 30) using a phosphitylation/oxidation

procedure,[25] which produced the fully protected phosphate **22**.

Once a successful protection strategy had been developed, further experiments

were conducted to elucidate the potential of the same phosphitylation procedure on the

unprotected β–pentenyl riboside **17** (Figure 31). These results (discussed in Chapter 3)

provided a shorter and more efficient synthesis of a similarly protected phosphate (**23**).

The attachment of the 5'-phosphate provided a further advantage for

spectroscopic characterization of the subsequent molecules. Due to the possible spin

states of ^{31}P ($I = \pm 1/2$), ^{31}P-NMR experiments easily verified product identity and purity.

Purity was tested by the presence or absence of a phosphorus singlet (in proton-

decoupled spectra), and identity could be elucidated from ^{1}H-coupled ^{31}P-NMR spectra,

if necessary. Interestingly, chemical shifts of the synthesized phosphates in this study

were relatively inconsistent. Accordingly, careful interpretation of the corresponding ^{1}H

and ^{13}C-NMR spectra was crucial for final product identification.
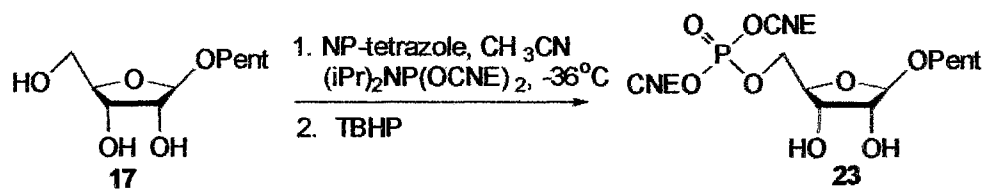
Figure 31. Synthesis of 23 via a selective phosphitylation.

The synthesis of the fully protected phosphate completed the final organic-phase step in the total synthesis. Upon deprotection, the phosphate yields a charged molecule, which then directs the remaining synthetic steps into aqueous-based chemistry.

The planned deprotection of **23** proceeded smoothly[25] to produce a respectable crude yield for the reaction. However, purification and further manipulation of the product created numerous technical difficulties (Figure 32). Fortunately, the insights
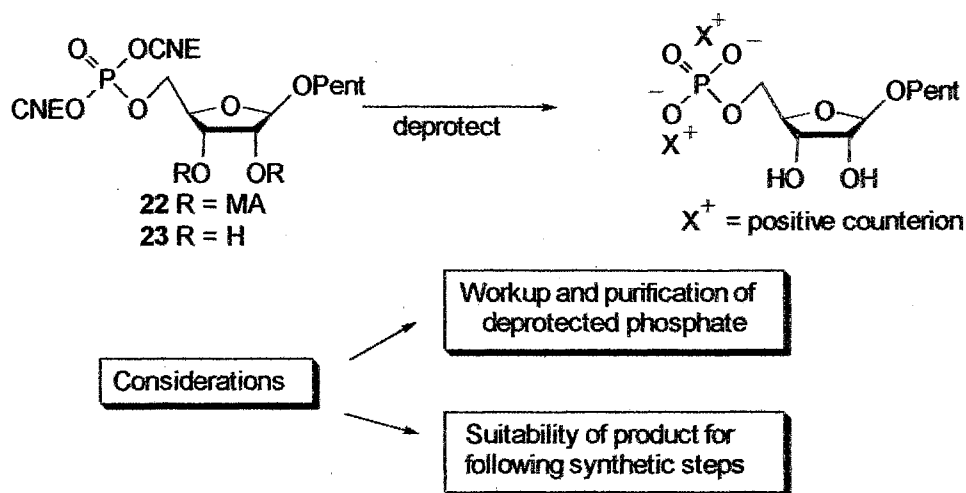
Figure 32. General deprotection scheme for the protected phosphates.

gained in preliminary studies of the deprotected phosphate served as precedents for the following synthetic steps (formation of the acyclic precursor **9** and cyclization to yield cADPR).

The general scheme for the deprotected phosphate (Figure 33) includes an initial
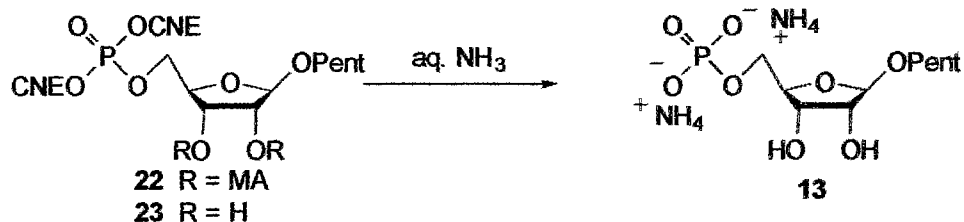
Figure 33. Actual deprotection scheme for the protected phosphates.

purification step, which separates the desired product 13 from any other side products or partially-deprotected molecules. Following this step, however, another step is necessary for conversion of the purified phosphate into a form suitable (see below) for its coupling with AMP. This conversion actually encompasses several steps, as it involves counterion exchange (shown schematically in Figure 34).

Initially, the crude deprotected phosphate is present as its bisammonium salt (13), following removal of the cyanoethyl (CNE) and methoxyacetyl groups by ammonium hydroxide. The resulting water solubility necessitates an aqueous-based purification step. A careful examination of the literature indicated that anion exchange might be a viable option, as it has been used extensively in the large-scale purification of various phosphates.[26-29] A salt gradient was then chosen for the column, in contrast to the alternative pH gradient. This selection was based primarily on the presence of the O-glycosidic bond; the possibility that the linkage may not be stable at a suitable pH of elution was high. Hypothetically, such a pH would be near the pKa of the most acidic phosphate proton (pH~1).

Several different gradients for anion exchange were attempted for the purification of 13. Triethylammonium bicarbonate, triethylammonium formate, and pyridinium formate were all unsuccessful. Interestingly, all three systems provided a simple means for purification by anion exchange. However, the major downfall in the aforementioned buffers was the lack of potential for product isolation. In most cases, desalting attempts following ion exchange were unsatisfactory, and utilized buffers did not demonstrate the expected volatility in the desalting step. This resulted in purified products containing extremely high (500 mg to 1.5 g for microscale deprotections) quantities of salt. Due to

the subsequent requirement for additional cation exchange (see below), a more

effective purification/desalting method was needed.

Literature procedures[26,27] have utilized a lithium chloride salt gradient in various

phosphate purifications by anion exchange. A key advantage to the procedure is
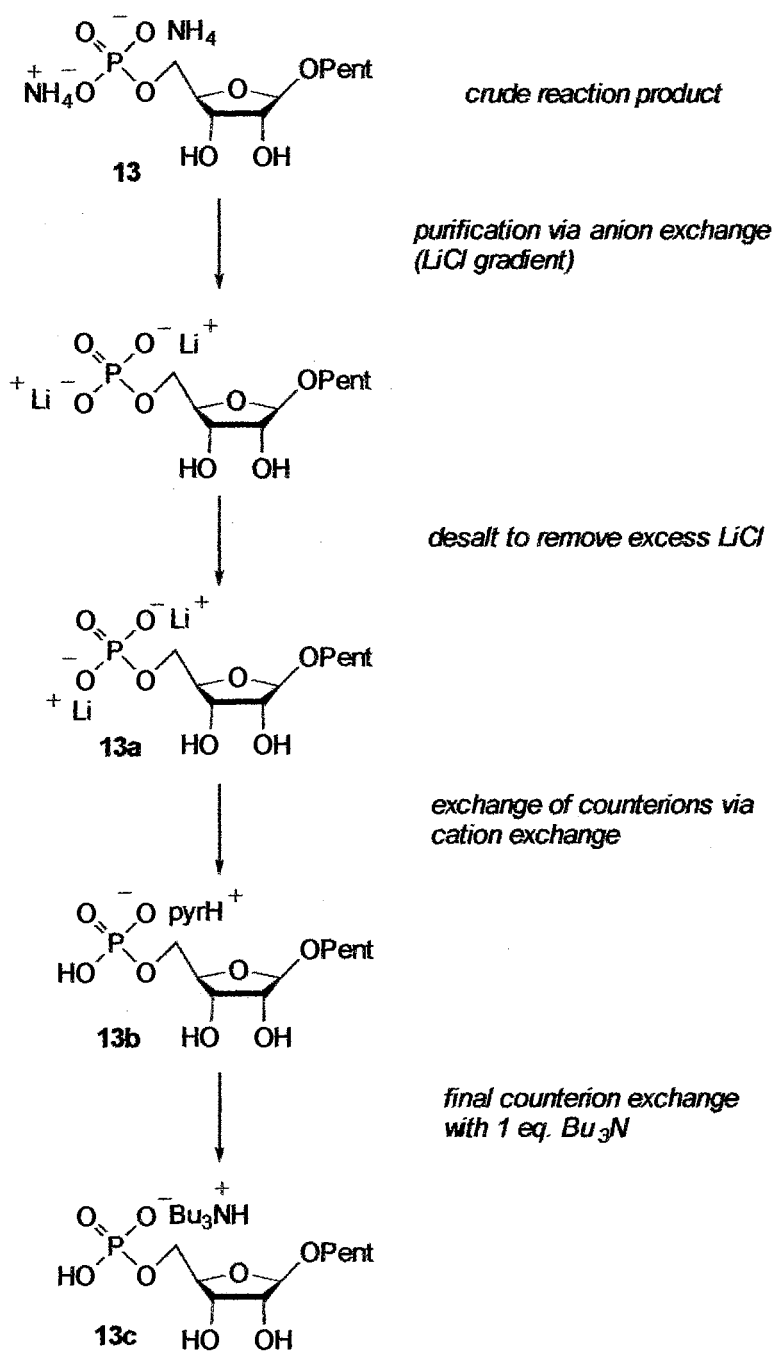
Figure 34. Counterion exchange strategy for the crude phosphate product 13.

the apparent ease of LiCl elution; in many cases, monophosphates have been

effectively eluted at relatively low (0.025-0.05 M) concentrations. An additional benefit

is present in the properties of the lithium cation. Due to its existence as a 'hard' ion, Li^+

can be predicted to be especially susceptible to (and easily removed by) subsequent

cation exchange.

Once the crude phosphate has been effectively purified and desalted, it exists as

its lithium dianion 13a (Figure 34). While this compound is extremely pure, it does not

possess the proper counterions for the upcoming coupling with AMP. Therefore, cation

exchange affords the corresponding monopyridinium salt 13b, which is then readily

converted to its monotributylammonium salt 13c, suitable for coupling with AMP.

With the tributylammonium salt in hand, an appropriate coupling strategy was

then investigated (Figure 35). Initial trials employed a strategy used by Hoard and Ott[29]

in the construction of pyrophosphate linkages. The approach includes coupling via 1,1'-

carbonyl diimidazole (Im_2CO), which catalyzes the formation of an imidazolium

intermediate. Subsequent treatment with a suitable nucleophile (in this case, AMP) then
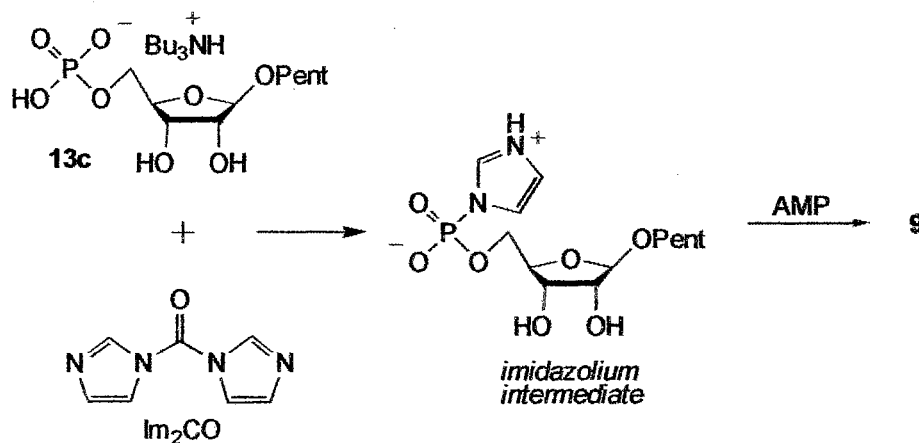
Figure 35. First attempted (unsuccessful) synthesis of 9.
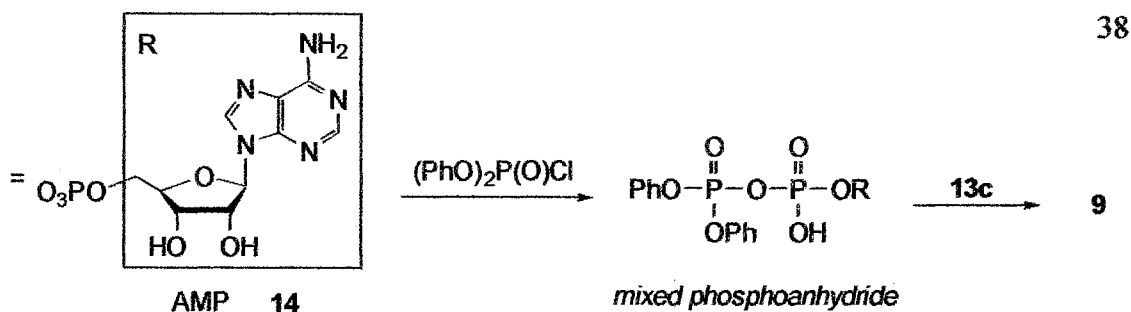
Figure 36. Successful synthesis of **9**.

produces the desired product. However, in the present study, this route proved to be problematic due to solubility limitations. Additionally, the reaction was difficult to monitor, owing to the instability of the formed intermediate.

Another published procedure used for the construction of pyrophosphate bonds includes the formation of a mixed phosphoanhydride (Figure 36).[27] Once formed, the anhydride undergoes nucleophilic attack by the remaining coupling fragment. A key advantage in the protocol results from the solubility of the anhydride; due to its organic nature, the reaction can be carried out in relatively nonpolar solvents (dioxan and pyridine). The anhydride (a white solid in the reaction solvent) can also be visually followed as it forms, thus enabling the partial observation of reaction progress.

The actual coupling reaction can be easily followed using high performance liquid chromatography (HPLC). Due to the ultraviolet activity of AMP, its relative amount in the reaction can be determined by integration. Under the developed conditions (pH = 3), the absorption of AMP can be effortlessly separated from that of the acyclic precursor, making the formation of the pyrophosphate quite apparent. The developed separation technique depends on the net charge of the mono- and pyrophosphate molecules; at a pH of 3, AMP and its own coupled product, diadenosine diphosphate (AppA), will be neutral, while the desired pyrophosphate **9** should possess a negative charge. This was
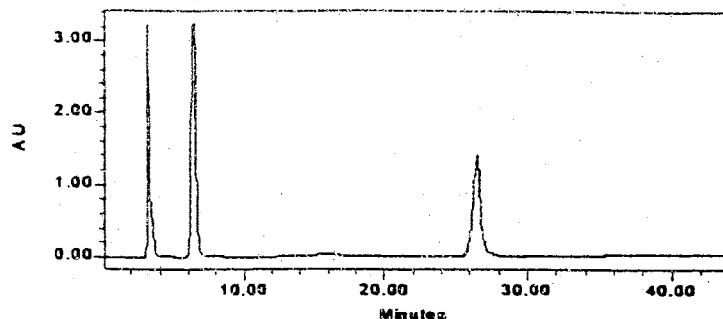
Figure 37. HPLC trace of A/AMP/ADP mixture (see Experimental Section for conditions).

further tested by an HPLC analysis of an adenosine-based mixture (Figure 37).

Current evidence indicates that, while the attempted coupling was successful, further modifications are necessary for optimization of reaction yield. HPLC analysis of reaction products showed two new peaks in the predicted region for the coupled product. Small-scale HPLC purification of the two peaks (Figure 38, retention time = 13.8 - 15.5 minutes) yielded a moderately pure sample.

Spectroscopic analysis by ^{1}H- and ^{31}P-NMR indicated that the obtained solid contains two basic pyrophosphate products. Gratifyingly, the product 9 was successfully synthesized, as evidenced by integration in the proton spectrum. Additionally, a structurally similar product was obtained without the desired pentenyl signals. A plausible hypothesis would include the acid-catalyzed loss of the pentenyl moiety (from 9) to yield adenosine diphosphate ribose (AppR).
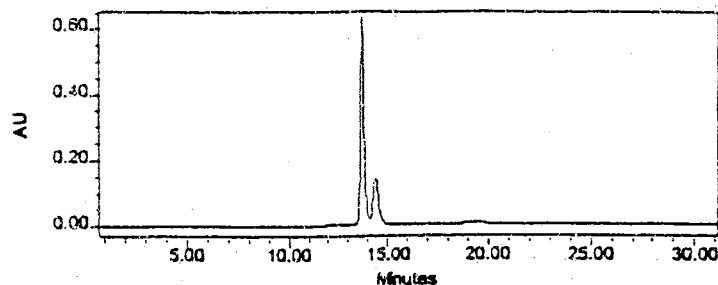
Figure 38. HPLC trace of coupling reaction products (see Experimental Section for conditions).

Crude reaction → Evaporate → Dissolve in
solution   solvent   water

↓

Purified ← Anion ← Adjust pH
pyrophosphate   exchange   (6.5)
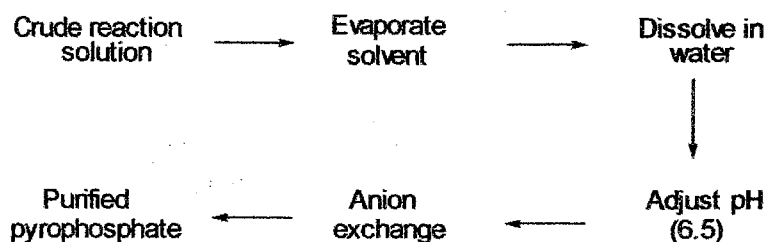
Figure 39. Purification details for the acyclic precursor 9.

Auspiciously, large-scale purification of the synthesized acyclic precursor 9 is

analogous to that of the pentenyl phosphate 13 (Figure 39). After adjusting the crude

solution to a pH ~ 6.5, the sample is loaded onto anion exchange resin and thoroughly

washed with 3 mM hydrochloric acid (HCl) to remove the uncharged AMP and AppA.

Once this elution is complete, a LiCl gradient is run, and the desired pyrophosphate is
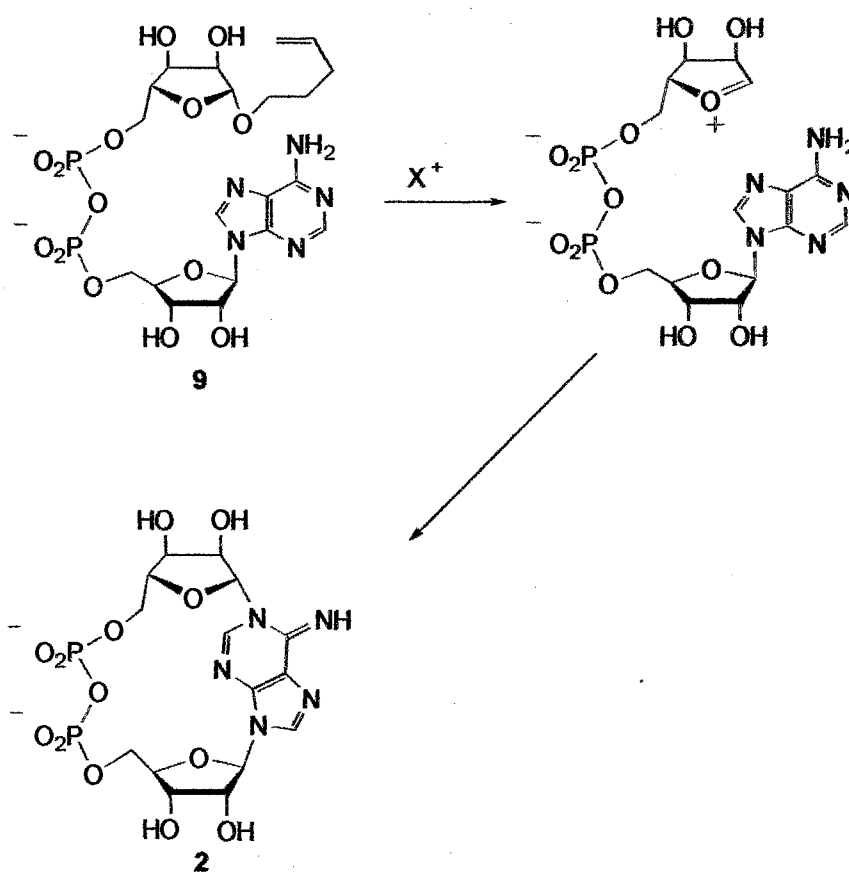
Figure 40. Remaining steps in the synthesis of cADPR.

eluted.

Pending final ion exchange, the obtained acyclic precursor **9** is now ready for final cyclization attempts (Figure 40). Although protection of the primary adenine nitrogen may prove necessary, a successful formation of the N-glycosidic bond should produce (in one step) the desired target cADPR (**2**).

Experimental Section

General. Pyridine and triethylamine were distilled from KOH; THF was distilled from LiAlH$_4$, and CH$_3$CN was distilled from CaH prior to use. DMF and methanol were stored over 4-Angstrom molecular sieves overnight. Bis(cyanoethyl) (-N,N-diisopropylamino)phosphoramidite was synthesized according to the published procedure.[25] All other reagents were commercially available. All reactions were performed under an atmosphere of dry nitrogen; glassware and syringes were dried at 100 °C overnight, prior to use. Spectral data was acquired using a Varian Gemini 300 MHz, an Inova 400 MHz, or a 600 MHz instrument. Unless otherwise noted, all spectra were acquired in CDCl$_3$ at room temperature, and were referenced to internal trimethylsilane.
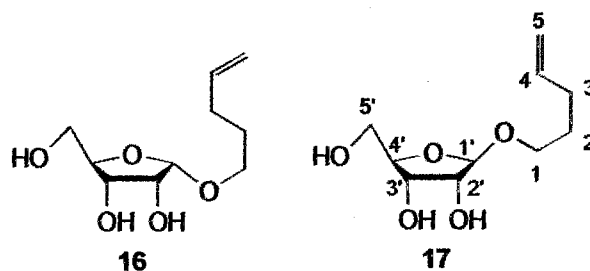
Pent-4-enyl-D-ribofuranoside (16 and 17)[16]: To a stirred suspension of D-ribose (**15**, 1.21 g, 8.07 mmol) in 4-penten-1-ol (16.0 mL, 154.9 mmol) was added a solution,

prepared by dissolving 10-camphorsulfonic acid (CSA, 162.4 mg, 0.70mmol) in 4-

penten-1-ol (2 mL 19.4 mmol), After stirring at rt for 16 hours, the reaction mixture was

quenched with Ag_2CO_3 (162.0 mg, 1.17 mmol), filtered, and the solvent evaporated. The

crude oil was then loaded onto a silica gel column and was eluted with medium pressure

(~40 psi) and a step gradient of 99:1 chloroform:ethanol ($CHCl_3$:EtOH) to 90:10

$CHCl_3$:EtOH, yielding the desired product as its α (**16**, 1.62 mmol, 20%), and β (**17**,

3.35 mmol, 41%) anomers.

<u>^{1}H-NMR (**16**, δ, 400 MHz):</u>

5.765 (ddt, J = 16.9, 13.2, 6.6 Hz, 1H, H4)

4.992 (dq, J = 17.1, 1.8 Hz, 1H, H5)

4.992 (d, J = 4.4 Hz, 1H, H1')

4.942 (ddt, J = 10.4, 2.1, 1.7 Hz, 1H, H5)

4.047 – 3.637 (m, 5H, H2', H3', H4', H5', H5'')

3.787 (dt, J = 9.7, 6.7 Hz, 1H, H1)

3.479 (dt, J = 9.7, 6.6 Hz, 1H, H1)

3.137 (d, J = 8.8 Hz, 1H, OH)

3.010 (d, J = 8.1 Hz, 1H, OH)

2.510 (bs, 1H, OH)

2.075 (q, J = 7.0 Hz, 2H, H3)

1.686 (quin, J = 6.5 Hz, 2H, H2)

¹³C-NMR (**16**, δ, 100 MHz):

137.501 (C4)

114.880 (C5)

101.325 (C1')

84.293 (C4')

71.209 (C2')

70.291 (C3')

67.600 (C1)

62.203 (C5')

29.892 (C3)

28.279 (C2)

FAB-MS (**17**):

219 (MH^+); 133 ($MH^+ - 85$), 69 ($MH^+ - 150$).

¹H-NMR (**17**, δ, 400 MHz):

5.792 (ddt, J = 17.1, 13.2, 6.6 Hz, 1H, H4)

5.027 (dq, J = 17.2, 1.6 Hz, 1H, H5)

4.978 (ddt, J = 10.3, 2.0, 1.3 Hz, 1H, H5)

4.914 (s, 1H, H1')

4.630 (bs, 1H, OH)

4.577 (bs, 1H, OH)

4.214 (app. q, J ~ 5.6 Hz, 1H, H4')

4.025 (m, 1H, H2')

3.774 – 3.638 (m, 5H, H1, H3',H5', H5", OH)

3.414 (dt, *J* = 9.6, 6.6 Hz, 1H, H1)

2.085 (q, *J* = 7.0 Hz, 2H, H3)

1.681 (quin, *J* = 6.8 Hz, 2H, H2)

^{13}C-NMR (**17**, δ, 100 MHz):

137.738 (C4)

115.113 (C5)

107.529 (C1')

83.941 (C4')

75.529 (C2')

71.554 (C3')

67.971 (C1)

63.428 (C5')

30.083 (C3)

28.651 (C2)

18a
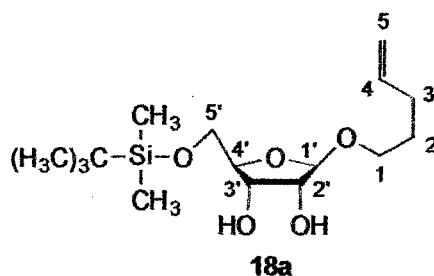
Pent-4-enyl 5-*tert*-butyldimethylsilyl-β-D-ribofuranoside (18a): To a solution of

pent-4-enyl β-D-ribofuranoside (**17**, 99.7 mg, 0.46 mmol) and imidazole (79.6 mg, 1.17

mmol) in DMF (0.5 mL, 6.5 mmol) was added *tert*-butyldimethylsilyl chloride (TBDMS-

Cl, 101.1 mg, 0.67 mmol). The resulting solution was stirred at room temperature for

three hours and was then diluted with ether (5 mL). After washing with water (2 x 3 mL)

and saturated NaCl solution (1 x 3 mL), the organic layer was dried over $MgSO_4$,

filtered, and the solvent evaporated. The crude oil was purified by silica gel

chromatography to yield the desired monosilylated product (**18a**, 0.22 mmol, 48%).

^{1}H-NMR (**18a**, δ, 400 MHz):

5.761 (ddt, J = 17.1, 13.2, 6.8 Hz, 1H, H4)

4.986 (dq, J = 17.2, 1.8 Hz, 1H, H5)

4.934 (ddt, J = 10.2, 1.3, 1.9 Hz, 1H, H5)

4.893 (s, 1H, H1')

4.198 (q, J = 5.9 Hz, 1H, H4')

4.015 (d, J = 4.4 Hz, 1H, H2')

3.855 (q, J = 6.3 Hz, 1H, H3')

3.763 (dd, J = 10.3, 5.4 Hz, 1H, H5')

3.692 – 3.620 (m, 2H, H5'', H1)

3.352 (dt, J = 9.5, 6.6 Hz, 1H, H1)

2.985 (bs, 1H, OH)

2.689 (bs, 1H, OH)

2.058 (q, J = 6.8 Hz, 2H, H3)

1.615 (quin, J = 6.7 Hz, 2H, H2)

0.877 [s, 9H, $(CH_3)_3CSi(Me)_2$]

0.055 [s, 6H, $(t\text{-Bu})Si(CH_3)_2$]

^{13}C-NMR (**18a**, δ, 100 MHz):

138.045 (C4)

114.832 (C5)

107.177 (C1')

82.771 (C4')

75.284 (C2')

73.237 (C3')

67.360 (C1)

65.078 (C5')

30.183 (C3)

28.678 (C2)

25.859 [$(CH_3)_3CSi(Me)_2$]

18.292 [$(CH_3)_3CSi(Me)_2$]

11.173 [$(CH_3)_3CSi(CH_3)_2$]

18b
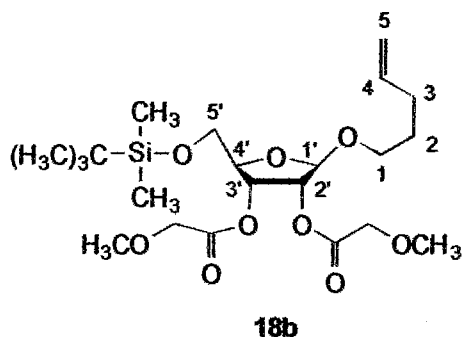
Pent-4-enyl 5-*tert*-butyldimethylsilyl-2,3-dimethoxyacetyl β-D-ribofuranoside

(18b): To a solution of pent-4-enyl 5-*tert*-butyldimethylsilyl-β-D-ribofuranoside (**18a**, 111.5 mg, 0.34 mmol) in pyridine (2.0 mL, 24.7 mmol) at 0 °C was added triethylamine (TEA, 0.16 mL, 1.15 mmol) and methoxyacetyl chloride (MA-Cl, 0.2 mL, 2.2 mmol), respectively. The resulting solution was stirred for two hours at 0 °C and was then quenched with 1:3 water:pyridine (4 mL). Solvent evaporation yielded a yellow oil, which was dissolved in CH_2Cl_2 (10 mL) and washed with saturated $NaHCO_3$ (10 mL) solution. After back-extracting the aqueous layer with additional CH_2Cl_2 (2 x 10 mL), the combined organic layers were evaporated, dried over $MgSO_4$, filtered and the solvent evaporated. Final isolation of the dimethoxyacetylated product (**18b**, 0.23 mmol, 68%) was accomplished using silica gel chromatography.

<u>¹H-NMR (**18b**, δ, 400 MHz)</u>:

6.219 (app. d, J = 6.0 Hz, 1H, H3')

6.030 (d, J = 4.5 Hz, 1H, H2')

5.759 (ddt, J = 17.1, 13.1, 6.7 Hz, 1H, H4)

4.990 (dq, J = 17.1, 1.7 Hz, 1H, H5)

4.928 (ddt, J = 10.2, 2.0, 1.8 Hz, 1H, H5)

4.887 (s, 1H, H1')

3.975 (s, 2H, COCH_2OMe)

3.912 (m, 2H, COCH_2OMe)

3.855 (q, J = 6.3 Hz, 1H, H4')

3.763 (dd, J = 10.3, 5.4 Hz, 1H, H5')

3.692 – 3.620 (m, 2H, H5'', H1)

3.451 (s, 3H, OCH_3)

3.352 (dt, J = 9.5, 6.6 Hz, 1H, H1)

3.397 (s, 3H, OCH_3)

2.058 (q, J = 6.8 Hz, 2H, H3)

1.615 (quin, J = 6.7 Hz, 2H, H2)

0.877 [s, 9H, (CH_3)$_3$CSi(Me)$_2$]

0.055 [s, 6H, (t-Bu)Si(CH_3)$_2$]

<u>^{13}C-NMR (**18b**, δ, 100 MHz):</u>

169.412 (C=O)

169.212 (C=O)

138.045 (C4)

114.832 (C5)

106.910 (C1')

80.559 (C4')

78.929 (C2')

76.899 (C3')

67.360 (C1)

65.078 (C5')

63.418 (2 x COCH_2Me)

55.048 (2 x OCH$_3$)

30.183 (C3)

28.678 (C2)

25.859 [(CH$_3$)$_3$CSi(Me)$_2$]

18.292 [(CH_3)$_3$CSi(Me)$_2$]

11.173 [(CH$_3$)$_3$CSi(CH_3)$_2$]
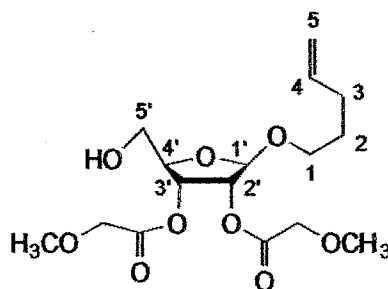
19 (not isolated)

Attempted synthesis of pent-4-enyl 2,3-dimethoxyacetyl-β-D-ribofuranoside (19):

To a solution of pent-4-enyl 5-*tert*-butyldimethylsilyl-2,3-dimethoxyacetyl -β-D-

ribofuranoside (**18b**, 107.6 mg, 0.23 mmol) in THF (0.5 mL, 6.2 mmol) at 0 °C was

added a solution of tetrabutylammonium fluoride (TBAF, 122.3 mg, 0.47 mmol) in THF

(0.61 mL, 7.5 mmol), and the solution was stirred at 0 °C. After 40 minutes, the reaction

was brought to room temperature, and was stirred for an additional 20 minutes preceding

dilution with ether (4 mL). The resulting solution was washed with water (2 x 4 mL) and

saturated NaCl solution (1 x 4 mL), and was dried over MgSO$_4$, filtered, and the solvent

evaporated to yield the crude product (~ 60 µmol, 26%). Due to the low crude yield

and the presence of multiple spots in TLC analysis, the attempted synthesis was aborted,

in favor of a more productive procedure (see following).

20a
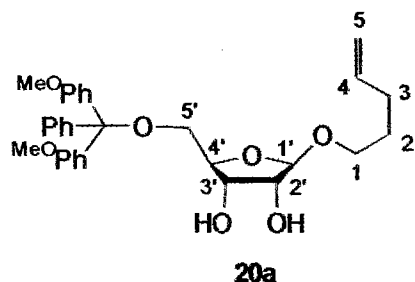
Pent-4-enyl 5-dimethoxytrityl-β-D-ribofuranoside (20a): To a solution of pent-4-

enyl β-D-ribofuranoside (17, 61.6 mg, 0.28 mmol) in pyridine (1.4 mL, 17.2 mmol) was

added 4-dimethylaminopyridine (DMAP, 6.2 mg, 0.05 mmol), triethylamine (0.05 mL,

0.36 mmol), and 4,4'-dimethoxytrityl chloride (DMT-Cl, 172.4 mg, 0.51 mmol),

respectively. The resulting solution was stirred at room temperature for 1.5 hours prior to

dilution with ether (5 mL). The solution was then washed with water (2 x 5 mL) and

saturated NaCl solution (1 x 5 mL), followed by drying over $MgSO_4$, filtration, and

solvent removal. The crude product was purified using a stepwise gradient (98:2:0.5

$CHCl_3$:CH_3OH:Et_3N – 95:5:0.5 $CHCl_3$:CH_3OH:Et_3N) in silica gel chromatography (**20a**,

0.23 mmol, 82%).

FAB-MS:

521 (MH$^+$); 303 (MH$^+$ – 218).

<u>1H-NMR (**20a**, δ, 400 MHz):</u>

7.479 – 6.791 (m, 13H, ArH)

5.737 (ddt, *J* = 17.0, 13.5, 6.7 Hz, 1H, H4)

4.944 (dq, *J* = 17.2, 1.7 Hz, 2H, H5)

4.931 (s, 1H, H1')

4.225 (dd, *J* = 6.1, 5.0 Hz, 1H, H5')

4.078 (q, *J* = 6.2 Hz, 1H, H4')

4.012 (d, *J* = 4.9 Hz, 1H, H5'')

3.780 (s, 3H, OCH$_3$)

3.764 (s, 3H, OCH$_3$)

3.671 (dt, *J* = 9.5, 6.6 Hz, 1H, H1)

3.436 (m, 1H, H3')

3.358 (dt, *J* = 9.5, 6.7 Hz, 1H, H1)

3.246 (d, *J* = 5.2 Hz, 1H, H2')

1.984 (q, *J* = 6.6 Hz, 2H, H3)

1.585 (quin, *J* = 6.9 Hz, 2H, H2)

<u>13C-NMR (**20a**, δ, 100 MHz):</u>

158.902 – 113.585 (Ar)

136.562 (C4)

115.247 (C5)

107.685 (C1')

86.544 [C(Ph₃)]

86.544 [C(Ph$_3$)]

82.667 (C4')

75.714 (C2')

73.163 (C3')

67.887 (C1)

65.559 (C5')

55.738 (2 x OCH$_3$)

30.703 (C3)

29.172 (C2)

20b
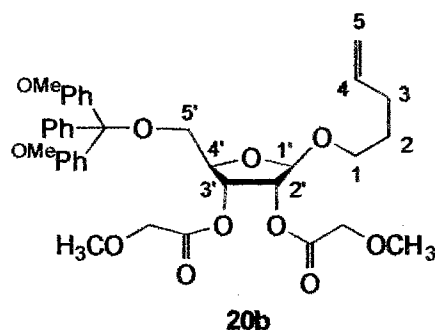
Pent-4-enyl 2,3-dimethoxyacetyl-5-dimethoxytrityl-β-D-ribofuranoside (20b): To

a solution of pent-4-enyl 5-dimethoxytrityl-β-D-ribofuranoside (**20a**, 114.6 mg, 0.22

mmol) in pyridine (1.4 mL, 17.3 mmol) was added triethylamine (TEA, 0.2 mL, 1.4

mmol). Methoxyacetyl chloride (MA-Cl, 64 μL, 0.70 mmol) was then added, and the

resulting solution was stirred at room temperature for two hours. After quenching with

5:2 water:pyridine (7 mL), the reaction solution was extracted with 50:50 CH$_2$Cl$_2$:water

(1 x 10 mL). The organic layer was then washed with water (10 mL) and saturated

NaHCO$_3$ solution (10 mL), dried over MgSO$_4$, filtered and the solvent evaporated. The

crude oil was purified on a silica gel column to yield the desired product (**20b**, 0.15

mmol, 67%).

<u>FAB-MS</u>:

664 (MH$^+$); 303 (MH$^+$ – 361).

<u>^{1}H-NMR (**20b**, δ, 400 MHz)</u>:

7.459 – 6.803 (m, 13H, ArH)

5.727 (ddt, J = 17.0, 13.3, 6.6 Hz, 1H, H4)

5.511 (dd, J = 4.7, 1.9 Hz, 1H, H3')

5.373 (d, J = 4.7 Hz, 1H, H2')

4.962 (m, 2H, H5)

5.028 (s, 1H, H1')

4.135 (q, J = 6.1 Hz, 1H, H4')

4.070 (s, 3H, OCH$_3$)

4.068 (s, 3H, OCH$_3$)

3.967 (m, 4H, 2 x COC*H$_2$*OCH$_3$)

3.690 (dt, J = 9.3, 6.7 Hz, 1H, H1)

3.451 (s, 3H, OCH$_3$)

3.397 (s, 3H, OCH$_3$)

3.382 (dt, J = 9.4, 6.6 Hz, 1H, H1)

3.340 (m, 2H, H5', H5'')

2.012 (q, J = 6.8 Hz, 2H, H3)

1.779 (quin, J = 7.1 Hz, 2H, H2)

^{13}C-NMR (**20b**, δ, 100 MHz):

169.179 (CO)

169.084 (CO)

158.428 – 126.739 (Ar)

135.789 (C4)

114.886 (C5)

104.923 (C1')

86.110 [C(Ph$_3$)]

79.469 (C4')

75.083 (C2')

72.513 (C3')

69.361 (2 x COCH$_2$OMe)

67.618 (C1)

64.223 (C5')

59.407 (2 x OCH$_3$, MA)

55.133 (3 x OCH$_3$, DMT)

30.068 (C3)

28.492 (C2)

21
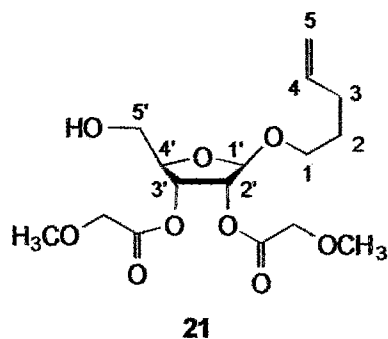
Pent-4-enyl 2,3-dimethoxyacetyl-β-D-ribofuranoside (21): To a solution of pent-4-

enyl 5-dimethoxytrityl-β-D-ribofuranoside (**20b**, 47.2 mg, 0.07 mmol) in methanol (0.7

mL, 20.0 mmol) was added a solution of 3% trichloroacetic acid in CH_2Cl_2 (TCA, 4.8

mL, 0.88 mmol). The resulting solution was stirred at room temperature for 20 minutes

before quenching with pyridine (0.48 mL, 5.9 mmol). The solution was then diluted with

ether (5 mL), washed with water (2 x 5 mL), saturated $NaHCO_3$ (1 x 5 mL) and NaCl (1

x 5 mL) solutions, and dried over $MgSO_4$. After filtration, the solvent was evaporated,

and the crude residue was purified via silica gel chromatography to yield the desired

deprotected product (**21**, 0.06 mmol, 84%).

FAB-MS:

664 (MH^+); 303 ($MH^+ - 361$).

^{1}H-NMR (**21**, δ, 400 MHz

5.792 (ddt, $J = 17.0, 13.4, 6.7$ Hz, 1H, H4)

5.518 (t, $J = 5.4$ Hz, 1H, H3')

5.354 (d, $J = 5.8$ Hz, 1H, H2')

5.062 (dq, J = 17.2, 1.6 Hz, 1H, H5)

5.040 (s, 1H, H1')

5.000 (ddt, J = 10.2, 2.1, 1.3 Hz, 1H, H5)

4.248 (m, 1H, H4')

4.090 (s, 2H, CH$_2$)

4.034 (m, 2H, CH$_2$)

3.846 – 3.658 (m, 3H, H1, H5', H5'')

3.519 – 3.414 (m, 7H, OCH$_3$, H1)

2.135 (q, J = 6.6 Hz, 2H, H3)

1.696 (quin, J = 6.9 Hz, 2H, H2)

^{13}C-NMR (**21, δ, 100 MHz**):

169.169 (C=O)

168.936 (C=O)

137.411 (C4)

114.865 (C5)

105.003 (C1')

81.729 (C4')

75.189 (C2')

71.366 (C3')

69.228 (2 x COCH_2OMe)

67.861 (C1)

62.600 (C5')

59.080 (2 x OCH$_3$)

30.703 (C3)

29.172 (C2)

22
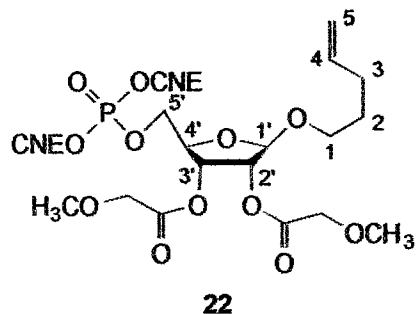
Bis(2-cyanoethyl) (pent-4-enyl 2,3-dimethoxyacetyl-β-D-ribofuranos-5-yl)

phosphate (22): Pent-4-enyl 2,3-dimethoxyacetyl-β-D-ribofuranoside was dried prior to

use (3 x 2 mL CH$_3$CN, followed by overnight vacuum). To a stirred suspension of pent-

4-enyl 2,3-dimethoxyacetyl-β-D-ribofuranoside (21, 337.3 mg, 0.93 mmol) and 1*H*-

tetrazole (138.0 mg, 1.97 mmol) in CH$_3$CN (44 mL) was added a solution of

bis(cyanoethyl)-*N,N*-diisopropylaminophosphoramidite (488.9 mg, 1.80 mmol) in

CH$_3$CN (6.0 mL), and the resulting solution was stirred at room temperature for two

hours. *m*-chloroperoxybenzoic acid (MCPBA, 283.2 mg, 1.80 mmol) was then added,

and the reaction was stirred for an additional 30 minutes before diluting with water (50

mL). Product was extracted with CH$_2$Cl$_2$ (3 x 80 mL), and the combined organic layers

were washed with saturated NaHCO$_3$ solution (1 x 250 mL), dried over MgSO$_4$, filtered

and the solvent evaporated. The crude residue was purified via silica gel chromatography

to yield the phosphorylated product (22, 0.81 mmol, 87%).

FAB-MS:

571 (MH$^+$ + Na); 463 (MH$^+$ − 85).

^{1}H-NMR (**22**, δ, 400 MHz):

5.776 (ddt, J = 17.1, 13.2, 6.6 Hz, 1H, H4)

5.4500 (dd, J = 5.0, 1.2 Hz, 1H, H3')

5.289 (d, J = 4.8 Hz, 1H, H2')

5.012 (s, 1H, H1')

5.007 (dq, J = 17.2, 1.6 Hz, 1H, H5)

4.955 (ddt, J = 10.3, 2.0, 1.3 Hz, 1H, H5)

4.196 (m, 7H, CH_2CH$_2$CN, H4', H5', H5'')

4.063 (s, 2H, COCH_2OMe)

4.003 (m, 2H, COCH_2Me)

3.747 (dt, J = 9.6, 6.6 Hz, 1H, H1)

3.426 (s, 3H, OCH$_3$)

3.404 (m, 4H, H1, OCH$_3$)

2.777 (td, J = 6.2, 1.0 Hz, 4H, 2 x CH$_2$$CH_2$CN)

2.084 (q, J = 7.0 Hz, 2H, H3)

1.650 (quin, J = 6.6 Hz, 2H, H2)

^{13}C-NMR (**22**, δ, 100 MHz):

168.926 (C=O)

167.992 (C=O)

137.543 (C4)

116.340 (CH$_2$CH$_2$*CN*)

114.763 (C5)

104.763 (C1')

78.417 (d, $^3J_{POCC}$ = 6.9 Hz, C4')

74.498 (C2')

70.967 (C3')

69.000 (2 x CO*CH$_2$*OMe)

68.955 (d, $^2J_{POC}$ = 6.0 Hz, C5')

67.549 (C1)

62.229 (d, $^2J_{POC}$ = 5.7 Hz, *CH$_2$*CH$_2$CN)

59.080 (2 x OCH$_3$)

29.715(C3)

28.118 (C2)

19.300 (d, $^3J_{POCC}$ = 8.0 Hz, CH$_2$*CH$_2$*CN)

23

Bis(2-cyanoethyl) (pent-4-enyl β-D-ribofuranos-5-yl) phosphate (23). To a stirred

solution of pent-4-enyl β-D-ribofuranoside (**17**, 91 mg, 0.42 mmol) and 5-(*p*-nitrophenyl

-1*H*-tetrazole (5-NPT 185 mg, 0.97 mmol) in CH$_3$CN (17 mL) at -36 °C was added

dropwise (0.02 mmol/min) a 0.45 M solution of bis(2-cyanoethyl) N,N-

diisopropylaminophosphoramidite (0.73 mL, 0.33 mmol) in CH_3CN, and the resulting

solution was stirred for 20 minutes. A 0.95 M solution of *tert*-butyl hydroperoxide

(TBHP, 4.0 mL, 3.8 mmol) in CH_2Cl_2 was then added, and the reaction was warmed to

room temperature with a water bath. After stirring for 20 minutes, the reaction solution

was evaporated to a small volume (~2-4 mL) and diluted with an equal volume of

CH_2Cl_2. The crude product was then loaded onto a silica gel column and eluted with a

step gradient of 60:40 CH_2Cl_2:ethyl acetate (MC:EA) to 100:0 MC:EA, followed by

90:10 EA:EtOH, yielding phosphate **23** (0.20 mmol, 59 % based on limiting

phosphoramidite; 81% based on total recovered carbohydrate) and recovered starting

material (**17**, 0.14 mmol).

^{1}H-NMR (**23**, δ, 600 MHz):

5.807 (ddt, J = 17.1, 13.2, 6.6 Hz, 1H, H4)

5.028 (dq, J = 17.1, 1.6 Hz, 1H, H5)

4.976 (ddt, J = 10.3, 2.0, 1.3 Hz, 1H, H5)

4.942 (s, 1H, H1')

4.328 (dt, J = 8.1, 6.1 Hz, 2H, CH_2CH$_2$CN)

4.325 (dt, J = 8.1, 6.1 Hz, 2H, CH_2CH$_2$CN)

4.290 (ddd, J = 10.9, 8.2, 4.5 Hz, 1H, H5' or H5")

4.262 (t, J = 5.3 Hz, 1H, H3')

4.216 (ddd, J = 10.9, 9.1, 5.9 Hz, 1H, H5' or H5")

4.145 (app. q, J ~ 6.2 Hz, 1H, H4')

4.030 (d, J = 4.9 Hz, 1H, H2')

3.719 (dt, J = 9.6, 6.6 Hz, 1H, H1)

3.563 (s, 1H, OH)

3.409 (dt, J = 9.6, 6.6 Hz, 1H, H1)

3.209 (s, 1H, OH)

2.807 (td, J = 6.1, 1.0 Hz, 4H, 2 x CH$_2$$CH_2$CN)
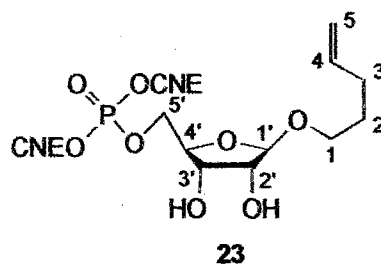
2.100 (q, J = 7.0 Hz, 2H, H3)

1.655 (quin, J = 6.6 Hz, 2H, H2)

^{13}C-NMR (**23**, δ, 151 MHz):

138.097 (C4)

116.578 (CH$_2$CH$_2$$CN$)

115.045 (C5)

107.366 (C1')

80.992 (d, $^3J_{POCC}$ = 6.9 Hz, C4')

75.027 (C2')

71.931 (C3')

69.701 (d, $^2J_{POC}$ = 6.0 Hz, C5')

67.561 (C1)

62.469 (d, $^2J_{POC}$ = 5.7 Hz, CH_2CH$_2$CN)

30.062 (C3)

28.575 (C2)

19.583 (d, $^3J_{POCC}$ = 8.0 Hz, CH$_2$$CH_2$CN)

^{31}P-NMR (δ, 162 MHz):

-0.550.

13a

Pent-4-enyl β-D-ribofuranos-5-yl phosphate (13a). Aqueous NH_3 was added to neat bis(2-cyanoethyl) (pent-4-enyl 2,3-dimethoxyacetyl-β-D-ribofuranos-5-yl) phosphate (**22**) and the resulting solution was refluxed for three hours. Following solvent evaporation under reduced pressure, the crude residue was loaded onto anion exchange resin (Dowex 1 x 8-100, Cl⁻ form). A stepwise gradient was performed (pH = 3), and the lithium dianion was eluted with 0.03 M LiCl. After desalting the product with 5:1 acetone:water, the purified phosphate was characterized by ^{1}H-NMR.

^{1}H-NMR (**13a**, δ, 400 MHz, D_2O):

5.845 (ddt, J = 17.2, 10.3, 6.7 Hz, 1H, H4)

5.035 (dq, J = 17.1, 1.6 Hz, 1H, H5)

5.013 (s, 1H, H1')

4.984 (ddt, J = 10.2, 2.1, 1.4 Hz, 1H, H5)

4.197 – 3.539 (m, 6H, H2', H3', H4', H5', H5'', H1)

3.502 (dt, J = 9.9, 6.8 Hz, 1H, H1)

2.387 (q, J = 5.9 Hz, 2H, H3)

1.646 (quin, J = 6.6 Hz, 2H, H2)

^{31}P-NMR (**13a**, δ, 162 MHz):

4.126 (s)

13b
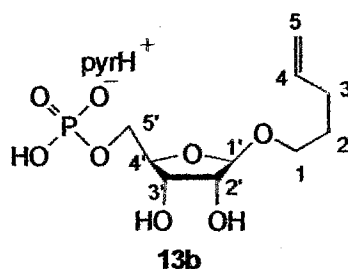
Pent-4-enyl β-D-ribofuranos-5-yl phosphate (13b). The purified phosphate **13a** was subjected to cation exchange chromatography (Dowex 50W x 8-100, pyrH$^+$ form). The monopyridinium salt **13b** was eluted with water, and the solvent was evaporated to yield the salt as a clear oil.

^{1}H-NMR (**13b**, δ, 400 MHz, CD$_3$OD):

8.879 – 7.852 (m, pyrH)

5.830 (ddt, J = 17.2, 10.2, 6.7 Hz, 1H, H4)

5.025 (m, 2H, H5)

5.011 (s, 1H, H1')

4.186 – 3.869 (m, 4H, H3', H4', H5', H5'')

3.868 (d, J = 4.8 Hz, 1H, H2')

3.691 (dt, J = 9.8, 6.8 Hz, 1H, H1)

3.388 (dt, J = 9.9, 6.8 Hz, 1H, H1)

2.086 (q, J = 6.9 Hz, 2H, H3)

1.416 (quin, J = 6.5 Hz, 2H, H2)

Bu₃NH⁺

13c
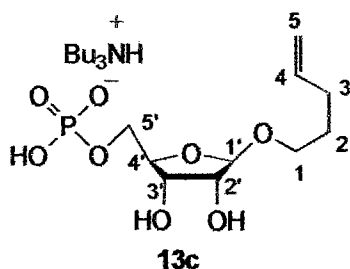
Pent-4-enyl β-D-ribofuranos-5-yl phosphate (13c). The monopyridinium salt

13b was dissolved in dry methanol, and tributylamine was added. The resulting solution

was stirred at room temperature for one hour, and the solvent was evaporated to yield the

monotributylammonium product **13c** as a light brown oil.

^{1}H-NMR (13c, δ, 400 MHz, CD₃OD):

5.804 (ddt, J = 17.1, 10.3, 6.8 Hz, 1H, H4)

5.020 (m, 2H, H5)

5.013 (s, 1H, H1')

4.162 – 3.844 (m, 4H, H3', H4', H5', H5'')

3.902 (d, J = 4.6 Hz, 1H, H2')

3.723 (dt, J = 9.8, 6.8 Hz, 1H, H1)

3.354 (dt, J = 9.9, 6.8 Hz, 1H, H1)

3.105 (t, J = 8.3 Hz, 6H, N(CH_2CH$_2$CH$_2$CH$_3$)$_3$)

2.086 (q, J = 6.9 Hz, 2H, H3)

1.729 – 1.588 (m, 12H, N(CH$_2$CH_2CH_2CH$_3$)$_3$

1.416 (quin, J = 6.5 Hz, 2H, H2)

0.994 (t, J = 7.3 Hz, 9H, N(CH$_2$CH$_2$CH$_2$CH_3)$_3$

^{13}C-NMR (**13c**, δ, 100 MHz, CD$_3$OD):

152.110, 125.700, 139.464 (pyr)

138.792 (C4)

114.841 (C5)

106.914 (C1')

81.294 (d, J_{POCC} = 6.7 Hz, C4')

74.155 (C2')

70.901 (C3')

68.083 (d, J_{POC} = 7.0 Hz, C5')

66.227 (C1)

29.570 (C3)

27.825 (C2)

9
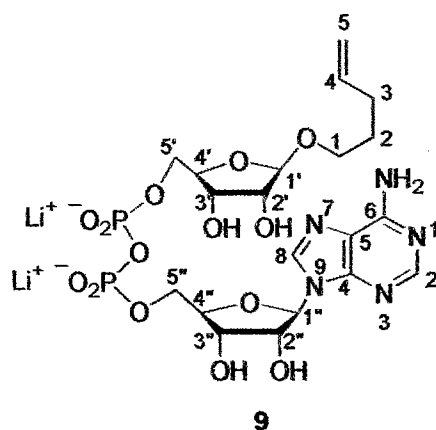
Adenosine diphosphate (pent-4-enyl β-D-)ribofuranose (9). To a solution of

adenosine 5'-monophosphate (**14**, 70.1 mg, 0.10 mmol) in dioxan (0.7 mL) was added

diphenyl phosphochloridate (0.03 mL, 0.15 mmol) and tributylamine (0.05 mL, 0.20

mmol), and the resulting solution was stirred at room temperature for three hours. After

solvent evaporation under reduced pressure, ether (2 mL) was added to precipitate the P^1-

nucleoside-5' P_2-diphenyl pyrophosphate. The suspension was kept at 0 °C for one hour.

Dioxan (3 mL) was the added, and subsequent solvent evaporation removed excess ether

and moisture. Then, a solution of the resulting P^1-nucleoside-5' P^2-diphenyl

pyrophosphate in dioxan (0.10 mL) was added to a solution of of pent-4-enyl β-D-

ribofuranos-5-yl phosphate (**13c**, 97.1 mg, 0.20 mmol)) in pyridine (0.20 mL). After

stirring at room temperature for 15 hours (followed progress by HPLC: Synchropak AX-

100, 4.6 x 250 mm, using 100 mM potassium phosphate buffer at a pH = 3, with a 0 – 2

M NaCl gradient, 1 mL/min), the solvent was evaporated, and the residue was loaded

onto anion exchange resin (Dowex 1 x 8-100, Cl⁻ form, pH = 3). After extensive washing

with 3 mM HCl, the product **9** was eluted with 0.03 M LiCl. The fractions were

combined, neutralized and the solvent evaporated to yield the desired product **9** as its

dilithium salt.

Using a sample purified by HPLC (sample ~ 1 mg)

^{1}H-NMR (9, δ, 600 MHz, D$_2$O):

8.512 (s, 1H, adenine CH)

8.320 (s, 1H, adenine CH)

6.105 (d, J = 5.3 Hz, 1H, H1'')

5.704 (ddt, J = 17.2, 10.3, 6.9 Hz, 1H, H4)

4.935 – 4.827 (m, 2H, H5)

4.868 (s, 1H, H1')

4.688 (t, J = 5.1 Hz, 1H, H3'')

4.454 (t, J = 4.8 Hz, 1H, H3')

4.332 – 3.992 (m, 6H, H2'', H4', H4'', H5', H5'')

3.952 (d, J = 4.8 Hz, 1H, H2')

3.847 (m, 1H, H5')

3.531 (dt, J = 9.7, 6.6 Hz, 1H, H1)

3.321 (dt, J = 10.3, 6.7 Hz, 1H, H1)

1.899 (q, J = 6.3 Hz, 2H, H3)

1,458 (quin, J = 6.6 Hz, H2)

References

1.   Clapper, D. L.; Walseth, T. F.; Dargie, P. J.; Lee, H. C. *J. Biol. Chem.*, **1987**, *262*, 9561-9568.

2.   Lee, H. C. *J. Biol. Chem*, **1991**, *266*, 2276-2281.

3.   Kim, H.; Jacobson, E. L.; Jacobson, M. K. *Biochem. Biophys. Res. Comm.*, **1993**, *194*, 1143-1147.

4.   Galione, A.; Lee, H. C.; Busa, W. B. *Science*, **1991**, *253*, 1143-1146.

5.   Walseth, T. F.; Aarhus, R.; Kerr, J. A.; Lee, H. C. *J. Biol. Chem*, **1993**, *268*, 26686-26691.

6.   Shirato, M.; Shuto, S.; Ueno, Y.; Matsuda, A. *Nuc. Acids Symp. Ser. No. 34* , **1995**, 165-166.

7.   Bailey, V. C.; Sethi, J. K.; Potter, B. V. L. *Chem. Commun.*, **1997**, 695-696.

8.   Zhang, F. J.; Sih, C. J. *Bioorg. Med. Chem. Lett.*, **1996**, *6*, 2311-2316.

9.   Yamada, S.; Gu, Q. M.; Sih, C. J. *J. Am. Chem. Soc.*, **1994**, *116*, 10787-10788.

10.   Prasad, G. S.; Levitt, D. G.; Lee, H. C.; Stout, C. D. *Prot. Struc. Func. Gen.*, **1996**, *24*, 138-140.

11.   Rusinko, N.; Lee, H. C. *J. Biol. Chem*, **1989**, *264*, 11725-11731.

12.   Sigma Catalog of Biochemicals and Reagents for Life Sciences Research (1999). Sigma: St. Louis, 310.

13.   Mootoo, D. R.; Date, V.; Fraser-Reid, B. *J. Am. Chem. Soc.*, **1988**, *110*, 2662-2663.

14.   Mootoo, D. R.; Konradsson, P.; Udodong, U.; Fraser-Reid, B. *J. Am. Chem. Soc.*, **1988**, *110*, 5583-5584.

15.   Fraser-Reid, B. *Synlett*, **1992**, *12*, 927-942.

16.   Chapeau, M. C.; Marnett, L. J. *J. Org. Chem.*, **1993**, *58*, 7258.

17.   Ludwig, J.; Eckstein, F. *J. Org. Chem.*, **1989**, *54*, 631-636.

18.   Corey, E. J.; Venkateswarlu, A. *J. Am. Chem. Soc.*, **1972**, *94*, 6190-6191.

19.   Ogilvie, K. K.; Beaucage, S. L.; Schifman, A. L.; Theriault, N. Y.; Sadan, K. L.
        Can. J. Chem., **1978**, *56*, 2768-2780.

20.   Ogilvie, K. K.; Schifman, A. L.; Penney.C. L. *Can. J. Chem.*, **1979**, *57*, 2230-2238.

21.   Reese, C. B.; Stewart, J. B. *Tetrahedron Lett.*, **1968**, *40*, 4273-4276.

22.   Gait, M. J. (1984): Oligonucleotide Synthesis: A Practical Approach. IRL Press:
        Oxford, 27.

23.   Takaku, H.; Morita, K.; Sumiuchi, T. *Chem. Lett.*, **1983**, 1661-1664.

24.   Gaffney, B. L.; Markey, L. A.; Jones, R. A. *Tetrahedron*, **1984**, *40*, 3-13.

25.   Bohler, C.; Bannwarth, W.; Luisi, P.; Giustini, M. , **1993**, *76*, 1341-1351.

26.   Grabowski, S.; Simon, E. S.; Whitesides, G. M. *J. Org. Chem.*, **1990**, *55*, 1834-
        1841.

27.   Michelson, A. M. *Biochim. Biophys. Acta*, **1964**, *91*, 1-13.

28.   Moffatt, J. G.; Khorana, H. G. *J. Am. Chem. Soc.*, **1958**, *80*, 3756-3761.

29.   Hoard, D. E.; Ott, D. G. *J. Am. Chem. Soc.*, **1965**, *87*, 1785-1788.

CHAPTER III

SELECTIVE PHOSPHITYLATION OF UNPROTECTED

RIBOSIDES AND CARBOHYDRATES

Synthesis of a Synthetic Intermediate En Route to cADPR

Introduction

An auxiliary challenge encountered en route to the total chemical synthesis of

cADPR (see Chapter 2) was the synthesis of a protected 5'-monophosphate (**22**, Figure

41). This molecule served as a precursor to the deprotected monophosphate **13** in a

coupling with adenosine monophosphate (AMP) to eventually yield cADPR (**2**). Due to

complexity and time issues, it was deemed appropriate to investigate additional and

preferably shorter methods for the synthesis of **22**. The alternative synthetic route
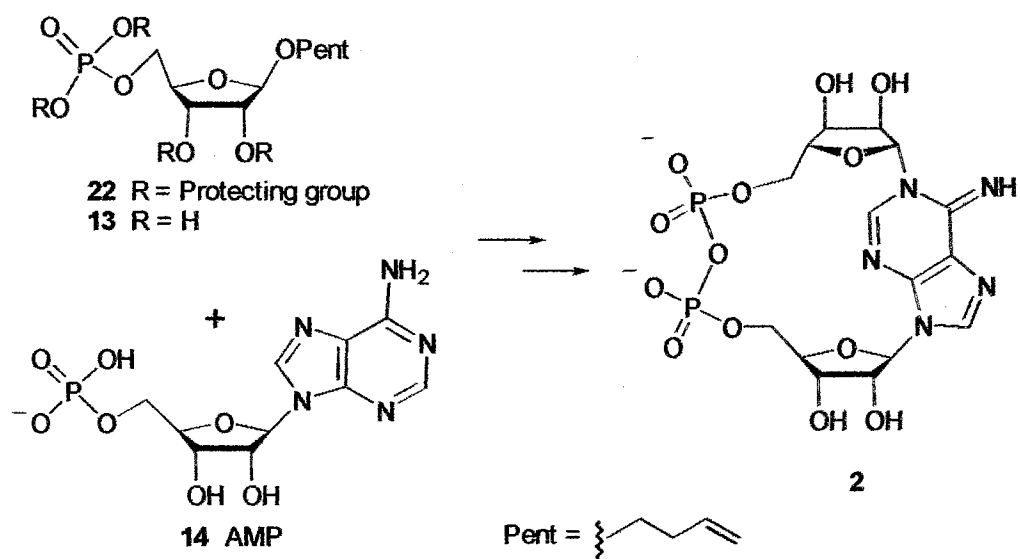
Figure 41. Outline of cADPR formation.
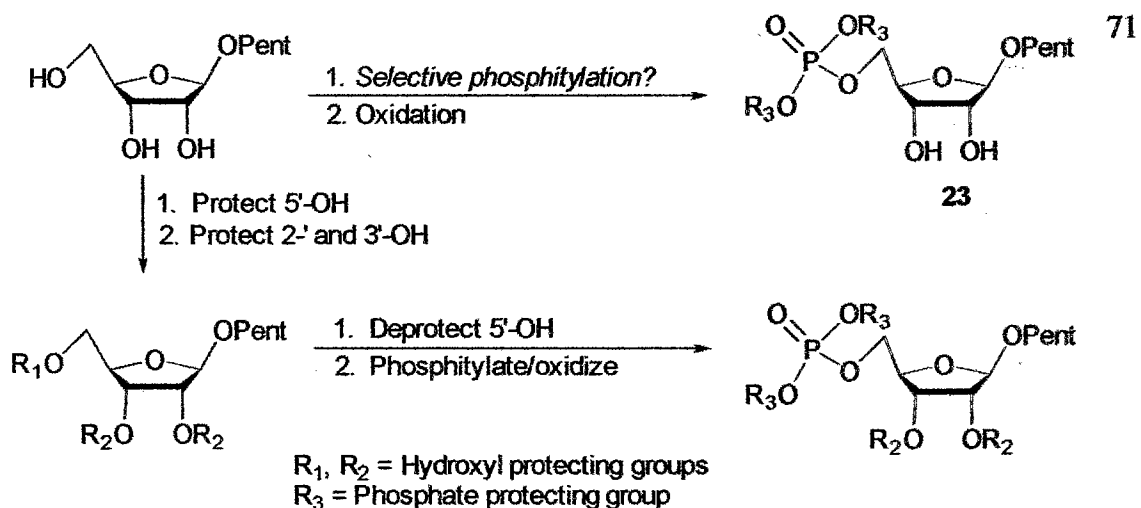
Figure 42. Syntheses of protected phosphates via both selective phosphitylation and a protection strategy.

individually evolved into an entire research study of its own.

The crucial aim of the project was the synthesis of the protected 5'-monophosphate **22** without the use of the previously developed (see Chapter 2) hydroxyl protection strategy (Figure 42). Although the protections may be useful in various syntheses of cADPR and cADPR analogues, the overall protocol possesses several drawbacks. Most prominently, the four-step reaction sequence is expensive in both time and effort. Protecting groups must be chosen in accordance with the functional groups already present in the reacting molecule. The observed yield for the protection strategy is relatively low; even with a yield of 90% for each step in the protection/deprotection procedure, the overall yield of **22** cannot exceed 60%. A successful selective phosphorylation protocol would bypass these obstacles, while providing a substantially simplified synthesis of a suitably protected monophosphate **23**.

Base = adenine, thymidine, uracil, or guanosine
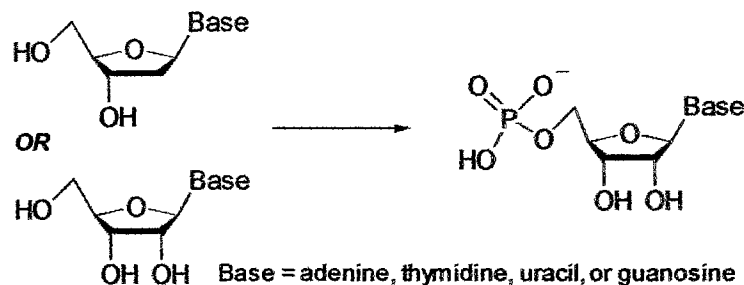
Table I. Literature precedents for selective phosphorylations.

Reagents	Yields	Limitations	Reference
$POCl_3/H_2O$/pyr, CH_3CN	81-99%	No isolation details given; Cleavage of the glycosidic bond in deoxyadenosine and deoxyguanosine.	1
m-cresol, $Cl_2P(O)OPCl_2$	55-85%	Purified by ion exchange	2
$POCl_3/PO(OMe)_3$	55-85%	Purified by ion exchange	3
$P(O)(Cl)(t-Bu)_2$, pyr	53-75%	Tedious workup	4

Historical Background

Several routes have been reported for the selective 5'-phosphorylation of

nucleosides,[1-4] in which phosphoryl chlorides are used as phosphorylating reagents

(Table I). However, several limitations exist for these protocols. The phosphates

produced in these cases are either the anionic or free acid forms, thereby requiring

aqueous ion exchange chromatography for product purification. Syntheses of similar

compounds, via a hydrogen phosphonate approach,[5] also produce charged phosphate

anions and require aqueous purification (Figure 43). In contrast, the previously successful

phosphoramidite method[6] provides a convenient route for monophosphate synthesis, as it

results in fully esterified, neutral phosphotriesters. Due to the resulting organic
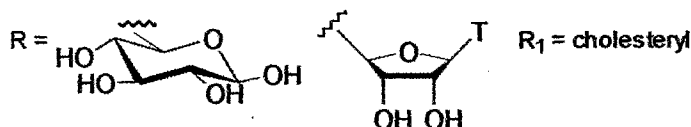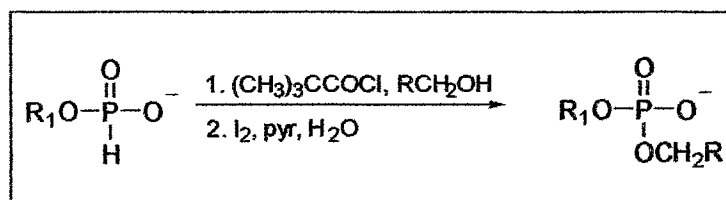
Figure 43. Selective phosphorylation via the hydrogen phosphonate approach.

solubility, the triesters can then be purified relatively easily via standard silica gel

chromatography (Figure 44). [7]

R = cyanoethyl
R$_1$ = methoxyacetyl

neutral molecule - purified
via standard chromatography
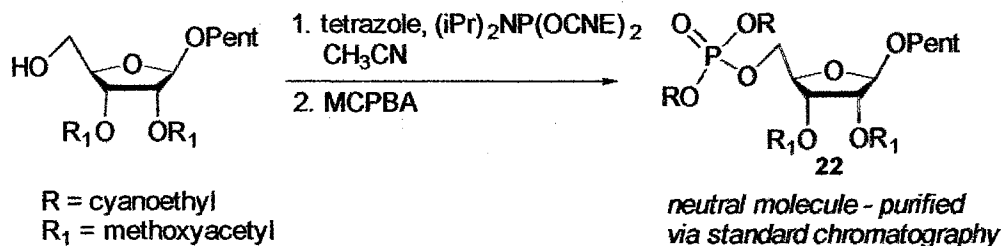
Figure 44. Synthesis of protected phosphate via phosphitylation/oxidation approach.

The successful synthesis of the fully protected 5'-monophosphate **22** via

phosphitylation/oxidation of the protected pentenyl riboside **17** (see Chapter 2) led to the

hypothetical possibility that similar conditions might be used to synthesize the same

compound from its unprotected precursor. The product of this selective phosphitylation

varies slightly in its protections. However, deprotection of **23** should yield the product

13, identical to deprotection of the fully protected phosphate **22** (Figure 45).

Consequently, the developed procedure was varied and optimized in relation to isolated

yield, percent recovery, and selectivity (see below).

R = cyanoethyl
R₁ = methoxyacetyl

22

OR

deprotect (aq. NH₃) →

13

*suitable for coupling
with AMP*

23
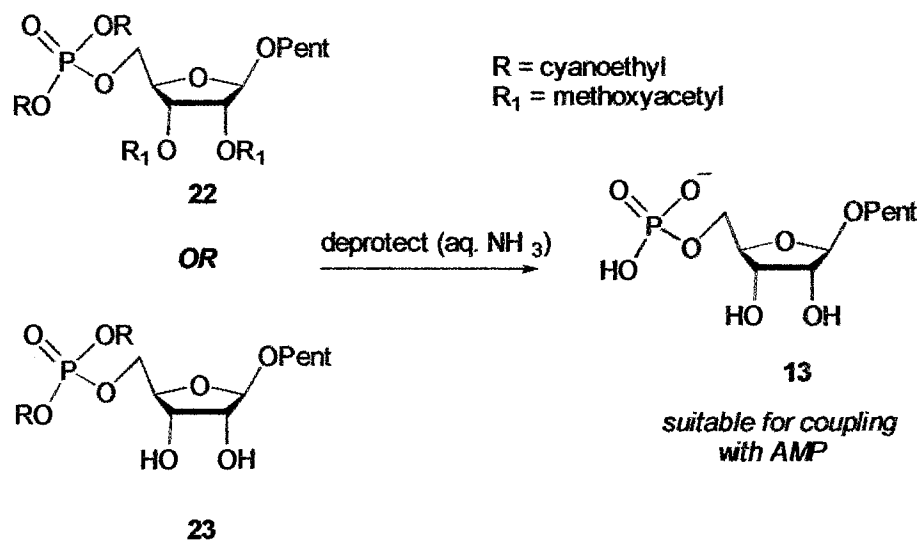
Figure 45. Deprotection of protected phosphates **22** and **23**.

Proposed reaction mechanism and synthetic strategy

The reaction actually proceeds in two basic steps (Figure 46).[8-11] Initial

protonation of the diisopropylamino moiety by tetrazole, in a relatively fast step, leads to

the formation of the diisopropylammonium leaving group. The

tetrazolylphosphoramidite intermediate is then activated towards the relatively slow

nucleophilic attack by a hydroxyl group of the riboside, thereby completing the

phosphitylation step. Once the attack has occurred, subsequent oxidation yields the

phosphorous (V) product **23** (Figure 47).

Given that the nucleophilic attack has been postulated to be the rate-determining

step of the phosphitylation,[8] various experiments were conducted to find optimal

conditions for the production of the desired phosphite. Unfortunately, the phosphite

triester was not observed to be stable enough for isolation. However, conditions were

developed that allowed for both product isolation as well as recovery of unreacted

riboside. Quantification of these compounds was then performed.
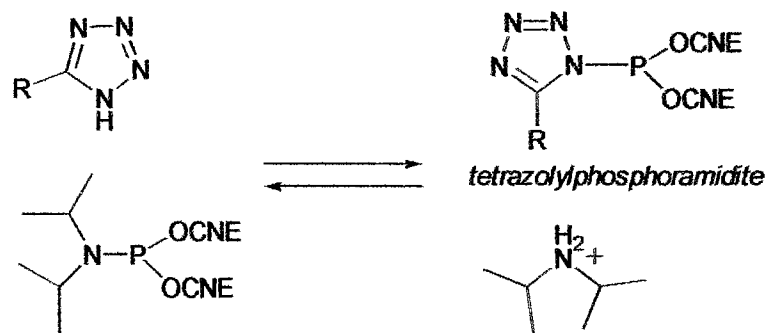
Step 2 - Attack of substrate hydroxyl
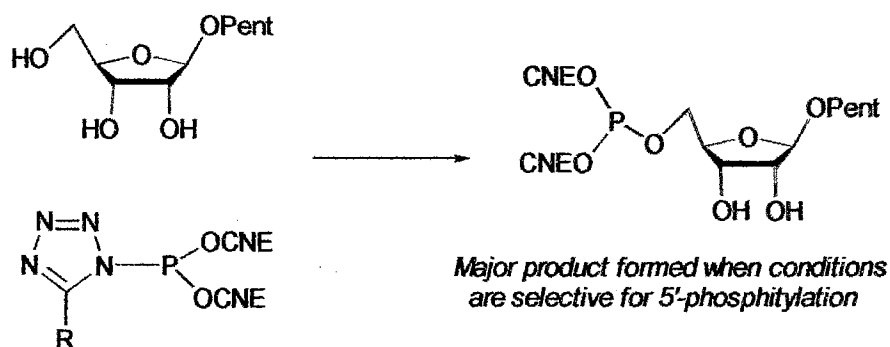
Figure 46. Formation of the phosphite triester.

The following data documented a substantially improved synthetic route to the

desired cADPR precursor. The study also developed an efficient and simple method for

selective phosphitylation of various riboside and carbohydrate substrates. Further

extensions of this work may have integral implications for other carbohydrate-based

syntheses, and in particular, syntheses currently based on hydroxyl protections.
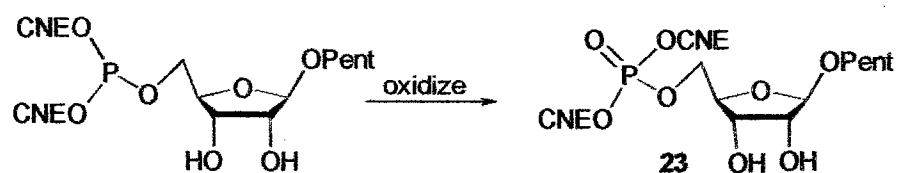
Figure 47. The formation of the phosphate triester **23**.

Results and Discussion

Initial experiments indicated (Table II) that the most integral factor in the selective phosphitylation was temperature. Previous evidence [1,2,4] indicated that low temperatures were necessary for the selective phosphorylation of unprotected ribosides. This is in accord with the current study, in which a selectivity with acceptable yield was observed at –36 °C (Entry 10). These optimal results may be directly related to the effective rate decrease for the secondary versus primary hydroxyl groups in the rate-determining phosphitylation step.
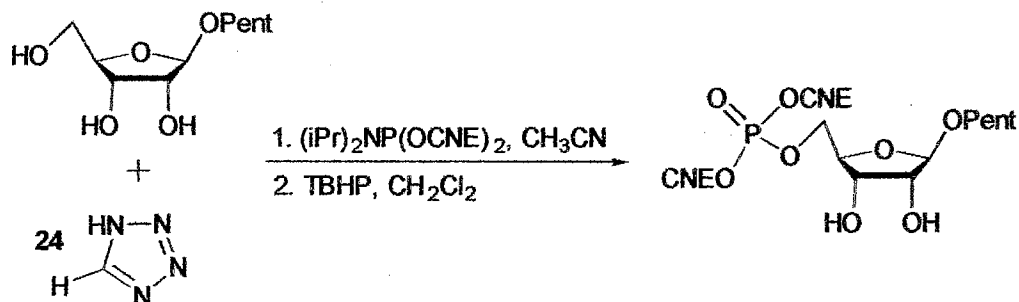
Table II. Selective phosphitylations using a tetrazole catalyst.

Entry	Phosphor-Amidite (eq.)	Addn. Time	Total time	Temp	Isolated yield	Selectivity	% Carb. Recovery
1	1.0	30	50	RT	33%	0.66	50%
2	1.2	26	50	RT	25%	0.43	41%
3	1.4	33	50	RT	36%	0.81	55%
4	1.6	37	50	RT	35%	0.61	43%
5	1.8	43	50	RT	38%	1.15	67%
6	2.0	44	50	RT	34%	0.75	55%
7	0.8	16	50	RT	40%	1.22	73%
8	0.8	16	50	0°C	40%	1.29	75%
9	0.8	16	50	-20°C	33%	1.03	75%
10	0.8	16	50	-36°C	31%	1.73	86%

While inferior results (Entries 1-9) were obtained at higher temperatures (0-25 °C), poor results were also observed at lower temperatures. Regardless of the desired phosphitylation rate decrease, temperatures lower than –36 °C present considerable solubility challenges, most substantially for the tetrazole. Under the developed conditions, the phosphitylation is run at the lower limit of solubility for the tetrazole catalyst. This low temperature is also near the freezing point of the acetonitrile solvent (~–42 °C).

In addition to temperature, the phosphoramidite reagent proved to be an instrumental consideration for the observed selective phosphitylation. The identity of the phosphoramidite, the procedure for its addition, and the stoichiometry of the added reagent were all investigated. Optimal results were obtained (Entries 7-10) with 0.8 equivalents (relative to the unprotected riboside) of the phosphoramidite, added gradually as a solution. Although different phosphoramidites[12-15] were observed in the study, the bis(cyanoethyl)-N,N-diisopropylaminophosphoramidite[13] remained the focal point, due to its desirable deprotection in subsequent steps.

Different substituted tetrazole derivatives were also studied, with hopes of improving yield and/or selectivity. In addition to tetrazole (24, Table II) itself, methylthio tetrazole (25, MTT, Table III)[18] and 5-p-nitrophenyl tetrazole (26, NPT)[16, 17] were used as catalysts for the formation of the intermediate phosphoramidite. The resultant MT- or NP-tetrazolylphosphoramidite was then subjected to nucleophilic attack by the unprotected hydroxyls of the riboside. Results indicated (Table III) that the chemical structures of the substituted tetrazolyl phosphoramidites provided enough steric

1. (iPr)$_2$NP(OCNE)$_2$, CH$_3$CN

2. TBHP, CH$_2$Cl$_2$
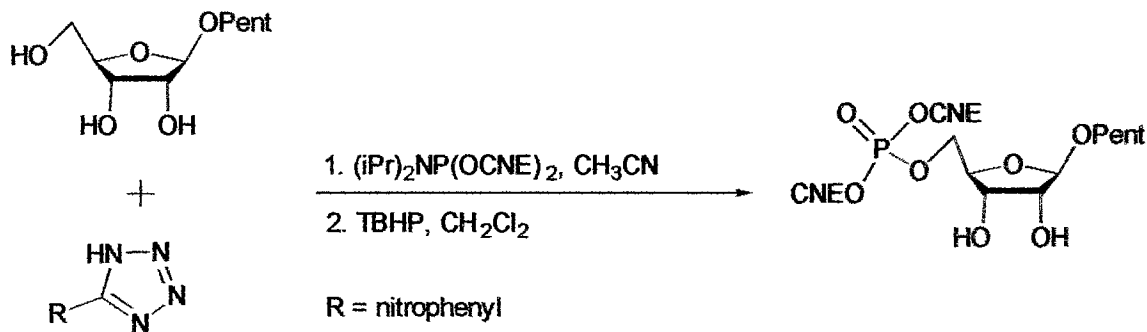
R = nitrophenyl

Table III. Selective phosphitylations using the 5-*p*-nitrophenyl (NPT)catalyst.

Entry	Phosphor-Amidite (eq.)	Addn. time	Total Time	Temp	Isolated yield	Selectivity	% Carb. Recovery
1	0.8	20	25	-36°C	59%	2.48	81%
2	0.8	16	300	-36°C	57%	2.66	82%
3	0.8	16	50	-36°C	60%	3.04	83%
4	1.0	35	75	-36°C	23%	0.77	71%
5	1.0	16	180	-36°C	31%	1.28	76%
6	0.8	16	50	0°C	50%	1.47	70%
7	0.8	20	25	-36°C	55%	5.23	92%
8	0.8	60	60	-36°C	54%	3.11	86%

Lastly, the identity of the oxidant was examined. Various control studies indicated that, while either of the two utilized oxidants (*tert*-butyl hydroperoxide, TBHP, or *meta*-chloroperoxybenzoic acid, MCPBA) would work, TBHP afforded slightly better results, in terms of starting material recovery. Accordingly, even though MCPBA remained an effective oxidant for oxidation of the phosphite in the protection strategy, TBHP was utilized in the selective phosphorylation attempts.

Preliminary results indicated that, despite its role as the rate-limiting step, the initial phosphitylation of the unprotected riboside was a relatively fast reaction, presumed complete in 25 minutes. A comparison of various times of reagent addition illustrates that the reaction appears to be complete soon after all of the phosphitylating reagent is added (Table III, Entries 1-4 and 8).

The optimal phosphitylation (Entries 1 and 7) was not performed under conditions dependent on the rate of addition for the phosphoramidite reagent. It was observed that the operative factor in the phosphoramidite's addition was not the actual time of addition, but rather the temperature of the phosphitylation reaction. Results indicate that phosphitylations run at temperatures above –36 °C produced a lower selectivity and carbohydrate recovery (Entry 6). Additionally, increases in the phosphitylation reaction time provided no major improvements in selectivity (Entries 2, 3, 6 and 9). Stoichiometric variations also produced inferior results (Entries 4 and 5).

Substantial improvements were noticed upon careful manipulation of the reaction workup procedure. Initial phosphitylation trials utilized a standard organic and aqueous phase workup. However, a crucial control study indicated that both the isolated product and the carbohydrate starting material demonstrated appreciable solubility in aqueous solvents. As a result, the standard workup was eliminated altogether. The post-oxidation reaction solution is instead evaporated down to a minimum volume (around 10 percent of the reaction volume), filtered to remove excess tetrazole, and loaded directly onto a silica gel column. The issue of extra water-soluble impurities provides little challenge; any remaining tetrazole can be quantified (and corrected for) using standard ^{1}H-NMR analysis, and residual starting carbohydrate can be easily recovered by chromatography.

Quantification of the phosphitylation results presented an initial challenge, in that a consistent and representative calculation of yield and selectivity had to be derived. This relationship was further complicated by the difficulty experienced in isolating undesired side products (poly-phosphitylated products and/or products which were phospitylated at one of the secondary hydroxyls). Therefore, it was deemed useful to establish both
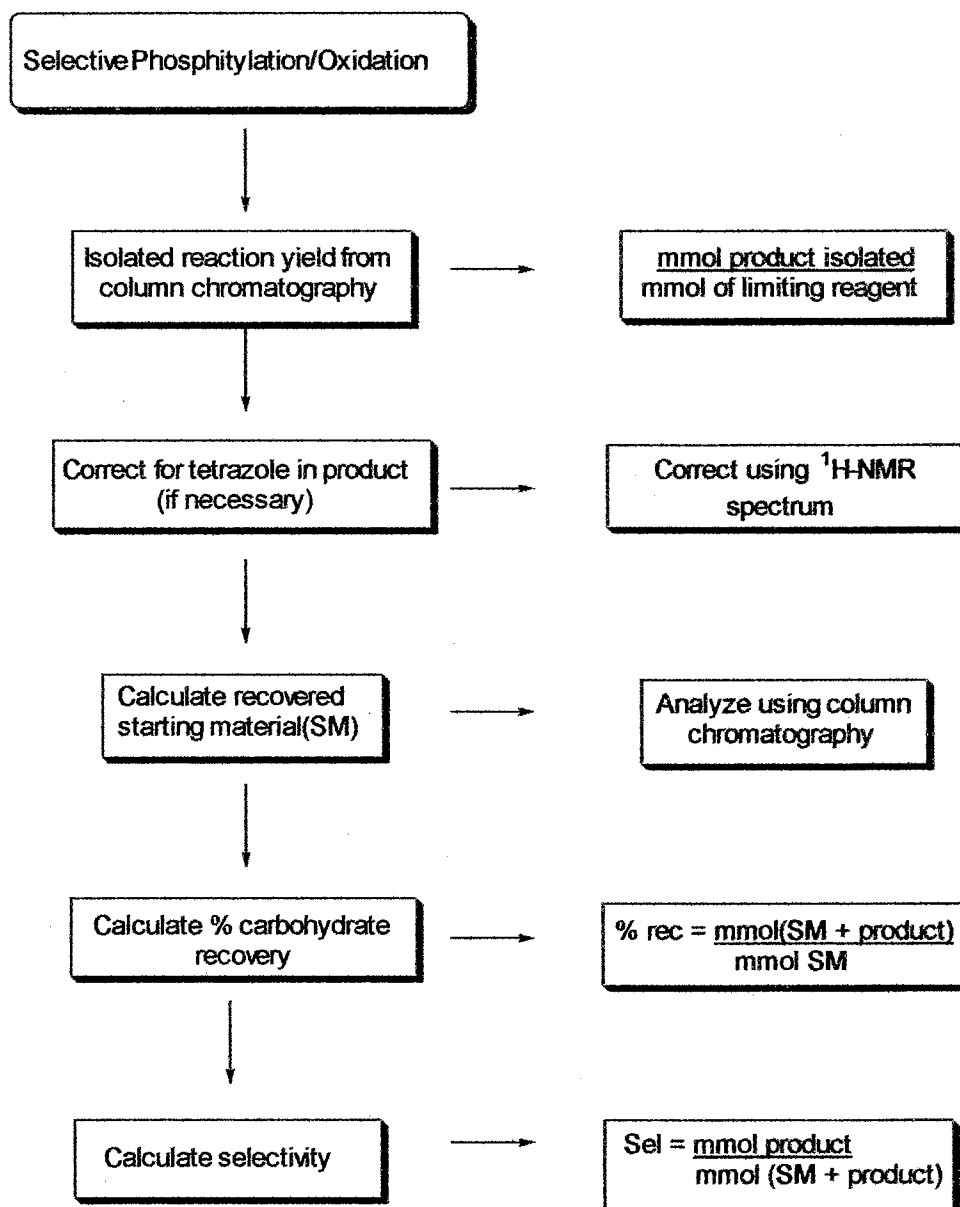
Figure 48. Calculation flow chart for selective phosphitylation data.

overall yield of the reaction as well as carbohydrate/nucleoside recovery (Figure 48). 'Missing' material was assumed to be undesired side products, which determined the overall recovery for the reaction trial. Once the isolated yield and recovery had been calculated, selectivity was then computed via the ratio of desired product versus the undesired product(s). Further improvements to the yield and selectivity could then be

established by correcting for the amount of starting carbohydrate recovered (the amount of starting material that did not react at all).

Product identity was confirmed using mainly spectroscopic techniques. One dimensional ^{1}H-NMR verified product purity, while providing the necessary integration for a tetrazole correction (small amounts of the various tetrazoles often remained in the isolated products). Subsequent ^{13}C-NMR offered further information regarding purity; however, ^{13}C-NMR analysis was most effective in determining the actual site of phosphitylation. Due to an observable ^{13}C-^{31}P coupling, the position of the phosphate could be easily confirmed by the presence of a doublet in the ^{13}C-NMR spectrum. This was usually accompanied by a slight downfield shift for the phosphorylated carbon. Further confirmation was available using the Attached Proton Test (APT), which separated methine and methyl carbons from methylene and quaternary carbons.

Product purity was also tested using one-dimensional ^{31}P-NMR experiments. A standard spectrum verified the presence of only one phosphate in the product. If necessary, ^{1}H-coupled ^{31}P experiments further confirmed the position of phosphate attachment.

Optimal yields and selectivities were observed under very specific conditions
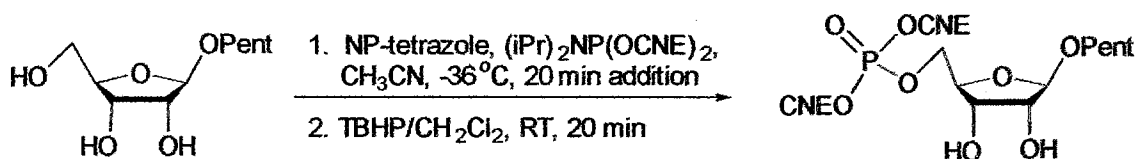
Workup: evaporate reaction solvent to minimum volume
Purification: standard column chromatography

Figure 49. Optimized conditions for selective phosphitylation/oxidation.

(Figure 49). The temperature for the phosphitylation was maintained at –36 °C, while

the phosphoramidite was added gradually over 20 minutes. Following a short interval of

stirring at –36 °C, the temperature was raised to room temperature, and the oxidant was

added. Twenty minutes later, the reaction solution was evaporated to a minimum volume

and loaded directly onto a silica gel column. Final results were determined by the

outcome of the chromatography step.

Despite the apparent success of the phosphitylation using tetrazole, vastly

improved yields and selectivities were observed with the use of the substituted tetrazoles

(Figure 50). As reported in Table II, the unsubstituted tetrazole afforded moderate yields

and selectivity, limited to 40% and 1.3, respectively. However, both nitrophenyl

tetrazole (26, Table III) and methylthiotetrazole (25) provided substantially enhanced

results, including 59-62% isolated yields with selectivities of 2.5-3.7.

The superior results for the substituted tetrazoles indicate that the nature of

substitution plays a key role in either the protonation and/or nucleophilic substitution

reaction of the phosphitylation, thereby effecting a certain selectivity. It is intriguing that

increasing acidity/decreasing pKa
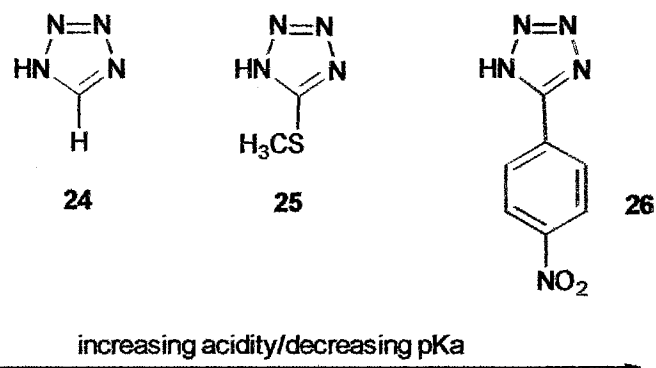
Figure 50. The three tetrazoles used in this study.

the methylthio and nitrophenyl derivatives possess a greater acidity than tetrazole (24),

due to the enhanced stabilities of the according conjugate bases. Appropriately, it is thus

reasonable to expect that protonation of the diisopropylamino functionality will proceed

more quickly with the substituted derivatives. However, this still does not account for the

selectivity of the phosphitylation itself. In this case, it is possible that steric factors

differentially facilitate the nucleophilic attack of the primary hydroxyl with the
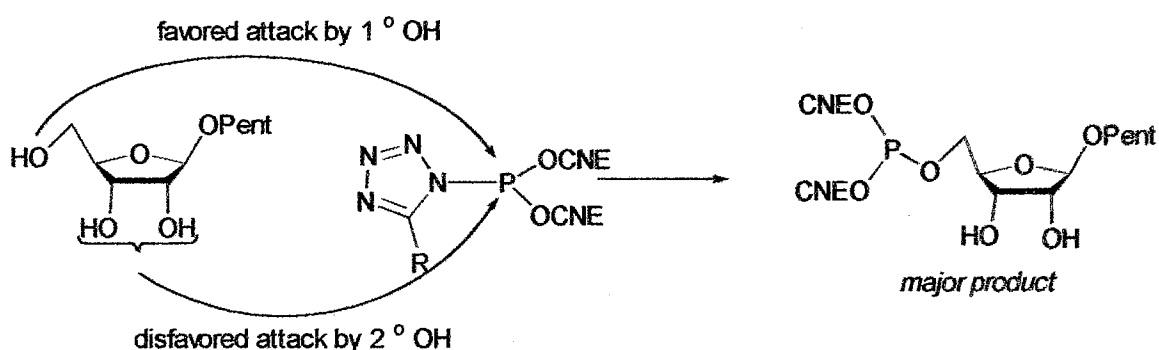
Figure 51. Rationale behind selective phosphitylation.

methylthio- or nitrophenyl tetrazolyl phosphoramidite intermediate, relative to the

same attack by any of the secondary hydroxyl groups (Figure 51).

Once optimal conditions had been determined, they were applied to a variety of

riboside and carbohydrate substrates. In addition to the central β-pentenyl riboside 17, [19]

other substrates included the α-pentenyl riboside 16[19] as well as glucopyranoside and 2'-

deoxy[20] derivatives (27 and 28, Figure 52). The reactions produced very respectable

isolated yields (54 – 69%).

Further research into this phosphitylation would potentially produce additional

β – pentenyl riboside 17   16

27   28
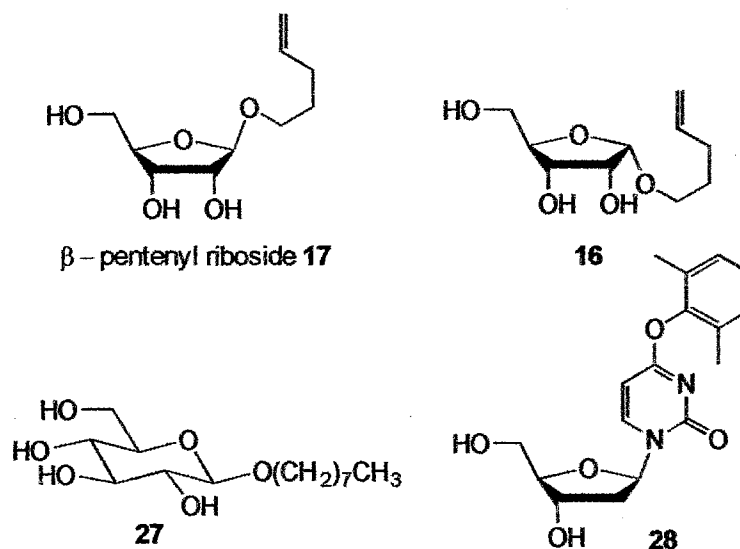
Figure 52. Substrates used in the present study.

insights into the mechanism and observed selectivity. One key focus of such

investigations could be a more detailed study of the steric factors involved. A potentially

important study would employ other substituted tetrazoles as phosphitylation catalysts.

Moreover, successful phosphitylations in other solvents[21] might produce effective

conditions for a larger variety of substrates, including nucleosides and more polar organic

compounds. Finally, the development of a spectroscopic protocol using ^{1}H- and ^{31}P-

NMR analyses to follow the phosphitylation and oxidation, would provide valuable

information regarding mechanism, rate, and side product formation.

Experimental Section

General. Acetonitrile was distilled from CaH_2. Carbohydrates 16 and 17[19] and

phosphoramidite 22[12, 13] were prepared as described. The synthesis of nucleoside 28 will

be reported in due course.[20] All other carbohydrates and reagents were commercially

available. The starting carbohydrate and tetrazole were dried together by evaporating

three times from dry acetonitrile. All reactions were performed under an atmosphere

of dry nitrogen; solutions of phosphoramidites in CH₃CN were added to the reaction

using a syringe pump and gastight syringes. ^{1}H (300 MHz) and ^{13}C (75 MHz) NMR

spectra were obtained in CDCl₃ solvent and referenced to internal tetramethylsilane or the

residual solvent peak unless otherwise stated; ^{31}P NMR spectra were referenced to

external 85% H₃PO₄ in D₂O. The proton and carbon assignments for **23** were made with

the aid of DQF COSY and HMQC spectra (not shown); the assignments for the

remaining compounds are in accord with these assignments but should be regarded as

tentative. In all cases, identification of the primary hydroxyl group as the site of

phosphorylation was confirmed using the Attached Proton Test as described in the

discussion.
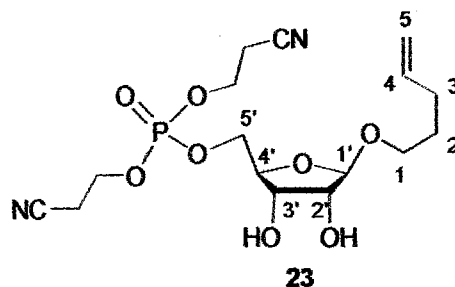
Bis(2-cyanoethyl) (pent-4-enyl β-D-ribofuranos-5-yl) phosphate (23). To a stirred

solution of pent-4-enyl β-D-ribofuranoside (**17**, 91 mg, 0.42 mmol) and 5-(*p*-nitrophenyl-

1*H*-tetrazole (5-NPT, **26**, 185 mg, 0.97 mmol) in CH₃CN (17 mL) at -36 °C was added

dropwise (0.02 mmol/min) a 0.45 M solution of bis(2-cyanoethyl)-*N,N*-

diisopropylaminophosphoramidite (**22**, 0.73 mL, 0.33 mmol) in CH₃CN, and the resulting

solution was stirred for 20 minutes. A 0.95 M solution of *tert*-butyl hydroperoxide

(TBHP, 4.0 mL, 3.8 mmol) in CH₂Cl₂ was then added, and the reaction was warmed to

room temperature with a water bath. After stirring for 20 minutes, the reaction

solution was evaporated to a small volume (~2-4 mL) and diluted with an equal volume

of CH_2Cl_2. The crude product was then loaded onto a silica gel column and eluted with a

step gradient of 60:40 CH_2Cl_2:ethyl acetate (MC:EA) to 100:0 MC:EA, followed by

90:10 EA:EtOH, yielding phosphate **23** (0.20 mmol, 59 % based on limiting

phosphoramidite; 81% based on total recovered carbohydrate) and recovered starting

material (**17**, 0.14 mmol).

^{1}H-NMR (**23**, δ, 600 MHz):

5.807 (ddt, J = 17.1, 13.2, 6.6 Hz, 1H, H4)

5.028 (dq, J = 17.1, 1.6 Hz, 1H, H5)

4.976 (ddt, J = 10.3, 2.0, 1.3 Hz, 1H, H5)

4.942 (s, 1H, H1')

4.328 (dt, J = 8.1, 6.1 Hz, 2H, CH_2CH_2CN)

4.325 (dt, J = 8.1, 6.1 Hz, 2H, CH_2CH_2CN)

4.290 (ddd, J = 10.9, 8.2, 4.5 Hz, 1H, H5' or H5")

4.262 (t, J = 5.3 Hz, 1H, H3')

4.216 (ddd, J = 10.9, 9.1, 5.9 Hz, 1H, H5' or H5")

4.145 (app. q, J ~ 6.2 Hz, 1H, H4')

4.030 (d, J = 4.9 Hz, 1H, H2')

3.719 (dt, J = 9.6, 6.6 Hz, 1H, H1)

3.563 (s, 1H, OH)

3.409 (dt, J = 9.6, 6.6 Hz, 1H, H1)

3.209 (s, 1H, OH)

2.807 (td, J = 6.1, 1.0 Hz, 4H, 2 x CH$_2$$CH_2$CN)

2.100 (q, J = 7.0 Hz, 2H, H3)

1.655 (quin, J = 6.6 Hz, 2H, H2)

^{13}C-NMR (23, δ, 150 MHz):

138.097 (C4)

116.578 (CH$_2$CH$_2$$C$N)

115.045 (C5)

107.366 (C1')

80.992 (d, $^{3}J_{POCC}$ = 6.9 Hz, C4')

75.027 (C2')

71.931 (C3')

69.701 (d, $^{2}J_{POC}$ = 6.0 Hz, C5')

67.561 (C1)

62.469 (d, $^{2}J_{POC}$ = 5.7 Hz, CH_2CH$_2$CN)

30.062 (C3)

28.575 (C2)

19.583 (d, $^{3}J_{POCC}$ = 8.0 Hz, CH$_2$$CH_2$CN)

^{31}P-NMR (δ, 162 MHz):

-0.550.

29

Bis(2-cyanoethyl) (pent-4-enyl α-D-ribofuranos-5-yl) phosphate (29). To a

stirred solution of pentenyl α-D-riboside **16** (71.9 mg, 0.33 mmol) and 5-NPT (**26**, 151.2

mg, 0.79 mmol) in CH_3CN (17 mL) at -36 °C was added dropwise (0.02 mmol/min) a

0.47 M solution of phosphoramidite **22** (530 μL, 0.25 mmol) in CH_3CN. After the

addition the resulting solution was stirred for an additional 20 minutes at -36 °C. A 0.95

M TBHP solution (1.3 mL, 1.2 mmol) in CH_2Cl_2 was then added, and the reaction

temperature was raised to room temperature and stirred for 20 minutes. The reaction

solution was then evaporated to a minimum volume (~2-4 mL) and diluted with an equal

volume of CH_2Cl_2. The crude product was then loaded onto a silica gel column and

eluted as described above, yielding phosphate **29** (0.14 mmol, 55% based on limiting

phosphoramidite; 92% based on total recovered carbohydrate) and recovered starting

material (**16**, 0.17 mmol).

^{1}H-NMR (**29**, δ, 400 MHz):

5.792 (ddt, J = 17.0, 13.2, 6.6 Hz, 1H, H4)

5.06-4.95 (m, 3H, =CH_2 and H1')

4.33-4.23 (m, 6H, H5', H5" 2 x CH_2CH_2CN)

4.13-4.06 (m, 2H, H4', H3')

3.951 (dd, J = 6.6, 4.4 Hz, 1H, H2')

3.813 (dt, J = 9.8, 6.6 Hz, 1H, H1)

3.520 (dt, J = 9.6, 6.6 Hz, 1H, H1)

3.02 (bs, 2H, 2 x OH)

2.785 (tt, J = 6.1, 1.0 Hz, 4H, 2 x CH$_2$$CH_2$CN)

2.114 (app. q, J ~ 6.6 Hz, 2H, H3)

1.713 (app. quint., J ~ 6.7 Hz, 2H, H2)

^{13}C-NMR (29, δ, 100 MHz):

137.900 (C4)

116.441 (CH$_2$CH$_2$$C$N)

115.167 (C5)

101.569 (C1')

81.917 (d, $^3J_{CCOP}$ = 6.8 Hz, C4')

70.899 (C2')

70.186 (C3')

68.077 (C1)

67.872 (d, $^2J_{COP}$ = 5.7 Hz, C5')

62.364 (d, $^2J_{COP}$ = 5.7 Hz, CH_2CH$_2$CN)

30.077 (C3)

28.484 (C2)

19.522 (d, $^3J_{CCOP}$ = 8.0 Hz, CH$_2$$CH_2$CN)

^{31}P-NMR (**29**, δ, 162 MHz):

-4.6.

30
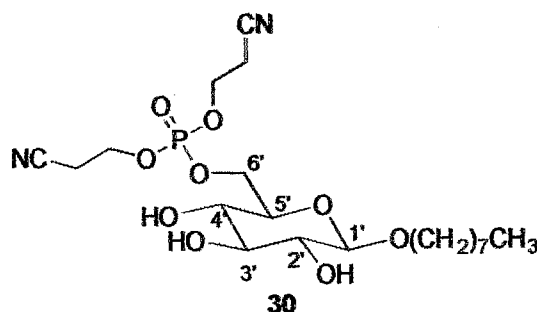
Bis(2-cyanoethyl) (*n*-octyl β-D-glucopyranos-5-yl) phosphate (30). To a stirred

solution of *n*-octyl β-D-glucopyranoside (**27**, 115.2 mg, 0.39 mmol) and 5-NPT (**26**,

182.4 mg, 0.95 mmol) in CH$_3$CN (30 mL) at -36 °C was added dropwise (0.02

mmol/min) a 0.43 M solution of phosphoramidite **22** (760 μL, 0.33 mmol) in CH$_3$CN.

After the addition the resulting solution was stirred for an additional 20 minutes at -36 °C.

A 0.88 M solution of TBHP (1.8 mL, 1.4 mmol) in CH$_2$Cl$_2$ was then added, and the

reaction temperature was raised to room temperature and stirred for 20 minutes. The

reaction solution was then evaporated to a minimum volume (~2-4 mL) and diluted with

an equal volume of CH$_2$Cl$_2$. The crude product was then loaded onto a silica gel column

and eluted as described above, yielding phosphate **30** (0.18 mmol, 54% based on limiting

phosphoramidite; 91% based on total recovered carbohydrate) and recovered starting

material (**1c**, 0.18 mmol).

^{1}H-NMR (**30**, δ, 600 MHz, DMSO-d$_6$ + D$_2$O):

4.296 (ddd, *J* = 11.0, 6.3, 1.6 Hz, 1H, H6' or H6")

4.26-4.19 (m, 5H, CH_2CH_2CN and H1')

4.131 (ddd, J = 11.0, 7.9, 5.6 Hz, 1H, H6' or H6")

3.732 [dt, J = 9.6, 6.8 Hz, 1H, $CH_2(CH_2)_6CH_3$]

3.457 [dt, J = 9.6, 6.8 Hz, 1H, $CH_2(CH_2)_6CH_3$]

3.41-3.37 (m, 1H, H5')

3.208 (t, 1H, J = 9.0 Hz)

3.119 (app. t, J ~ 9.4 Hz), and 2.990 (dd, J = 9.0, 7.9 Hz) [(3H, H2', H3', and H4')]

2.925 (t, J = 5.6 Hz, 4H, 2 x CH_2CN)

1.508 [quint, J = 7.1 Hz, 2H, $CH_2CH_2(CH_2)_5CH_3$]

1.274 [bs, 10H, $CH_2CH_2(CH_2)_5CH_3$]

0.861 (t, 3H, J = 6.6 Hz, CH_3)

In a sample without D_2O the following were observed:

5.225 (bs, 1H, OH)

5.066 (bs, 2H, 2 x OH)

^{13}C-NMR (30, δ, 150 MHz, DMSO-d₆):

118.778 (CN)

103.355 (C1')

76.751 (C3')

74.573 (d, $^3J_{CCOP}$ = 6.0 Hz, C5')

73.785 (C4')

69.840, 69.688 [C2' and $CH_2(CH_2)_6CH_3$]

68.004 (d, $^2J_{COP}$ = 5.0 Hz, C6')

63.184 (d, $^2J_{COP}$ = 5.0 Hz, CH_2CH$_2$CN)

63.181 (d, $^2J_{COP}$ = 5.0 Hz, CH_2CH$_2$CN)

31.924, 29.891, 29.512, 29.337, 26.136, 22.783 (octyl CH$_2$'s)

19.692 (d, $^3J_{CCOP}$ = 6.9 Hz, CH_2CN)

14.643 (CH$_3$)

^{31}P-NMR (30, δ, 162 MHz, DMSO-d$_6$):

0.317.
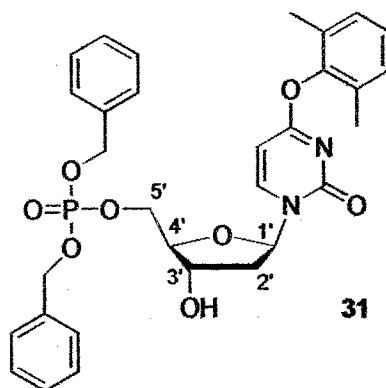
Dibenzyl (4-*O*-(2,6-dimethylphenyl)-2'-deoxyuridin-5'-yl) phosphate (31). To a
stirred solution of 4-*O*-(2,6-dimethylphenyl)-2'-deoxyuridine (**28**, 166.8 mg, 0.50 mmol)
and 5-NPT (**26**, 198 mg, 1.04 mmol) in CH$_3$CN (40 mL) at -36 °C was added dropwise
(0.02 mmol/min) a 0.47 M solution of dibenzyl-*N*,*N*-diisopropylaminophosphoramidite
(890 μL, 0.42 mmol) in CH$_3$CN. After the addition the resulting solution was stirred for
an additional 20 minutes at -36 °C. A 0.77 M solution of TBHP (2.3 mL, 1.7 mmol) in
CH$_2$Cl$_2$ was then added, and the reaction temperature was raised to room temperature and
stirred for 20 minutes. The reaction solution was then evaporated to a minimum volume
(~2-4 mL) and diluted with an equal volume of CH$_2$Cl$_2$. After the suspended solid was

removed by filtration through a bed of sand, the crude product was loaded onto a silica

gel column and eluted as described above, yielding phosphate **31** (0.29 mmol, 69% based

on limiting phosphoramidite; 75% based on total recovered carbohydrate) and recovered

starting material (**28**, 0.09 mmol).

^{1}H-NMR (**31**, δ, 400 MHz):

8.007 (d, $J = 7.4$ Hz, 1H, H6)

7.39-7.32 (m, 10H, 2 x CH_2Ph)

7.036 (s, 3H, Me_2ArH_3)

6.191 (t, $J = 6.1$ Hz, 1H, H1')

5.880 (d, $J = 7.4$ Hz, 1H, H5)

5.10-5.00 (m, 4H, 2 x CH_2Ph)

4.24-4.12 (m, 3H, H3', H5', H5")

4.043 (app. quintet, $J \sim 3.3$ Hz, 1H, H4')

3.4-3.0 (bs, 1H, OH)

2.507 (ddd, $J = 13.8, 6.0, 4.7$ Hz, 1H, H2' or H2")

2.101 [s, 6H, $Ar(CH_3)_2$]

1.911 (dt, $J = 13.8, 6.4$ Hz, 1H, H2' or H2")

^{13}C-NMR (**31**, δ, 100 MHz):

170.655, 155.544, 148.990, 143.885 (C6)

135.924 (d, $^3J_{CCOP} = 6.9$ Hz, benzyl C1)

130.116, 128.857, 128.834, 128.690, 128.675, 128.045, 128.008 (Ar CH)

125.868 (DMP C4)

94.303 (C5)

86.801 (C1')

84.784 (d, $^3J_{CCOP}$ = 7.6 Hz, C4')

70.097 (C3')

69.728 (d, $^2J_{COP}$ = 5.3 Hz, CH$_2$Ph)

69.699 (d, $^2J_{COP}$ = 5.3 Hz, CH$_2$Ph)

66.558 (d, $^2J_{COP}$ = 5.3 Hz, C5')

41.179 (C2')

16.389 (ArMe_2)

^{31}P-NMR (**31**, δ, 162 MHz):

-4.18.

32
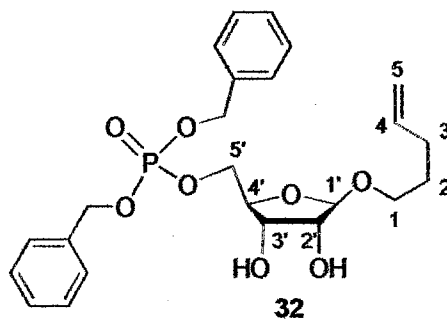
Dibenzyl (pent-4-enyl β-D-ribofuranos-5-yl) phosphate (32). To a stirred solution

of pentenyl β-D-riboside **17** (80.8 mg, 0.37 mmol) and 5-NPT (**26**, 167.7 mg, 0.88 mmol)

in CH$_3$CN (17 mL) at -36 °C was added dropwise (0.02 mmol/min) a 0.38 M solution of

dibenzyl-N,N-diisopropylaminophosphoramidite (650 µL, 0.25 mmol) in CH$_3$CN. After

the addition the resulting solution was stirred for an additional 20 minutes at -36 °C. A 0.95 M solution of TBHP (675 µL, 0.64 mmol) in CH_2Cl_2 was then added, and the reaction temperature was raised to room temperature and stirred for 20 minutes. The reaction solution was then evaporated to a minimum volume (~2-4 mL) and diluted with an equal volume of CH_2Cl_2. The crude product was then loaded onto a silica gel column and eluted as described above, yielding phosphate **32** (0.17 mmol, 70% based on limiting phosphoramidite; 80% based on total recovered carbohydrate) and recovered starting material (**17**, 0.12 mmol).

^{1}H-NMR (**32**, δ, 400 MHz):

7.4-7.2 (m, 10H, 2 x Ph)

5.758 (ddt, J = 16.9, 13.3, 6.7 Hz, 1H, H4)

5.047 (d, J = 8.2 Hz, 2H, CH_2Ph)

5.043 (d, J = 8.1 Hz, 2H, CH_2Ph)

5.02-4.92 (m, 2H, CH_2, overlap with CH_2Ph and H1')

4.918 (s, 1H, H1')

4.219 (t, 1H, J = 5.4 Hz, H3')

4.10-4.07 (m, 3H, H4', H5', H5")

4.014 (d, J = 4.7 Hz, 1H, H2')

3.881 (bs, 1H, OH)

3.647 (dt, J = 9.6, 6.6 Hz, 1H, H1)

3.344 (dt, J = 9.6, 6.6 Hz, 1H, H1)

3.130 (bs, 1H, OH)

2.031 (qt, J = 6.6, 1.2 Hz, 2H, H3)

1.583 (quin, J = 6.6 Hz, 2H, H2)

^{13}C-NMR (**32**, δ, 100 MHz):

138.036 (C4)

135.411 (d, $^3J_{CCOP}$ = 5.7 Hz, benzyl C1)

128.779, 128.703, 128.066, 124.348 (Ar CH)

114.909 (C5)

107.215 (C1')

81.098 (d, $^3J_{CCOP}$ = 7.6 Hz, C4')

75.103 (C2')

71.947 (C3')

69.693 (d, $^2J_{COP}$ = 5.7 Hz, C5')

68.790 (d, $^2J_{COP}$ = 6.9 Hz, CH_2Ph)

67.318 (C1)

30.112 (C3)

28.572 (C2)

^{31}P-NMR (**32**, δ, 162 MHz):

-3.438.

23
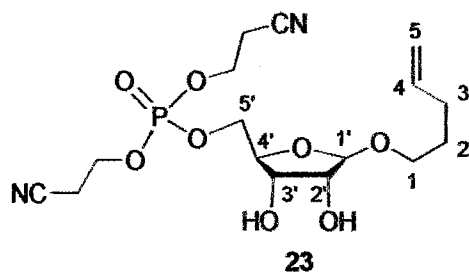
Preparation of phosphate 23 using 5-methylthio-1*H*-tetrazole (5-MTT, 25). To a stirred solution of pentenyl β-D-riboside **17** (91.2 mg, 0.42 mmol) and 5-MTT (117.3 mg, 1.01 mmol) in CH_3CN (20.5 mL) at -36 °C was added dropwise (0.02 mmol/min) a 0.40 M solution of bis(cyanoethyl)-*N,N*-diisopropylaminophosphoramidite (825 μL, 0.33 mmol) in CH_3CN. After the addition the resulting solution was stirred for an additional 20 minutes at -36 °C. A 1.1 M solution of TBHP (3.5 mL, 3.85 mmol) in CH_2Cl_2 was then added, and the reaction temperature was raised to room temperature and stirred for 20 minutes. The reaction solution was then evaporated to a minimum volume (~2-4 mL) and diluted with an equal volume of CH_2Cl_2. The crude product was then loaded onto a silica gel column and eluted as described above, yielding phosphate **23** (0.20 mmol, 62% based on limiting phosphoramidite; 87% based on total recovered carbohydrate) and recovered starting material (**17**, 0.16 mmol). The obtained product was spectroscopically equivalent to the previously-obtained phosphate **23** (see above spectral information).

23
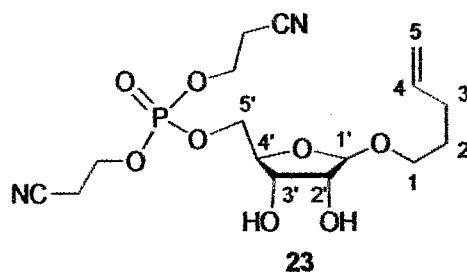
Preparation of phosphate 23 using 1*H*-tetrazole (24). To a stirred solution of

pentenyl β-D-riboside **17** (68.8 mg, 0.32 mmol) and tetrazole (**24**, 55.1 mg, 0.79 mmol) in

CH$_3$CN (20.5 mL) at -36 °C was added dropwise (0.02 mmol/min) a 0.40 M solution of

bis(cyanoethyl)-*N*,*N*-diispropylamino phosphoramidite (625 µL, 0.25 mmol) in CH$_3$CN.

After the addition the resulting solution was stirred for an additional 50 minutes at -36 °C.

A 0.94 M solution of TBHP (0.6 mL, 0.6 mmol) in CH$_2$Cl$_2$ was then added, and the

reaction temperature was raised to room temperature and stirred for 20 minutes. The

reaction solution was then evaporated to a minimum volume (~2-4 mL) and diluted with

an equal volume of CH$_2$Cl$_2$. The crude product was then loaded onto a silica gel column

and eluted as described above, yielding phosphate **23** (0.08 mmol, 31% based on limiting

phosphoramidite; 86% based on total recovered carbohydrate) and recovered starting

material (**17**, 0.20 mmol). The obtained product was spectroscopically equivalent to the

previously-obtained phosphate **23** (see above spectral information).

23
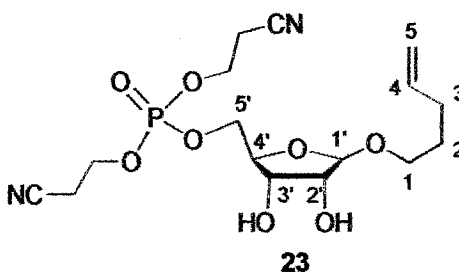
Preparation of phosphate 23 (large scale). To a stirred solution of pentenyl β-

D-riboside **17** (1.02 g, 4.7 mmol) and 5-NPT (**26**, 2.13 g, 11.1 mmol) in CH₃CN (230

mL) at -36 °C was added dropwise (0.2 mmol/min) a 0.5 M solution of bis(cyanoethyl)-

N,N-diisopropylamino phosphoramidite(7.0 mL, 3.5 mmol) in CH₃CN. After the addition

the resulting solution was stirred for an additional 20 minutes at -36 °C. A 0.88 M

solution of TBHP (18.8 mL, 16.5 mmol) in CH₂Cl₂ was then added, and the reaction was

warmed to room temperature with a water bath. After stirring for 20 minutes, the

reaction solution was evaporated to a small volume (~15-20 mL) and diluted with an

equal volume of CH₂Cl₂. After the suspended solid was removed by filtration through a

bed of sand the crude product was loaded onto a silica gel column and eluted as described

above, yielding phosphate **23** (2.29 mmol, 65% based on limiting phosphoramidite; 80%

based on total recovered carbohydrate) and recovered starting material (**17**, 1.43 mmol).

The obtained product was spectroscopically equivalent to the previously-obtained

phosphate **23** (see above spectral information).

References:

1.   Sowa, T.; Ouchi, S. *Bull. Chem. Soc. Japan*, **1975**, *48*, 2084-2090.

2.   Imai, K.; Fujii, S.; Takanohashi, K.; Furukawa, Y.; Masuda, T.; Honjo, M. *J. Org. Chem.*, **1969**, *34*, 1547-1550.

3.   Yoshikawa, M.; Kato, T.; Takenishi, T. *Bull. Chem. Soc. Japan*, **1969**, *42*, 3505-3508.

4.   Hes, J., Mertes, M. *J. Org. Chem.*, **1974**, *39*, 3767-3769.

5.   Knerr, L.; Pannecouke, X.; Schmitt, G.; Luu, B. *Tetrahedron*, **1996**, *37*, 5123-5126.

6.   Beaucage, S. L.; Caruthers, M. H. *Tet. Lett.*, **1981**, *22*, 1859-1862.

7.   Still, W. C.; Kahn, M.; Mitra, A. *J. Org. Chem.*, **1978**, *43*, 2923-2925.

8.   Dahl, B. H.;Nielsen, J.; Dahl, O. *Nucleic Acids Res.*, **1987**, *15*, 1729-1743.

9.   Berner, S.; Muhlegger, K.; Seliger, H. *Nucleic Acids Res.*, **1989**, *17*, 853-865.

10.   Berner, S.; Muhlegger, M.; Seliger, H. *Nucleosides Nucleotides*, **1988**, *7*, 763-767.

11.   Stec, W. J.; Zon, G. *Tet. Lett.*, **1984**, *25*, 5279-5282.

12.   Pederson, R. L.; Esker, J.; Wong, C. H. *Tetrahedron*, **1991**, *47*, 2643-2648.

13.   Bannwarth, W.; Trzeciak, A. *Helv. Chim. Acta*, **1987**, *70*, 175-186.

14.   Uhlmann, E.; Engels, J. *Tet. Lett.*, **1986**, *27*, 1025-1026.

15.   Yu, K.-L.; Fraser-Reid, B. *Tet. Lett.*, **1988**, *29*, 979-982.

16.   Froehler, B. C.; Matteucci, M. D. *Tet. Lett.*, **1983**, *24*, 3171-3174.

17.   Hayakawa, Y.; Kataoka, M. *J. Am. Chem. Soc.*, **1997**, *119*, 11758-11762.

18.   Wright, P.; Lloyd, D.; Rapp, W.; Andrus, A. *Tet. Lett.*, **1993**, *34*, 3373-3376.

19.   Chapeau, M. C.; Marnett, L. J. *J. Org. Chem.*, **1993**, *58*, 7258.

20.   Graham, S. M.; Spinnato, D. S. **1999**, in press.

21.   Wolter, A.; Biernat, J.; Koster, H. *Nucleosides Nucleotides*, **1986**, *5*, 65-77.

CHAPTER IV

THE SOLUTION STRUCTURE OF CADPR

Characterization by 400 MHz NMR

General Background

Due to its known calcium-releasing activity, cADPR[1] has become an attractive target for future study. Unfortunately, relatively little is known regarding its actual mechanism of action. Additional structural information would potentially provide such crucial details, thus promoting elucidation of the cADPR pathway.

The basic goal of this study included the structural deduction of cADPR in solution, as supported by NMR data. The processed and resolved experiments afford this information, while offering additional avenues for future cADPR research. Continuation of experimentation in this arena would potentially produce key insights pertaining to the conformation and binding of cADPR in biological systems.

cADPR Background

In biological systems, cADPR is formed from NAD^+ in an enzymatic reaction catalyzed by ADP-ribosyl cyclase (Figure 53). The relatively ubiquitous cyclase produces the cyclic product, which includes a new N-glycosidic bond between adenine and the anomeric position of the opposite ring (the "R ring", previously occupied by the NAD^+ moiety). Initial studies[1,2] were unsuccessful in determining the
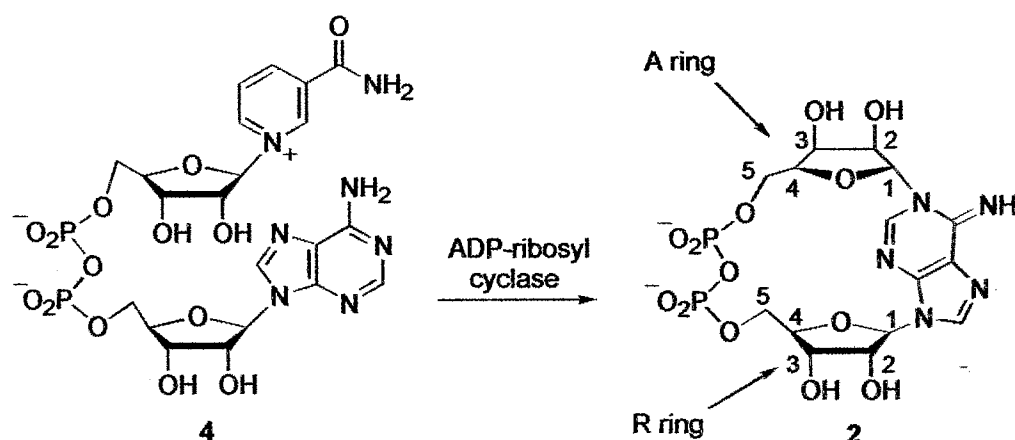
Figure 53. Biological synthesis and ring-labeling of cADPR (2).

exact nature of the new glycosidic bond. However, subsequent UV spectroscopy[3] and X-ray crystallography[4] data characterized the new bond as a β-linkage between the adenine N_1 and the R-ring C1. To date, several cADPR analogues[5-11] have been successfully synthesized via the enzymatic approach. Further correlations of structure and activity for cADPR and these analogues are necessary for an understanding of the biological activities of these compounds. The following investigation commences the integral interpretation of cADPR conformation in solution. The applications of the initial data would potentially yield further conclusions regarding these calcium-releasing agents.

Results and Discussion

1D and VT experiments

The 1D ^{1}H-NMR spectrum of cADPR (Figure 54) initially indicated that data obtained at room temperature would be inadequate for precise elucidation of
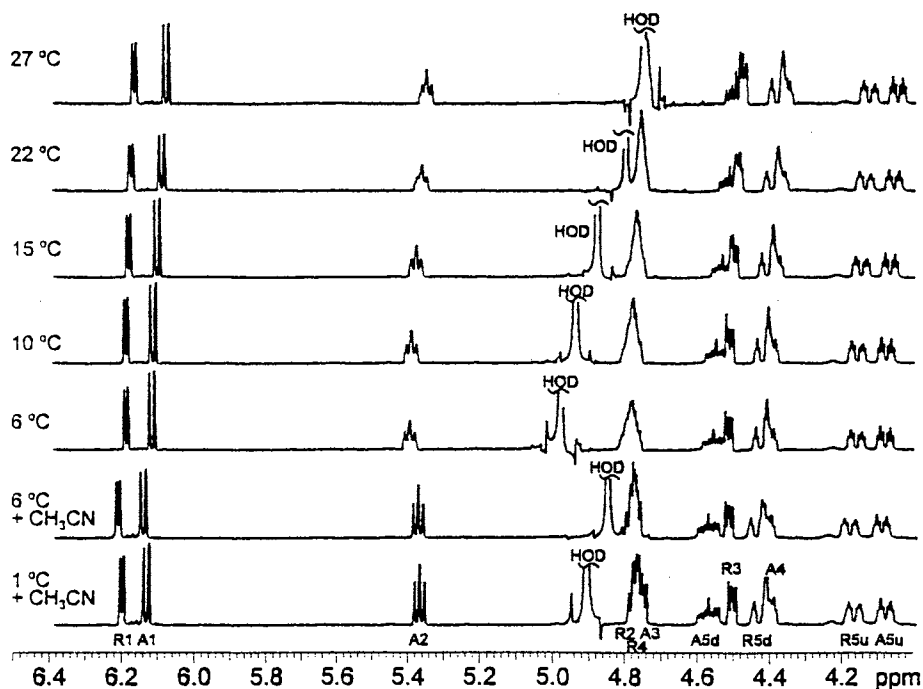
Figure 54. ¹H-NMR spectra of cADPR at various temperatures.

conformation. Most prominent was the absence of three carbohydrate signals (14 non-

exchangeable signals expected versus 11 observed by integration at RT). Equally

problematic was the observed lack of resolution in the multiplets centered around 4.4 and

4.5 ppm, necessary for subsequent simulation trials. As it seemed likely that the missing

signals were masked by the residual HOD signal (~4.8 ppm), variable temperature (VT)

experiments were conducted in an attempt to shift the position of the HOD signal. After

gradually lowering the temperature to 6 °C, two significant improvements were observed.

As expected, the HOD signal shifted downfield by approximately 0.2 ppm, thereby uncovering the missing three-proton multiplet at 4.8 ppm. Additionally, the two-proton multiplet centered at 4.5 ppm became more dispersed, yielding two separate, well-defined multiplets.

In order to further lower the temperature, while correspondingly improving the physical appearance of the resultant spectrum, an NMR solvent titration (Figure 54) was performed. Addition of CD_3CN and continued decrease of the temperature produced further improvements. Ultimately the superior data was obtained (bottom spectra, Figure 54) using an approximate 5:2 v/v mixture of D_2O/CD_3CN at 1 °C. The produced spectrum was deemed sufficient for the subsequent assignment of the sugar signals using ^1H-^1H correlated spectroscopy (COSY).

COSY Assignments

Figures 55 and 56 show the full and expanded COSY spectra, respectively, of the $D_2O/CD_3CN/1$ °C sample of cADPR. The assignment of the sugar signals by ^1H-NMR was greatly aided by the observation that the anomeric signals (H1) are usually the most downfield aliphatic signals and/or that the diastereotopic (upfield and downfield in ^1H-NMR spectra) methylene signals (H5'd, H5'u in ribose rings) are the most upfield. Given sufficient resolution, each ribose ring of cADPR (A or R) should show six cross peaks (H1'-H2', H2'-H3', H3'-H4', H4'-H5', H4'-H5", and H5'-H5").

Of the downfield sugar signals, the ~6.20 ppm signal was assigned to R1 (i.e., the proton on C1' of the R ring) and the ~6.13 ppm signal to A1 (Figure 55). The A1 signal
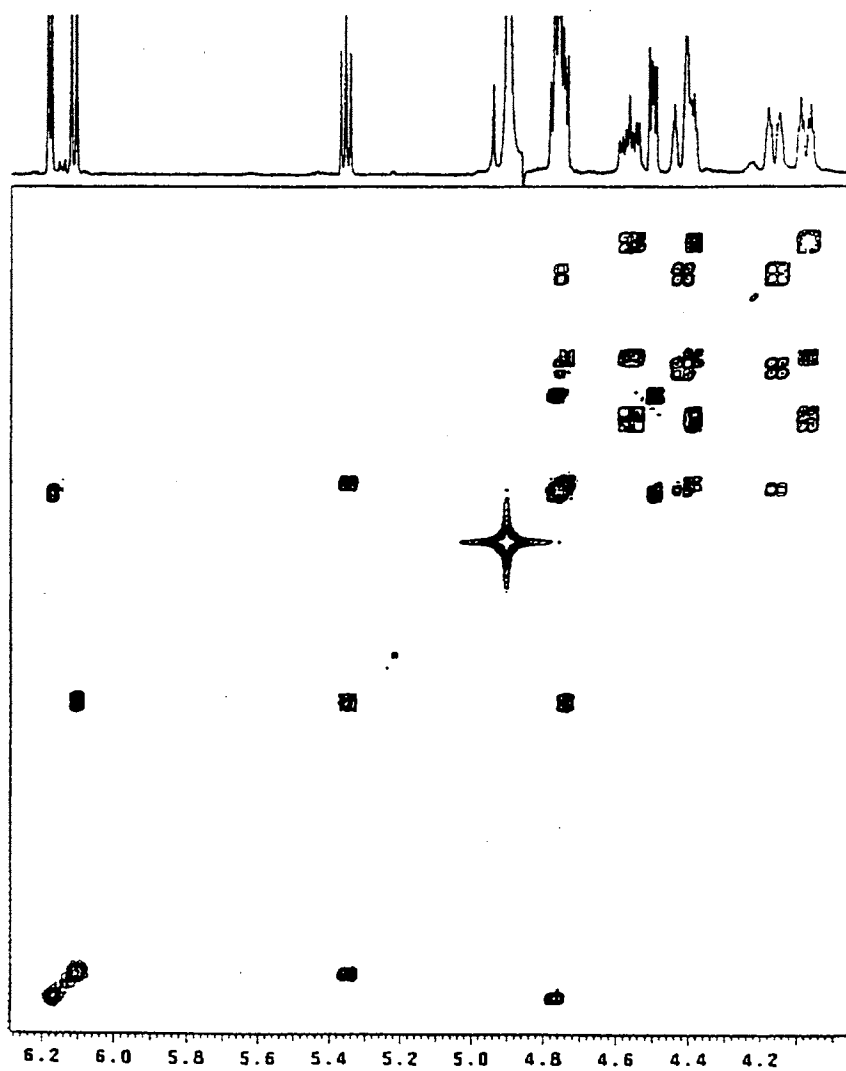
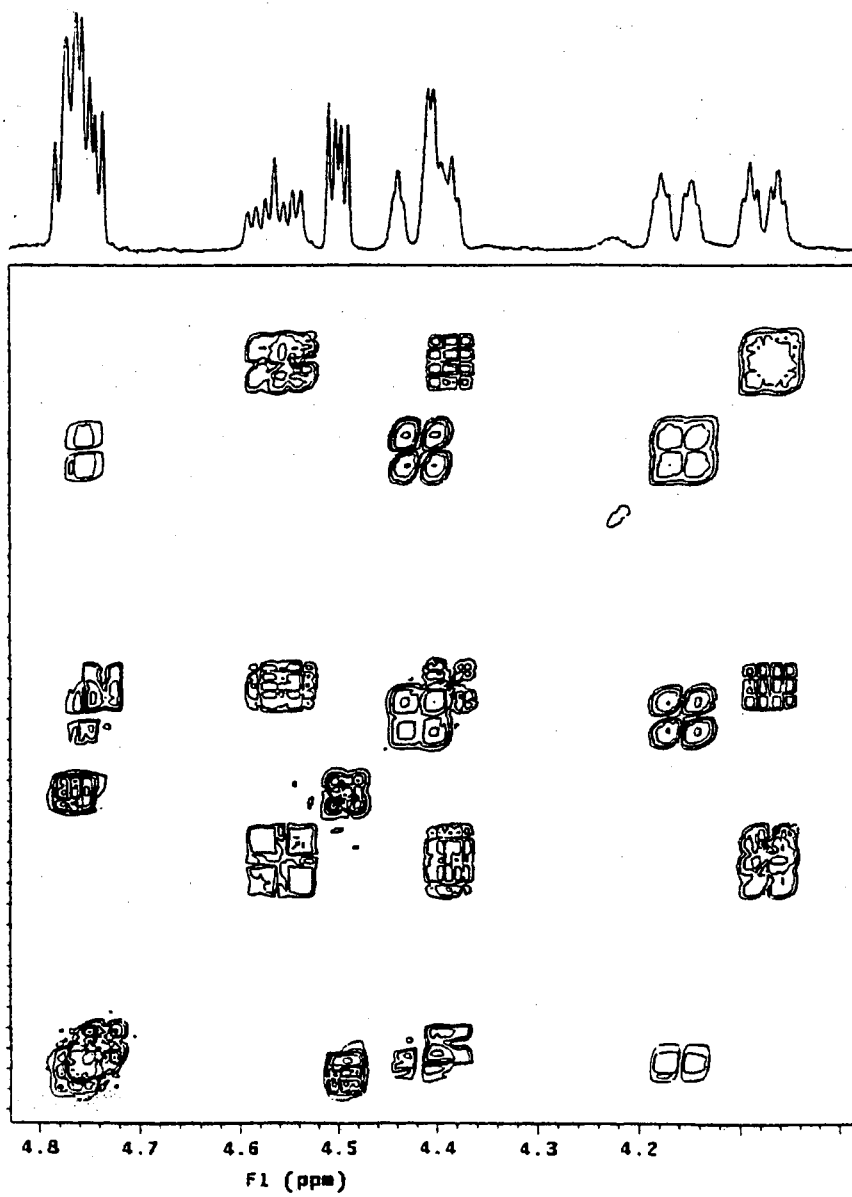**Figure 55.** COSY spectrum of 2.

Figure 56. Expanded COSY spectrum of 2.

correlates to the A2 signal at ~5.4 ppm; as A2 is an apparent triplet in the 1D spectrum,

$J_{A1'-A2'} \sim J_{A2'-A3'}$. Expansion of the COSY spectrum (Figure 56) reveals that A2 correlates

with the upfield portion of the three-proton multiplet at ~4.80 ppm, thus revealing A3.

The A3 signal leads to A4, which is the upfield portion of the two-proton multiplet at

~4.4 ppm. Finally, A4 shows cross peaks to both[12] the upfield (A5u) and downfield

(A5d, the seven peak pattern at ~4.6 ppm) signals of the A ring methylene group. The R

ring analysis is slightly complicated by the near chemical shift coincidence of R2 and R4.

Careful analysis reveals that R1 correlates to the upfield portion of the three-proton

multiplet at ~4.80 ppm and that R5u and R5d correlate to the central portion of the

multiplet.

Coupling constants and conformational analysis

With a relatively well-resolved, assigned spectrum of cADPR obtained, the

extraction of coupling constants for conformational analysis was then performed. The

relationship between observed coupling constants in sugar rings and the torsional angle

required to produce these coupling constants has been described using

pseudorotation.[12,13] In this treatment, the conformation of a sugar is described in terms of

a phase angle, P (a location on the pseudorotation wheel), and a sugar puckering

amplitude, Φ_m. A two-state model is assumed (see below), in which a particular

observed coupling constant is the weighted average of the respective coupling constants

of the rapidly equilibrating conformations. Analysis of a large number of nucleosides

has shown that the majority of furanose rings adopt sugar puckers in the "north" (N, $P \sim 0$,

or C2'-exo-C3'-endo) or "south" (S, $P\sim180$, or C2'-endo-C3'-exo) domains of the

pseudorotational wheel. The relationship between the observed coupling constant and

the conformational equilibrium is described by Equation 1:

$$J_{a,b \; (obs)} = J_{a,b \; (N)}X_N + J_{a,b \; (S)}X_S \qquad (1)$$

where $J_{a,b(N)}$ and $J_{a,b(S)}$ are the particular coupling constants of the pure N and S

conformers and X_N and X_S are the mole fractions of the N and S conformers. Given

enough coupling constants (and consequently, enough furanose torsional angles) the ratio

of conformers can be calculated for certain observed coupling constants.[14]

The observed coupling constants for the A and R rings of cADPR ($D_2O/CD_3CN/1$

°C) are summarized in Table IV. The R1, R3, and R5u signals were all well-resolved and

provide almost all of the information needed to estimate all but one of the R ring

coupling constants. Inspection of the R1 doublet reveals $J_{R1,R2}\sim3.7$ Hz.

J	A ring (Hz)	R ring (Hz)
$J_{1,2}$	5.9	3.7
$J_{2,3}$	5.0	4.8
$J_{3,4}$	3.0	2.8
$J_{4,5u}$	2.7	2.8
$J_{4,5d}$	7.2	2.2
$J_{5u,5d}$	11.0	12.1
$J_{P,5u}$	2.9	2.8
$J_{P,5u}$	3.5	2.2

Table IV. Observed coupling constants for the A and R rings of cADPR.

R3 is a doublet of doublets (J = 4.8, 2.8 Hz), giving the magnitude, but not the actual

assignments, of $J_{R2,R3}$ and $J_{R3,R4}$. R5u is an apparent doublet of triplets, with a large

$^2J_{R5u,R5d}$ of ~12 Hz; the "triplet" portion of the signal is caused by the nearly similar

values (~2.5 Hz) of $J_{R4,R5u}$ and $^3J_{R5u-C5-O5-P}$. A similar treatment of the A ring coupling

constants allowed estimation of all of the coupling constants except $J_{A3,A4}$. The extracted

coupling constants, although imprecise, were sufficiently well-determined to allow

spectral simulation[15] and further refinement (Figures 57 and 58).

The comparison of the observed coupling constants to those calculated by

Altona[16] for a ribose ring is given in Table V. For Φ_m = 35° we explored combinations of

P_N and P_S regions from 0 - 36° and 144 - 216°, respectively; for Φ_m = 40 combinations of

P_N = 351 - 36° and P_S = 144 - 216° regions were explored. For a given ratio of N and S

conformers a good fit was defined as one where each calculated J was within ± 0.5 Hz of

the observed value. The observed J's for the A ring are consistent with N:S ratios ranging

from 30:70 to 20:80 for P_N values of 0 - 36° and P_S values of 162 - 171° (Φ_m = 35°).

When Φ_m was increased 40° the relative populations were unchanged (30:70 N:S), while

P_N and P_S localized to the high end of their observed ranges (P_N = 36° and P_S = 171 -

180°). The analysis of the R ring revealed a generally poor fit when Φ_m = 35°, and only

when Φ_m = 40° was a good fit observed. Again the N:S ratios ranged from 30:70 to

20:80, with P_N spanning the range from 351 - 180°. Interestingly, the R ring P_S localized

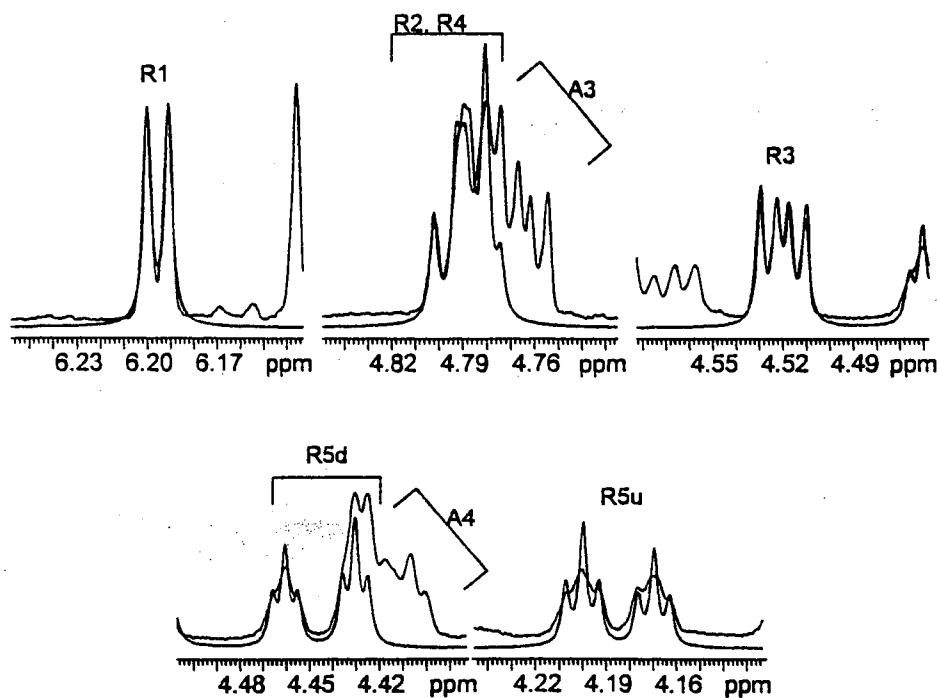to 216°. In the published crystal structure of cADPR the A ring was found to adopt a C2'-
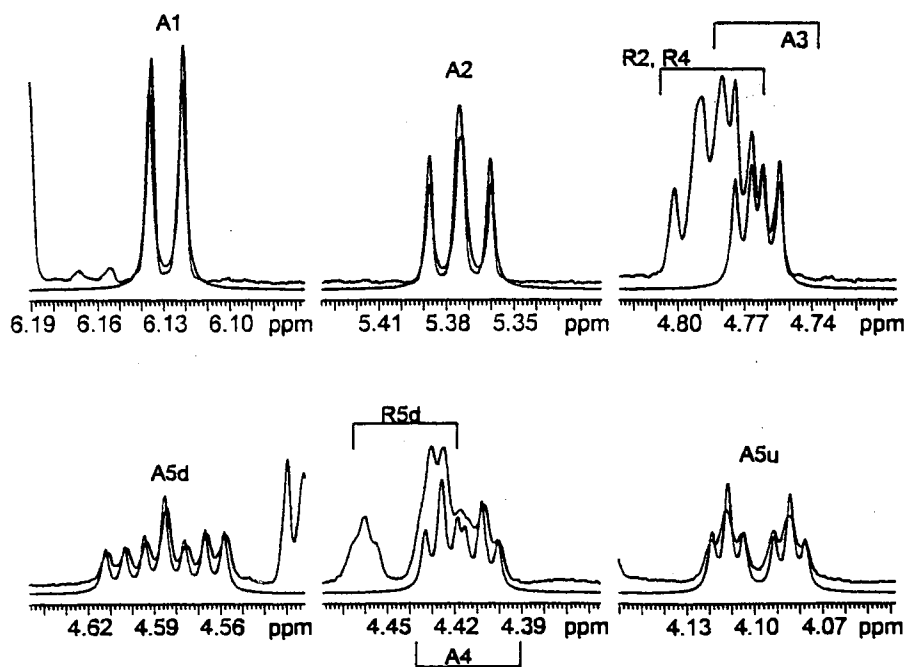
Figure 57. R ring simulation.

Figure 58. A ring simulation.

A Ring ($\Phi_m = 35°$)

P_N, P_S	%S:%N	$J_{1'2'}$	$J_{2'3'}$	$J_{3'4'}$
0,162	80:20	6.24	5.27	2.65
0,162	70:30	5.59	5.24	3.34
9,162	80:20	6.26	5.28	2.72
9,162	70:30	5.61	5.26	3.44
18,162	80:20	6.29	5.31	2.77
18,162	70:30	5.51	5.19	3.32
27,171	80:20	6.17	5.23	2.57
27,171	70:30	5.59	5.27	3.36
36,171	80:20	6.25	5.31	2.58
36,171	80:20	5.72	5.39	3.37

R Ring ($\Phi_m = 35°$)

P_N, P_S	%S:%N	$J_{1'2'}$	$J_{2'3'}$	$J_{3'4'}$

A Ring ($\Phi_m = 40°$)

P_N, P_S	%S:%N	$J_{1'2'}$	$J_{2'3'}$	$J_{3'4'}$
36,171	70:30	5.99	4.73	3.38
36,180	70:30	5.76	4.68	3.32
OBSERVED		5.90	5.00	3.00

R Ring ($\Phi_m = 40°$)

P_N, P_S	%S:%N	$J_{1'2'}$	$J_{2'3'}$	$J_{3'4'}$
351,216	80:20	4.10	5.24	2.32
351,216	70:30	3.72	5.14	3.05
0,216	80:20	4.08	5.23	2.42
0,216	70:30	3.70	5.11	3.19
9,216	80:20	4.08	5.24	2.48
9,216	70:30	3.70	5.14	3.29
18,216	80:20	4.11	5.28	2.52
OBSERVED		3.70	4.80	2.80

Table V. Comparison of obtained data with calculated J values.

endo (major)-C3'-exo (minor) conformation ($P_S \sim 171°$), and an R ring conformation of

C3'-exo ($P_S \sim 198°$). Limiting attention to the major solution conformers of the A and R

rings (P_S = 162 - 180° and 216°, respectively), agreement between the crystal structure and the obtained solution states was found to be quite reasonable.

The observed coupling constants were also used to determine the backbone torsional angles β (P-O5'-C5'-C4' via the $^3J_{P-H5d/5u}$ coupling)[17,18] and γ (O5'-C5'-C4'-C3' via the $^3J_{H4-H5u/5d}$ coupling). For the A ring the coupling of the phosphorus to both the A5u and A5d protons was quite similar, thereby suggesting a symmetrical relationship. The consequent assumption of a staggered conformation about the β-bond leads to the conclusion that the phosphorus is *gauche* to both H5 hydrogens (*trans* to C4'). Analogous behavior was observed for the R ring, and thus both the A and R ring β-bonds are likely to be exclusively (>90%) *trans* (torsion angle = ±180°). The crystal structure β-bonds are in the same general range as the solution values, with an A ring β of -138° and an R ring β of +160°. In the case of the R ring γ-bond,[19] near equivalence of $J_{R4, R5u}$ and $J_{R4,R5d}$ was observed. An extension of the previously applied logic yields an R4' proton gauche to both R5u and R5d (i.e., the R ring C3 and O5 are gauche and the R ring γ-bond is (>85%) $γ^+$ (pure $γ^+$ = +60°; +54° was observed in the crystal structure). Analysis of the A ring γ-bond is hindered by the lack of stereospecific assignments for A5u and A5d, especially in correlation to H5d and/or H5u.[20] In the absence of this data, a "small" $J_{A4,A5u}$ (2.7 Hz) and a "large" $J_{A4,A5d}$ (7.2 Hz) coupling were interpreted as evidence for either $γ^t$ (±180°) or $γ^-$ (-60°). This is in direct contrast to the crystal structure, in which the observed A ring γ (+66°) was clearly in the $γ^+$ range. One possible interpretation includes the role of packing forces in the crystal as the principal determinant of the γ configuration, e.g., rotation about the γ in the solid state may

relieve an electrostatic repulsion caused by the anionic phosphates of a neighboring molecule.

The high-resolution NMR data presented above supports a solution structure for cADPR. Future extensions of this research would potentially produce additional structural details. Useful experiments, such as Nuclear Overhauser Effect (NOE) protocols, could be used in the stereospecific assignments of H5u and H5d. NOE experiments would also further the determination of the glycosidic torsion angles.

Experimental Section

Synthesis of cADPR

cADPR was synthesized and purified as described,[21] substituting ADP ribosyl cyclase (Sigma) for pig brain acetone powder.

NMR studies of cADPR

^{1}H (400 MHz) and ^{31}P (121.5 MHz) NMR spectra were obtained in D_2O (>99.8%) solvent. Pure D_2O samples were referenced to the residual HOD peak in a temperature-dependent fashion as described.[22] Samples run in D_2O/CD_3CN were referenced to the previous samples (not containing CD_3CN). ^{31}P-NMR spectra were referenced to external 85% H_3PO_4 in D_2O. NMR samples were lyophilized three times from D_2O prior to final dissolution in D_2O. 1D NMR spectra were acquired for 2.7 seconds (32 transients) with a 5 second pulse delay, using a spectral width of 6000 Hz,

32K data points, and zero-filling to 64K. No solvent suppression was used, and the resultant data was processed with weighting functions (line broadening = -0.9, guassian function = 0.7). Simulated spectra were acquired using a simulated line width (1.5 Hz). The COSY experiment was performed in absolute value mode using 16 transients, 512 increments, with an acquisition time of 1.11 seconds, a 2.0 second delay, a spectral width of 3600 Hz, and zero-filling to 8K x 8K points. After sine bell weighting (0.3 seconds) in both dimensions, the data was symmetrized.

2
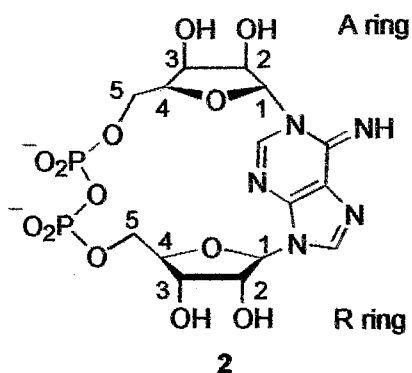
^{1}H-NMR (2, δ, 400 MHz)

9.104 (s, 1H, adenine H8)

8.469 (s, 1H, adenine H2)

6.196 (d, J = 3.7 Hz, 1H, R1)

6.129 (d, J = 5.9 Hz, 1H, A1)

5.374 (t, J = 5.3 Hz, 1H, A2)

4.783 - 4.767 (m, 3H, R2, R4)

4.752 (dd, J = 5.0, 2.9 Hz, 1H, A3)

4.584 (ddd, J = 10.9, 7.3, 3.5 Hz, 1H, A5d)

4.496 (dd, 1H, J = 4.8, 2.8 Hz, R3)

4.461 (app. dt, J = 11.9, ~2 Hz, 1H, R5d)

4.419 (app. dt, J = 7.0, 2.8 Hz, 1H, A4)

4.189 (app. dt, 1H, J = 12.3, ~3 Hz, R5u)

4.099 (dt, 1H, J = 11.1, 2.9 Hz, A5u)

^{31}P-NMR (2, δ, 162 MHz)

-10.4 (d, J = 14 Hz)

-11.7 (d, J = 14 Hz)

References

1. Lee, H.C.; Walseth, T.F.; Bratt, G.T.; Hayes, R.N.; Clapper, D.L. *J. Biol. Chem.* **1989**, *264*, 1608-1615.

2. Clapper, D.L.; Walseth, T.F.; Dargie, P.J.; Lee, H.C. *J. Biol. Chem.* **1987**, *262*, 9561-9568.

3. Kim, H.; Jacobsen, E.L.; Jacobsen, M.K. *Biochem. Biophys. Res. Comm.* **1993**, *194*, 1143-1147.

4. Lee, H.C.; Aarhus, R.; Levitt, D. *Nature Struct. Biol.* **1994**, *1*, 143-144.

5. Graeff, R.M.; Walseth, T.F.; Hill, H.K.; Lee, H.C. *Biochemistry* **1996**, *35*, 379-386.

6. Zhang, F.J.; Sih, C.J. *Bioorg. Med. Chem. Lett.* **1997**, *7*, 1753-1756.

7. Walseth, T.F.; Lee, H.C. *Biochim. Biophys. Acta* **1993**, *1178*, 235-242.

8. Ashamu, G.A.; Sethi, J.K.; Galione, A.; Potter, B.V.L. *Biochemistry* **1997**, *36*, 9509-9517.

9. Bailey, V.C.; Sethi, J.K.; Galione, A.; Potter, B.V.L. *Chem. Commun.* **1997**, 695-696.

10. Ashamu, G.A.; Galione, A.; Potter, B.V.L. *J. Chem. Soc., Chem. Commun.* **1995**, 1359-1360.

11. Shuto, S.; Shirato, M.; Sumita, S.; Ueno, Y.; Matsuda, A. *J. Org. Chem.* **1998**, *63*, 1986-1994.

12. The H5 protons have not been stereospecifically assigned at the current time.

13. de Leeuw, F.A.A.M.; Altona, C. *J. Chem. Soc.* **1982**, *94*, 375-384.

14. In the full treatment described in the literature, $^3J_{HH}$ is a function of five variables - P_N, Φ_N, P_S, Φ_S, and X_N (or X_S, since $X_S + X_N = 1$). Deoxy sugars can be completely determined, as there are five observable values related to the endocyclic torsion angles - $J_{1'2'}$, $J_{1'2''}$, $J_{2'3'}$, $J_{2''3'}$, and $J_{3'4'}$. Ribo sugars have only three coupling constants related to the endocyclic torsion angles - $J_{1'2'}$, $J_{2'3'}$, and $J_{3'4'}$. Ribo sugars are therefore "underdetermined" and assumptions concerning two of the variables must be made. In practice, $^3J_{HH}$ shows relatively little dependence on the puckering amplitude, Φ (the variation in Φ is typically 1 Hz or less over most of its allowed range). The

current study has constrained Φ to two values, 35° and 40°.

15. Simulations were performed using LAME (Varian Associates).

16. Altona, C.; Sundaralingam, M. *J. Am. Chem. Soc.* **1972**, *94*, 8205-8212.

17. Lankhorst, P.P.; Haasnoot, C.A.G.; Erkelens, C.; Altona, C. *J. Biomolec. Struct. Dyn.* **1984**, *1*, 1387.

18. Haasnoot, C.A.G.; de Leeuw, F.A.A.M.; De Leeuw, H.P.M.; Altona, C. *Recl. Trav. Chim. Pays Bas.* **1979**, *98*, 576.

19. Altona, C. *Recl. Trav. Chim. Pays Bas.* **1982**, *101*, 413.

20. The rule of Shugar and Remin, which states that H5″ is typically upfield from H5′, has not been invoked. In the current study, the cyclic and presumably conformationally restricted nature of the sugar-phosphate backbone in cADPR may render this observation invalid. See Remin, M.; Shugar, D. *Biochem. Biophys. Res. Comm.* **1972**, *48*, 636.

21. Gu, Q.M.; Sih, C.J. *J. Am. Chem. Soc.* **1994**, *116*, 7481-7486.

22. Gottlieb, H.E.; Kotlyar, V.; Nudelman, A. *J. Org. Chem.* **1997**, *62*, 7512-7515.

VITA

Sarah Christine Pope

Candidate for the Degree of

Doctor of Philosophy

Thesis: I.   STUDIES TOWARD THE TOTAL CHEMICAL SYNTHESIS OF CYCLIC ADENOSINE 5'-DIPHOSPHATE RIBOSE (CADPR)

II.   SELECTIVE PHOSPHITYLATION OF UNPROTECTED CARBOHYDRATES

III.   THE SOLUTION STRUCTURE OF CADPR

Major Field: Chemistry

Biographical:

Personal Data: Born in Louisville, Kentucky, on November 17, 1972.

Education: Graduated from LeMars Community High School, LeMars, Iowa in June 1990; received Bachelor of Arts degree in Chemistry from Earlham College, Richmond, Indiana, in June 1994; completed the requirements for the Doctor of Philosophy degree with a major in Chemistry at Oklahoma State University in December, 1999.

Experience: Served as a deskworker in Science Reference at Earlham College, 1990-1994; employed by Oklahoma State University, Department of Chemistry, as a graduate teaching assistant and as a graduate research assistant, 1994-present.

Professional Memberships: American Chemical Society, Phi Lambda Upsilon.